2016

Flow Sensing in the Deep Sea: Morphology of the Lateral Line System in Stomiiform Fishes

Ashley Marranzino
University of Rhode Island, amarranzino@my.uri.edu

FLOW SENSING IN THE DEEP SEA: MORPHOLOGY OF THE LATERAL LINE SYSTEM IN STOMIIFORM FISHES

BY

ASHLEY N. MARRANZINO

A THESIS SUBMITTED IN PARTIAL FULFILLMENT OF THE REQUIREMENTS FOR THE DEGREE OF

MASTER OF SCIENCE

IN

BIOLOGICAL AND ENVIRONMENTAL SCIENCES

UNIVERSITY OF RHODE ISLAND

2016

MASTER OF SCIENCE

OF

ASHLEY N. MARRANZINO

APPROVED:

Thesis Committee:

Major Professor

Jacqueline Webb

Brad Seibel

Karen Wishner

Nasser H. Zawia
DEAN OF THE GRADUATE SCHOOL

UNIVERSITY OF RHODE ISLAND
2016

ABSTRACT

The deep sea is characterized by extreme environmental conditions including limited light availability, which makes non-visual sensory capabilities quite important. In addition to the visual, auditory, olfactory and gustatory systems found in all vertebrates, all fishes have a mechanosensory lateral line system. This system is composed of neuromast receptor organs on the skin and in bony canals on the head and trunk and is sensitive to unidirectional water flows and low frequency vibrations. Our knowledge about the lateral line system (LL) in deep-sea fishes is limited.

Of the taxa in which the LL has been described, there appears to be two morphologies: widened LL canals with large canal neuromasts, and a reduced LL canal system with a proliferation of superficial neuromasts (SNs). However, the one published description of the LL in a species of the prominent midwater order Stomiiformes, suggests that there is a third LL morphology defined by a reduction in canals on the head accompanied by just a few, small SNs. The goal of Chapter 1 was to use traditional and modern morphological methods to provide the first detailed description of the LL system in two groups of stomiiform fishes (*Argyropelecus* [Family Sternoptychidae] and *Cyclothone* [Family Gonostomatidae]) as well as other fishes in the Families Gonostomatidae, Phocichthyidae, and Stomiidae in order to test the hypothesis that reduced canals and a reduced number of SNs is a strategy in the evolution of the LL in stomiiform fishes. A total of 27 species in 17 genera in four families were studied using one or more morphological approaches (including histology and micro computed tomography, or μCT).

In depth analysis of four *Argyropelecus* species (Sternoptychidae) revealed the presence of several incompletely ossified LL canals on the head, including the supraorbital (SO), mandibular (MD) and preopercular (PO) canals. Examination of whole preserved specimens of other taxa also revealed the presence of SO, MD, PO, and IO (infraorbital) canals with varying degrees of ossification. Few species had all canals typically found in bony fishes, but all taxa, with the exception *Cyclothone* species, had some cranial LL canals.

A proliferation of SNs was revealed using histological material and scanning electron microscopy in fishes in the families Sternoptychidae, Gonostomatidae, and Stomiidae. These domed, circular structures (= "white dots") stood out against darkly pigmented skin and were visible under low magnification in very well preserved specimens. They appeared to be innervated, and had a similar morphology and distribution on the head and/or body in all species. Thus, it appears that there is a proliferation of SNs in many stomiiform genera, that the initial description of just a few SNs in *Argyropelecus* is incorrect, and that the LL is more important to these deep-sea fishes than has been previously suggested.

The discovery of a proliferation of SNs in these fishes made it necessary to be able to distinguish them from the numerous bioluminescent photophores and other structures found in in the skin of these fishes. In Chapter 2, specimens were imaged under different wavelengths of light as a new tool to distinguish SNs from both complex and simple photophores. A total of 34 stomiiform species (in four families) and representatives of two other deep-sea taxa (Myctophidae, Melamphaidae) were examined under brightfield illumination, and at three different excitation wavelengths (390, 470,

545 nm). Complex photophores were visible under all wavelengths, while SNs and simple photophores were only visible at 390 and 470 nm. SNs and simple photophores were brighter under different wavelengths, allowing for SNs to be differentiated from photophores when illuminated under different wavelengths of light. This technique also revealed variation in the size, distribution, density, and orientation (direction of light emission) of numerous, minute, complex photophores on the head and trunk of stomiids. Additionally, the fragile, gelatinous coating found in some stomiid fishes and the simple photophores found within it were described in *Chauliodus sloani* and *Stomias boa ferox.*

ACKNOWLEDGEMENTS

I would like to thank Cindy Klepaldo (Scripps Institute of Oceanography) and Karsten Hartel (Museum of Comparative Zoology at Harvard) for specimen loans used for this research. Thank you to Dr. Jacqueline Webb, Dr. Brad Seibel, Dr. Tracey Sutton (Nova Southeastern University), Dr. Steve Haddock (MBARI) for providing specimens from personal collections or for collecting specimens for my research. I would also like to give special thanks to Dr. Chris Kenaley (Boston College and Harvard University) for providing μCT data, histological slides of *Astronesthes niger*, and unpublished innervation data.

I would like to acknowledge and thank undergraduate Ben Sevey for training me to use OsiriX and for generating μCT images. Thank you to undergraduate Danielle Jordan for collecting data from histological material. Thank you to undergraduates Ciara Dawson and John Psaltis (Boston College, working in the Kenaley Lab) for preliminary analysis of photophore morphology and distribution.

I would like to thank Dr. Nathan Bird for his mentorship and help through this project. I would also like to thank my labmates, Lauren Carter, Julia Johnstone, Andrea Schlunk, and Dr. Yinan Hu for their ongoing support, encouragement and help. Finally I would like to thank my advisor, Dr. Jacqueline Webb for her continued mentorship, support, and guidance and my committee members, Dr. Brad Seibel and Dr. Karen Wishner, for their guidance during this project.

This research was funded by a NSF Graduate Research Fellowship (#ADW03561), the American Museum of Natural History (NY) Lerner Grey Fund and by a URI Enhancement of Graduate Research Award.

PREFACE

This thesis is composed in Manuscript format. Each chapter is formatted for separate submission to the *Journal of Morphology*.

TABLE OF CONTENTS

LIST OF TABLES

TABLE **PAGE**

CHAPTER 1

CHAPTER 2

LIST OF FIGURES

FIGURE **PAGE**

CHAPTER 1

CHAPTER 1

This manuscript has been formatted for submission to the *Journal of Morphology*

Introduction

Approximately 65% of the surface of the earth lies at depths below 200 m, in the dark waters of the deep sea, making this habitat one of the largest on our planet. Yet, we know less about the deep sea than we do about the surface of the moon (Nouvian, 2007). This prominent habitat is characterized by extreme environmental conditions (Fig. 1.1). The waters of the deep sea reach near freezing temperatures and experience high pressures (increasing 1atm per 10 m depth increase). Furthermore, only 1% of visible sunlight from surface waters penetrates below 200 m into the mesopelagic zone (~200 – 1,000 m), while no detectable light extends into the bathypelagic zone (~1,000 – 4,000 m). This light limitation prevents photosynthesis from occurring in the deep sea, resulting in lower biomass in this environment compared to that in shallow water habitats (Angel, 1997; Haedrich, 1997; Montgomery et al., 2014). Additionally, low-light levels define the sensory environment, limiting the detection of visual stimuli and thus challenging processes of prey and mate location and predator avoidance, which are otherwise dependent on vision in shallow water. In order to cope with these extreme environmental conditions, fishes have evolved some interesting sensory adaptations, such as enlarged olfactory structures and eyes capable of detecting lower levels of light including those generated by bioluminescence. While adaptive visual morphologies have been fairly well described in several deep-sea fish taxa (i.e. Douglas and Partridge, 2011; Gagnon et al., 2013; Busserolles et al., 2014), little information is available on the non-visual sensory systems including the mechanosensory lateral line system.

The mechanosensory lateral line system is a primitive vertebrate sensory system found in all fishes (and in larval and adult aquatic amphibians), that detects

hydrodynamic stimuli (water flows and vibrations). It is known to mediate many important behaviors including prey detection, predator avoidance, and communication (reviewed in Webb et al., 2014a). The sensory organs of the lateral line system, the neuromasts, are composed of directionally sensitive hair cells that respond to unidirectional water flows and vibrations. Neuromasts are located either superficially, on the skin surface (superficial neuromasts), or within cylindrical pored canals (canal neuromasts), which run through a conserved set of dermal bones of the skull and the lateral line scales on the trunk (Webb, 1989). Variation in the morphology of the lateral line system is defined by variation in cranial canal phenotype (narrow, narrow with widened tubules, narrow with branched tubules, widened, or reduced; Webb, 2014b; Fig. 1.2), development and placement of the trunk canal, morphology of individual neuromasts, and the size, shape, and location of these neuromasts within canals or on the surface of the body (Webb, 1989; 2014b).

This morphological variation is thought to contribute to variation in flow sensing capabilities among fishes (Coombs and Bleckmann, 2014; Montgomery et al., 2014). For example, it has been shown that superficial neuromasts detect flow velocity, whereas, canal neuromasts detect flow acceleration and pressure gradients (McHenry and Liao, 2014). Further, neuromasts in widened lateral line canals are more sensitive to hydrodynamic stimuli than neuromasts in narrow canals, but exhibit slower response times (Denton & Gray, 1989; Schwalbe et al., 2012). It has been suggested that such variation in the morphology of the lateral line system is adaptive, and correlates with variation in the behavioral and ecological characteristics of fishes.

The Lateral Line System in the Deep Sea

The morphological specializations of the lateral line system found among diverse groups of fishes living in extreme environments, such as the deep sea, can be used to explore patterns of adaptive evolution of the lateral line system. In an environment with lower light levels, fishes need to rely more heavily upon non-visual sensory modalities. The deep sea is an environment with relatively low hydrodynamic noise in which a more sensitive lateral line system can function effectively. Therefore, it is reasonable to expect the lateral line system to be well-developed and relatively important for mediating behaviors in deep-sea fishes

The lateral line systems of shallow water taxa have been studied extensively, but data on deep-sea fish lateral line systems are scattered in the literature and are often incomplete (reviewed by Webb, 2014). The lateral line system has been described in a small number of deep-sea taxa (i.e. Saccopharyngidae, Nielsen & Bertelsen, 1985; Myctophidae, Lawry, 1972a,b; Macrouridae, Marshall, 1965, Fange et al., 1972; Lophiiformes, Caruso, 1989, Marshall, 1996; Trachichthyiformes, Jakubowski, 1974, Moore, 1993; Melamphidae and Melanonidae, Marshall, 1996). These studies suggest that the lateral line system in deep-sea fishes demonstrates two evolutionary strategies, which have each arisen convergently in multiple fish taxa.

1) Widened canal system with large canal neuromasts. This morphology is found in fishes such as the melamphaids (Stephanoberyciformes), macrourids (Gadiformes), and Ophidiformes (Fig. 1.3A-C; Jakubowski, 1974; Marshall, 1996). Neuromasts in such widened canals are more sensitive than those in narrow canals, but

also react slower to flow stimuli (Denton & Gray, 1988; 1989). Fishes with widened canals feed in low light or darkness and have been shown to feed more successfully (i.e. Eurasian ruffe) in light-limited environments than fishes with narrow canals (discussed in Schwalbe et al., 2012). These studies have led to the hypothesis that widened canals evolved convergently as an adaptation for feeding in light-limited environments (Coombs et al., 1988; Janssen, 1997).

2) Canal reduction with a proliferation of superficial neuromasts. Some deep-sea anglerfishes (Lophiiformes, e.g., *Phrynichthys wedli*), gulper eels (Saccopharyngiformes), and snipe eels (Nemichthyidae) lack cranial lateral line canals. The absence of canals may be explained by selection for reduced bones, including those bones in which cranial lateral line canals are typically found. Bone reduction serves to reduce overall density of a fish providing it with more buoyancy that reduces sinking rates allowing fish to remain in the water column (Fig.1. 4). Although these fishes lack cranial lateral line canals, they have a proliferation of superficial neuromasts on the head and body (Fig. 1.3D-F; Marshall, 1996). In the anglerfishes (i.e. *Phrynicthys wedli*; Fig. 1.3D) and in the snipe eels and gulper eels (Fig. 1.3E – F), these superficial neuromasts sit upon papillae or stalks that extend into the environment, which possibly increases sensitivity to flows. At least some neuromasts are found in locations where cranial canals would typically be present (i.e. above and below the eye, along the lower jaw and the operculum, and around the nares), and likely represent "replacement neuromasts", where canals have been lost (Coombs et al., 1988).

Handrick (1901) reported what appears to be a third morphological strategy in the hatchetfish, *Argyropelecus hemigymnus* (Sternoptychidae: Stomiiformes; Fig. 1.5), where

a reduction of lateral line canals is accompanied by only a very small number of superficial neuromasts. The only other observations on lateral line morphology in these fishes were made by Marshall (1954), who made incidental comments on the "lateral line organs, which are particularly numerous on top of the head" in hatchetfishes. He also stated that "*Cyclothone* spp., the commonest bathypelagic fishes, have both canal organs and free-ending organs" (Marshall, 1979), and suggested that "compared to [myctophids], the other fishes of the twilight zone the [stomiids] have small or poorly developed lateral line organs" (Marshall, 1954). With these few, conflicting reports on the lateral line system of stomiiform fishes, it is unclear if *Argyropelecus* has a reduced canal system with few neuromasts (as suggested by Handrick, 1901) and further, if this morphology is characteristic of other taxa within the Family Sternoptychidae, or more broadly within the Order Stomiiformes.

Two of the most abundant and well-known stomiiform fishes are those of the sister genera (as per Harold and Weitzman, 1996) *Argyropelecus* (hatchetfishes: Sternoptychidae) and *Cyclothone* (bristlemouths: Gonostomatidae). Both genera are widely distributed, frequently collected in midwater trawls, and commonly found in museum collections, making specimens readily available for detailed morphological analyses. *Cyclothone* is often referred to as the most numerous vertebrate genus on the planet (Grey, 1960; Bigelow, 1964; Maynard, 1982).

The ten genera of sternoptychids (hatchetfishes) are known to inhabit the mesopelagic zone circumglobally (Biard, 1971). They are distinguished by their laterally compressed body, large, sometimes tubular eyes, and reflective silvery coloration. The seven recognized species of *Argyropelecus* range in size from approximately 40 to 90

mm SL (fishbase.org). *Argyropelecus* spp. typically undergo diel vertical migrations from mesopelagic waters into shallower waters to feed on planktonic prey (Biard, 1971; Merrett & Roe, 1974; Kinzer & Shultz, 1988; Andersen & Sardou, 1992).

Similarly, gonostomatids (bristlemouths) comprise eight genera, inhabit the mid-waters of the meso- and bathypelagic zones, and have been recorded from all oceans (Grey, 1960). The most speciose genus of the gonostomatids is *Cyclothone*. These fishes have elongate bodies with long jaws, numerous teeth, and relatively small eyes. The 13 recognized *Cyclothone* species range in size from ~2.5 to 8 cm SL (Marshall, 1984; fishbase.org) and feed on zooplanktonic prey (Marshall, 1964; Dewitt & Cailliet, 1972; Merrett & Roe, 1974; Smith & Laver, 1981; Maynard, 1982, Marshall, 1984). Different *Cyclothone* species have discrete depth distributions within their geographic ranges (Fig. A.5). They also undergo ontogenetic migrations, in which larvae and juveniles inhabit shallower waters and eventually move into deeper waters as they grow. Furthermore, *Cyclothone* species tend to be divided into three ecological groups based on the depth distribution of adults (Bond and Tighe, 1974; Maynard, 1982; Marshall, 1984; Miya & Nemoto, 1991):

1) Shallow-dwelling (upper mesopelagic), light-colored species that undergo vertical migrations into the epipelagic (e.g. *C. alba, C. braueri, C. signata.*). These species usually reach sexual maturity early in life, have short lifespans, are semelparous, and produce relatively fewer gametes**. 2)** Deep-dwelling (bathypelagic), darkly pigmented species, which do not undergo vertical migrations (e.g. *C. acclinidens, C. atraria, C. livida, C. microdon C. obscura, C. pallida, C. pygmaea*). These are larger, reach sexual maturity later in life, have a longer lifespan, are iteroparous, and are more

fecund than shallow dwelling species. Several of these species have also been confirmed to be protogynous hermaphrodites. **3)** Intermediate species that occupy intermediate depth ranges and have morphological and reproductive characteristics somewhere between the other two groups (e.g. *C. pseudopallida, C. kobayashii*; Bond and Tighe, 1974; Maynard, 1982; Marshall, 1984; Miya & Nemoto, 1991).

Both *Argyropelecus* and *Cyclothone* are delicate fishes with many "larval" characteristics (Maynard, 1982; Marshall, 1984). They lack scales and have a very thin epithelium (only 1 – 2 cell layers thick; personal observation). As is common in stomiiforms and in deep-sea fishes in general, they exhibit extreme cranial bone reduction, including the loss or reduced size of many lateral line canal-bearing bones (Fig. 1.4B-C). Weitzman (1967, 1974) and Fink (1985) provide detailed osteological descriptions of several stomiiform genera and make reference to lateral line canals or to canal pores in the canal-bearing bones in some species (Table 1.1). Based on descriptions and figures in these papers, it appears that stomiiforms have few cranial canals, but there are no explicit references to canal or neuromast morphology. Furthermore, these studies say little about the lateral line canals in *Argyropelecus* in particular, and say nothing at all about those in *Cyclothone*. However, *Cyclothone* does have enlarged centers in the brain that suggest heightened importance of the lateral line system (Maynard, 1982) and Marshall (1977) mentions the presence of superficial and canal neuromasts. However, in a detailed study of the ecology of *Cyclothone* spp., Maynard (1982) was unable to locate superficial neuromasts when closely inspecting specimens.

The goal of this project was to use a combination of traditional and modern methods to carry out the first detailed description of the lateral line system in

Argyropelecus (Sternoptychidae) and *Cyclothone* (Gonostomatidae) species in order to test the hypothesis that reduced canals and a reduced number of superficial neuromasts, as reported by Handrick (1901), is a strategy in the evolution of the lateral line system in deep-sea fishes. Furthermore, a comparison of lateral line morphology in *Cyclothone* and *Argyropelecus* to that in other stomiid genera will shed light on potential adaptive significance of variation in lateral line morphology among Stomiiformes.

Methods

Specimen Collection and Identification:

Study specimens were obtained from the Museum of Comparative Zoology at Harvard University (MCZ) or were collected on several cruises and provided for this study. See Table 1.2 for a complete list of species used and their collection data and Table 1.3 for list of specimens used for each method.

Specimens collected in 1988 by Dr. J. F. Webb (University of Rhode Island) in the Catalina Basin, CA were collected at night using an Isaacs-Kidd Midwater Trawl (IKMT) and fixed in 4% formalin in seawater (some subsequently transferred to 70% ethanol). Specimens from the Northwest Atlantic and the Eastern Pacific were collected in 2010 and 2014, respectively, by Dr. B. Seibel (University of Rhode Island) using a 3x3 m Tucker trawl (Childress, 1978) with a modified 30 m thermally-insulated cod end (TTIC) and fixed in 4% formalin in seawater. Fish from the Eastern Pacific (Monterey Bay, CA; 2014) were collected by Dr. S. Haddock (Monterey Bay Aquarium Research Institute) using a 2x2 m open-closing tucker trawl with 50 µm mesh (OCTT) and preserved in 4% formalin in seawater.

Specimens were identified to species level using several sources. Harold (2002) was used to identify stomiiforms to family level. Specimens were then identified to genus and species level using other, more specific keys. Stomiids from the Western North Atlantic were identified using keys in *Fishes of the Western North Atlantic* (Bigelow et al., 1964) and were referenced against *fishbase.org* to check for recent name changes. *Fishbase.org* was used to determine geographic ranges of the specimens from the Eastern Pacific. In most cases, species had a circumglobal distribution (so identification using *Fishes of the Western North Atlantic* was sufficient).

Identification of sternoptychids was carried out using keys and species descriptions in Schultz (1961) and Baird (1971). Phylogenetic revisions of Sternoptychidae done after these keys had been published tended to group taxa into a single species (Harold, 1993). Thus, *fishbase.org* and Harold (1993) were used to find the most recently accepted species distinctions.

Gonostomatid taxonomy is not as straightforward as Sternoptychid taxonomy. *Gonostoma* specimens collected in the Western North Atlantic were identified using *Fishes of the Western North Atlantic* (Bigelow et al., 1964). Identification of *Cyclothone* specimens was relatively challenging because a key including all 13 named species was not available. Furthermore, locality and depth data were not available for all specimens used in this study, restricting the use of regional *Cyclothone* identification guides. Thus, data from Mukhacheva (1966), DeWitt (1972), DeWitt and Cailliet (1972), Badcock (1982), Bond and Tighe (1984), Miya and Nemoto (1987), Miya (1994a, b), and Miya and Nishida (1996) were used to form a character matrix (Appendix 1) which was then used to construct a new dichotomous key including ten of the 13 species of *Cyclothone*

(Appendix 2). This is now the most complete dichotomous key of the genus to my knowledge, incorporating 10 of the 13 recognized *Cyclothone* species. However, it is not locality-specific and should be referenced against species distributions when collection locality is known.

Morphological Analysis:

A combination of standard histological protocols was used to describe lateral line canal and neuromast morphology. Specimens were sampled from collections mentioned above focusing on those specimens in good condition. This resulted in a detailed morphological analysis of a relatively small number of specimens in a limited range of species.

Examination of Whole Specimens:

All specimens were first examined and imaged using a dissecting microscope (Nikon SMZ1500 with SPOT RT3 25.2 2 MP color mosaic camera) and SPOT 5.2 imaging software (Diagnostic Instruments, Inc.). Images in multiple planes of focus were combined into a single image using Helicon Focus (Helicon Soft LTD.). Imaging revealed the locations of putative superficial neuromasts (= “white dots”) and the presence/absence of canal pores in the epithelium, indicative of the presence of cranial lateral line canals. The location of putative superficial neuromasts was noted and manually counted using Photoshop (Adobe Systems Incorporated) or ImageJ (nih.gov).

Whole Mount Hematoxylin Staining:

Whole preserved specimens were stained with full strength Meyer's hematoxylin (Sigma MHS16), a nuclear stain that stains superficial neuromasts in shallow water species (personal observation). Meyer's hematoxylin staining was used as a proxy to determine if putative superficial neuromasts (= "white dots") seen in images of preserved specimens were indeed superficial neuromasts. Due to variation in skin pigmentation in *Argyropelecus*, hematoxylin staining was only effective identifying neuromasts on the dorsal surface of the head where skin was less pigmented. Darkly pigmented *Cyclothone* specimens were first bleached in a solution of 3% hydrogen peroxide in 1% potassium hydroxide (1 part 3 % H_2O_2 to 5 parts 1% KOH). Specimens were left in the bleaching solution under a light for 30 – 90 min and then placed in Meyer's hematoxylin for 1 – 45 min (depending on the batch and age of hematoxylin used). Specimens were removed from the hematoxylin when the putative neuromasts had been stained, but before the skin began to stain, allowing for the differentiation of neuromasts from general epithelium. The location of putative neuromasts was noted and they were counted using ImageJ (nih.gov).

Clearing and Staining:

Cranial lateral line canals within dermatocranial bones were examined using specimens enzymatically cleared and stained for bone and cartilage (Pothoff, 1984). In addition, a modified clearing and staining procedure (Song and Parenti, 1995) using Sudan Black B was used to visualize nerve innervation (due to staining of lipids in the myelin sheath) in order to locate innervated superficial neuromasts in the skin.

Histology:

Histological material was used to study canal morphology and to locate and count both canal and superficial neuromasts. Observations indicated that the canals in many of the species examined had what appear to be incompletely developed canals or canal segments. Thus, canal morphology was described using the stages of canal morphogenesis as described by Webb (2014a) and Bird and Webb (2014; Fig. 1.6).

Specimens were decalcified in Cal-Ex (Thermo Fisher Scientific) for 2 hours, dehydrated in ascending concentrations of ethanol and t-butyl alcohol, embedded in Paraplast (Thermo Fisher Scientific), serially sectioned (8µm thickness, transverse sections), and mounted on slides subbed with 10% albumin in 0.9% NaCl. Sections were stained with a modified HBQ stain (Hall, 1986) and coverslipped with Entellan (Electron Microscopy Sciences).

Other specimens (or in some cases portions of specimens) were embedded in glycol methacrylate plastic resin (Technovit 7100, Electron Microscopy Sciences) and sectioned at 5µm (to obtain transverse sections; on a Leica 4M2265 microtome) and every third section was mounted out of dH_2O on clean slides, dried on a slide warmer overnight, stained with 0.5% aqueous cresyl violet (5 min followed by 1 - 2 min tap water rinse), air dried overnight, and coverslipped with Entellan (Electron Microscopy Sciences).

Histological material was imaged on a compound microscope with either an Olympus BH2 Insight 414.2 color mosaic camera or a Zeiss AxioImager A1 Axiocam MRC camera, using SPOT 5.2 imaging software (Diagnostic Instruments, Inc.) or

AxioVision (Zeiss) imaging software, respectively. Neuromast length was determined by counting the number of sections in which neuromast tissue was present. For canal neuromasts, the diameter (width) of the neuromast was measured in the rostro-caudal midpoint of the neuromast using ImageJ (nih.gov) or SPOT 5.2 (Diagnostic Instruments, Inc.). The preopercular canal (and therefore, its canal neuromasts) runs dorso-ventrally so methods used to measure length and diameter were reversed. Observations of superficial neuromasts in whole preserved specimens revealed that they are round, so length (along the rostro-caudal axis) was used to approximate neuromast diameter.

The number and distribution of superficial neuromasts were determined in histological material by digitally superimposing a 14x14 box grid (generated by SPOT 5.2, Diagnostic Instruments, Inc.) on the image on the computer screen. The center of the grid was placed at a stable landmark (i.e. in the center of a large bone or mid-dorsal on the head). The location of each neuromast was noted with reference to the landmark at the center of the grid, to ensure that sections of one neuromasts in sequential sections were identified appropriately, especially when neuromasts were located in very close proximity to each other in certain areas on the specimen.

µCT Imaging:

Micro computed tomographic (µCT) imaging was utilized to visualize the presence/absence and morphology of partially and fully ossified canals as determined by the presence of canal pores or open troughs, which represented incompletely ossified canals (Fig. 1.6). Specimens were imaged at the Museum of Comparative Zoology at Harvard (Bruker SkyScan 1173, pixel size range = 14.9 – 54.7µm). Canal presence or

absence was also confirmed by examining 2-D slices. 3-D µCT data were reconstructed using OsiriX (v3.6.1 64 bit, volume rendering).

Scanning Electron Microscopy:

Scanning Electron Microcopy (SEM) was used to assess superficial neuromast morphology (neuromast shape and size, sensory strip shape, and hair cell orientation). Specimens were dehydrated in an ascending ethanol series at room temperature, critical point dried out of liquid CO_2 (Tousimis Samdri-780A), mounted on aluminum stubs with adhesive carbon discs, and coated with 15 nm platinum (Leica MED 020). Specimens were viewed at 3 KV at a working distance of ~10 mm on a Zeiss NTS Supra 40VP or JEOL 5900 LV SEM to generate digital images.

Results

The morphology of the lateral line canals and canal and superficial neuromasts was examined in 27 species representing 17 genera in four families of stomiiform fishes. Of these, all but one genus (*Cyclothone*) had cranial lateral line canals (Table 1.4). Variation in the subset of canals present and the morphology of canals (Fig. 1.6) was found among families and among genera (for Gonostomatidae and Stomiidae).

Small, densely placed white dots were observed in linear series on the head and trunk in fairly conserved distributions in whole preserved specimens from five genera (*Argyropelecus*, *Cyclothone*, *Gonostoma*, *Idiacanthus*, and *Tactostoma*) representing three families (Sternoptychidae, Gonostomatidae, and Stomiidae). These white dots appeared as circular, domed structures ranging from ~30 – 100 µm in diameter. They

were found around the nares, in vertical lines ventral and caudal to the orbit, along the lower jaw in association with photophores, and in discrete vertical lines on the trunk between major photophores ventrally (except in *Argyropelecus* spp.), extending onto the caudal fin, and on the pectoral and pelvic fins (in *Argyropelecus aculeatus* and *Cyclothone* spp.). Small, brown, circular depressions in the skin on the head and trunk were observed in whole preserved *Gonostoma* and stomiids in the same locations as those described for white dots in other taxa.

The distribution and morphology of cranial lateral line canals and neuromasts are described below for each species examined. Table 1.3 summarizes the methods used to examine specimens. Table 1.4 provides a summary of presence or absence of each lateral line canal and its morphology in each genus based on examination of whole preserved specimens, cleared and stained specimens, nerve staining, histology, μCT imaging, and SEM.

Family Sternoptychidae

The family Sternoptychidae (marine hatchetfishes) is comprised of ten genera in two subfamilies. These fishes are characterized by a deep, compressed body with preopercular and postabdominal spines, a keel-like structure on the abdomen, a spine-like blade rostral to the dorsal fin, and series of photophores on the head and body. Species in the genus *Argyropelecus* are further characterized by having tubular eyes. Four of the seven *Argyropelecus* species (recognized by Nelson et al., 2016) were examined in this study.

Argyropelecus spp.

Whole preserved specimens of four species of *Argyropelecus* (*A. aculeatus*; *A. affinis*; *A. hemigymnus*; *A. lychnus*) were examined. Between 1 and 11 individuals of each species were studied using hematoxylin staining (*A. aculeatus*), histology (*A. aculeatus*; *A. lychnus*), SEM (*A. aculeatus*; *A. lychnus*), clearing and staining (*A. lychnus*), nerve staining (*A. affinis*; *A. hemigymnus*; *A. lychnus*), and µCT imaging (*A. aculeatus*).

The cranial bones in *Argyropelecus* are very thin and some appear to have a honeycomb structure. Cleared and stained specimens of *A. affinis*, *A. hemigymnus*, and *A. lychnus* and µCT imaging of *A. aculeatus* revealed similar features of lateral line canal-bearing bones (i.e. frontal, preopercle, and dentary), but ossified lateral line canals (Fig. 1.7) and infraorbital bones were absent. Ossified canals were also absent in the mandible and preopercle, but troughs were present, which represent incompletely ossified canals (Stage 2b/3 as per Bird & Webb, 2014; Fig 1.7D – E). The most distinctive feature of the cranial skeleton of *Argyropelecus* spp. is the pair of bilaterally symmetrical, longitudinal bony ridges extending dorsally from the frontal bone. Viewed dorsally, each ridge starts rostral to the orbit. As it extends caudally, it moves medially, so that the left and right longitudinal ridges nearly touch medial to the orbits, but never fuse. Caudal to the orbits, the ridges move laterally once again before terminating (Fig.1.7A, C)**.**

Clearing and staining and µCT revealed no ossified canals in *A. aculeatus*, but histological analyses of three individuals revealed largely enclosed, but unossified SO, MD, and PO canals (St. 3; Table 1.4). The SO canal runs in close association with the longitudinal bony ridge of the frontal bone (Fig. 1.8), and forms rostral to the orbit,

medial to the bony ridge. The first SO neuromast is found in a depression in the epithelium over the frontal bone (St. 2a/b; Fig. 6C-D). Moving caudally, soft tissue canal walls enclose the next SO canal neuromast (St. 3; Fig. 6G-H). As the left and right canals extend caudally, they also move medially and merge into a single canal medial to orbits (between the ridges) and two canal neuromasts sit side-by-side within the median canal. Caudal to the orbits, the left and right SO canals move laterally and separate so that the next canal neuromasts sit in left and right paired SO canals. Moving caudally, each canal continues to move laterally, through the bony ridge. The next SO canal neuromast is fully enclosed in an ossified canal (St. 4; Fig. 1.6I-J) for a short distance. When the canal terminates, the next neuromast in the series (interpreted as a canal neuromast homologue, given the similarity in size to the enclosed canal neuromasts) is on the skin surface (St. 1; Fig.1.7A-B**)**.

This histological analysis of *A. aculeatus* also revealed the presence of enclosed, but only partially ossified (St. 3) MD and PO canals. The MD canal is a trough in the lower jaw, which is covered by a thin layer of epithelium (1-2 cell layers thick), and contains two canal neuromasts (Fig.1.9F). The PO canal originates just caudal to the posterior end of the MD canal (Fig. 1.10A) and is enclosed and fully ossified (St. 4) ventrally and the first PO canal neuromast is beneath a preopercular spine. In the portion of the PO canal that runs dorsal-ventrally, the canal is only partially ossified (St. 3), forming a narrow trough that is enclosed by a thin epithelium (Fig. 1.9G). This portion of the canal contains three neuromasts so that a total of four PO canal neuromasts are present. It appears that the MD and PO canals are more easily damaged during collection

than the SO canal because the epithelium and bones of the MD and PO canals were often damaged and their condition was variable within and among specimens.

The canal neuromasts in the SO, PO, and MD canals all appear to be elliptical or diamond-shaped with the major axis parallel to the axis of the canal. The SO and PO canal neuromasts are longer in larger individuals, while the MD canal neuromasts do not appear to demonstrate this same trend (26 – 39 mm SL, n = 3 specimens). PO canal neuromasts are slightly longer (mean = 273 µm, range = 117 – 440 µm, n = 14 neuromasts) than SO canal neuromasts (mean = 260 µm, range = 112 – 645 µm, n = 24 neuromasts) and MD canal neuromasts were the shortest (mean = 219 µm, range = 72 - 320 µm, n = 8 neuromasts) of the neuromasts in these three canals. Canal neuromast width (diameter) followed the same trend, with PO canal neuromasts being the widest (mean = 113 µm, range = 48 – 195 µm, n = 14 neuromasts). The SO and MD canal neuromasts were narrower (SO mean = 105 µm, range = 54 – 233 µm, n = 24 neuromasts; MD mean = 66 µm, range = 44 – 88 µm, n = 8 neuromasts). Within an individual, the size of neuromasts in the SO and PO canals (both length and width) varied a good deal, while size of the MD canal neuromasts appeared to be more consistent.

Careful examination of whole preserved specimens (*A. aculeatus, A. affinis, A. hemigymnus, A. lychnus*) confirmed histological data. Lateral line canals were found in the epithelium medial to the longitudinal bony ridge on the dorsal surface of the head and on the lateral surface of the head where the SO canal ends lateral to the bony ridge. This, in conjunction with the similarity in morphology of the frontal bone between species, shows that SO canal morphology is similar among *Argyropelecus* species. In whole *A. hemigymnus* (n = 5), opaque, white, oval shaped structures (= canal neuromasts) sit in the

troughs (incompletely formed canals; St. 2b/3) in the lower jaw and the preopercle, and are thus interpreted as canal neuromasts. Similar structures were found in whole *A. aculeatus* in the same locations as where canal neuromasts were observed in histological material. The MD and PO canal morphology are therefore similar in *A. aculeatus* and *A. hemigymnus*. However, *A. hemigymnus* specimens examined had two MD canal neuromasts and three PO canal neuromasts (possibly a fourth beneath the preopercular spine), contrary to the one MD and two PO canal neuromasts illustrated by Handrick (1901, Fig. 1.5).

Numerous small white dots were found on the head and body of several *Argyropelecus* species (*A. aculeatus, A. affinis, A. hemigymnus, A. lychnus*) and these were identified as superficial neuromasts in histological material prepared from *A. aculeatus*. The superficial neuromasts had the same overall morphology in all species examined, appearing as small (~50 – 100 µm in diameter), circular, domed structures. Superficial neuromasts were easily seen against darkly pigmented skin, but were much less obvious on lighter colored or transparent epithelium (Fig. 1.11) where what appear to be nerves or blood vessels were seen running to them, suggesting that they are innervated and/or vascularized. In *A. hemigymnus*, larger (approximately twice as large), oval structures were found in predictable locations on all specimens. These are interpreted as canal neuromast homologues based on their similarity to the MD and PO canal neuromasts visible in whole preserved specimens.

In all *Argyropelecus* specimens examined, superficial neuromasts (white dots) were quite numerous. Approximately 420 were found on one side of the head and trunk of an *A. affinis* (49 mm SL; Fig. 1.10B, 12) and ~220 were found in an *A. lychnus* (29

mm SL). A mean of ~74 superficial neuromasts were found on each of several specimens of *A. aculeatus* (26 – 40.5 mm SL; range = ~42 – 131 superficial neuromasts per specimen; n = 11 specimens; Fig. 1.10A) and a mean of ~178 in *A. hemigymnus* (30 – 36.5 mm SL; range = ~46 – 215 superficial neuromasts per specimen; n = 5 specimens; Fig. 1.10C).

Superficial neuromasts were found in similar locations in all *Argyropelecus* species examined (Fig.1.10). They are distributed around the nares, in vertical lines ventral and caudal to the orbit, along the lower jaw, above the orbit and medial to the longitudinal bony ridge of the frontal bone on the dorsal surface of the head. On the trunk, they are found in association with the photophores, and in discrete vertical lines, approximately at the level of each body segment. They were also found extending onto the caudal fin in *A. hemigymnus* and on the pectoral fin in *A. aculeatus.* In all cases, they are densely placed, with 6 – 8 per millimeter in linear series.

In *A. aculeatus*, the superficial neuromasts located on the dorsal side of the head, ventral and caudal to the eye, around photophores, and along the trunk stained positively with hematoxylin, which was correlated with the location of superficial neuromasts found in histological material (Fig. 1.9A – E). In a single specimen (39 mm SL; MCZ 159086) ~248 superficial neuromasts were identified in serial histological sections in just a portion of the head (from snout to operculum extending just dorsal to the preopercular photophore). In all three *A. aculeatus* examined histologically, superficial neuromasts were quite small (between 25 – 45 µm in diameter ± 8 or 15 µm for paraffin and plastic histology, respectively) about one fifth of the size of canal neuromasts. The size of superficial neuromasts did not appear to vary with location or with fish size. Superficial

neuromast width was smaller as measured in histological material than that measured in whole preserved specimens, indicating the effects of shrinkage during histological preparation.

Nerve staining revealed nerves running along the horizontal septum with branches extending vertically (with approximately one nerve branch per body segment) in two *A. lychnus* specimens. The nerve branches begin near the spinal column and move towards the skin surface, and appear to innervate the small superficial neuromasts on the skin, which were in the same location as the superficial neuromasts typically observed in whole preserved specimens. Superficial neuromasts also stained positively with Sudan Black B (a lipid stain). Unfortunately, nerve branches could not be traced to their origin in the central nervous system to confirm their identity. Similar nerve-like structures were visible in several unstained, whole preserved specimens of four species (*A. aculeatus*, *A. affinis*, *A. hemigymnus*, and *A. lychnus*). They followed the same pattern as those in nerve stained specimens and seemed to be closely associated with superficial neuromasts, suggesting that they are innervating these structures.

Given the similarity of the distribution and morphology of superficial neuromasts in *A. aculeatus* to the white dots and nerve-stained structures in other *Argyropelecus* species, it is concluded that all *Argyropelecus* species examined have a proliferation of superficial neuromasts.

The distribution of superficial neuromasts was highly dependent on specimen condition. The epithelium of whole preserved specimens appeared to be easily damaged, and both scales and epithelium were easily flaked off the surface of the fish. Histology revealed that the epithelium in *A. aculeatus* is indeed very thin (1 – 2 cell layers thick;

Fig. 1.9) and SEM revealed that the skin in both *A. aculeatus* and *A. lychnus* was fragile and was apparently completely smooth with no evidence of cellular boundaries or the microridges characteristic of the epithelium of teleost fishes. Although round, domed structures were found medial to the longitudinal bony ridges on the dorsal surface of the head in the same location as superficial neuromasts had been observed prior to specimen preparation, no superficial neuromasts could be detected using SEM. It is possible that there was tissue covering the superficial neuromasts, or that the epithelium in which they were contained was entirely missing, thus removing any traces of superficial neuromasts.

Finally, the variability in specimen condition made it difficult to accurately determine the exact number and distribution of superficial neuromasts in all specimens of a given species. However, a comparison of superficial neuromast distributions in multiple specimens of the same species revealed that as many as ~357 superficial neuromasts are on one side of the head and body of *A. aculeatus* and ~521 superficial neuromasts are on one side of the head and body of *A. hemigymnus* (Table 1.5). This is in stark contrast to the report of only 17 superficial neuromasts and 6 canal neuromasts by Handrick (1901).

Family Gonostomatidae

The fishes in the family Gonostomatidae (the bristlemouths) have elongate bodies and rows of ventral and lateral photophores. Two of the eight gonostomatid genera were examined here: *Cyclothone* and *Gonostoma*. Both are characterized by elongate jaws with numerous, fine teeth. They are similar in morphology, but *Cyclothone* spp. have much smaller eyes and smaller body size than *Gonostoma* spp. (Harold, 2002). Here the morphology of the lateral line system in eight of the thirteen species of *Cyclothone* and in

one of the two species of *Gonostoma* (as recognized by Nelson et al., 2016) are described.

Cyclothone

Examination of 2-4 whole preserved *Cyclothone* specimens in each of three species (*C. acclinidens, C. braueri, C. microdon*), hematoxylin staining of 1 – 4 individuals in each of two species (*C. microdon, C. signata*), histology of two *C. microdon,* SEM of 1 – 2 individuals in each of 4 species (*C. braueri, C. microdon, C. pseudopallida, C. signata*), clearing and staining of 1 – 5 individuals in each of 4 species (*C. acclinidens, C. alba, C. pseudopallida, C. signata*), and µCT imaging of one *C. microdon* revealed that all of the cranial lateral line canals are absent in these fishes (Table 1.4), but that numerous small, white dots are present on the skin. The cranial bones in *Cyclothone* are very thin, and needle-like. Unlike in other stomiiforms, there is no evidence of bony ridges or troughs in the bones that may indicate the presence of partially ossified lateral line canals (Fig. 1.12A, 1.13). Histology (*C. microdon,* 52 – 60 mm SL) confirmed this and showed no evidence of the unossified, soft tissue lateral line canals seen in *Argyropelecus*.

"White dots", the small, domed (~55 – 80 µm in diameter), circular structures found in *Argyropelecus,* were also found covering the head and trunk of well-preserved *Cyclothone* spp. These were more apparent on the darkly pigment skin of deeper dwelling *Cyclothone* species (i.e. *C. acclinidens* and *C. microdon*), but could still be visualized in lighter colored, more transparent specimens (i.e. *C. braueri, C. pseudopallida*, C. *signata*. Furthermore, the white dots stained positively with hematoxylin, appearing darker than

the surrounding epithelium (Fig. 1.14A, D; 15A). In whole preserved specimens, and in hematoxylin stained specimens, these structures appeared to be innervated by nerves.

Histological analysis of two *C. microdon* and SEM of 1 – 2 individuals from each of 2 species (*C. braueri*, *C. microdon*) revealed superficial neuromasts in the same locations as the white dots in whole preserved specimens. These appeared smaller than those in *Argyropelecus* and had a mean diameter of only ~53 µm (range = 8 – 128 µm, with the majority being 45 – 75 µm; n = 85 superficial neuromasts; Fig. 1.14B – C, E - F). SEM revealed hair cells (with axis of best physiological sensitivity parallel to the axis of the sensory strip of the neuromast) in superficial neuromasts with an equilateral diamond shape (Fig. 1.16 G – I).

These superficial neuromasts were numerous and were found on the head and body of *C. microdon* (mean = 268 superficial neuromasts, range = 164 – 385, n = 4 specimens). They had similar distributions in all *Cyclothone* species examined and were found in clusters along the head, in rows along the upper and lower jaw, near the nares, in a row along the 3rd fin rays of both the pectoral and pelvic fins, in vertical lines on the trunk, in horizontal rows running between vertical lines (one more dorsally and another row near the horizontal septum), in lines ventrally running vertically between the ventral photophores, and extending onto the caudal fin rays (Fig. 1.15B). Cursory observations of at least 10 specimens of each of 4 other species (*C. acclinidens, C. braueri*, *C. microndon, C. signata*) revealed superficial neuromasts in these same locations.

Interestingly, SEM did not reveal neuromasts in *C. microdon* specimens that had obvious superficial neuromasts that had stained positively with hematoxylin prior to preparation for SEM. Instead, SEM revealed concave, circular depressions in the skin,

which were sometimes filled with debris with no signs of hair cells. These depressions were numerous and prominent against the otherwise smooth skin, and were found in the same pattern as the superficial neuromasts observed in the whole specimen prior to being prepared for SEM. This suggested that the superficial neuromasts were damaged during specimen preparation, leaving behind only the depressions in the skin seen using SEM.

C. acclinidens stained for nerves revealed vertical nerve branches on the trunk, with approximately one branch per body segment. They started near the spinal column and moved towards the skin surface. In whole preserved *Cyclothone*, opaque, white, branching filaments were visible against darkly pigment skin or through lighter, transparent skin and followed the same pattern as the nerves identified in the nerve stained *C. acclinidens* (Fig. 1.15C). They appear at or near the horizontal septum with branches extending both dorsally and ventrally. The ventral branches diverge around the lateral photophores and then around the ventral photophores, forming a pentagon mid-ventrally. A similar pattern is found where the dorsal branches extend dorsally from the horizontal septum. Dorsally, the branch diverges, connecting with another horizontal segment, which is visible laterally at the dorsal portion of the trunk. In whole preserved specimens, superficial neuromasts are found in discrete lines either directly aligned or in close association with these putative nerves (Fig. 1.15C).

Cyclothone specimens were very fragile and the description of superficial neuromast morphology (using SEM) and distribution (using observations of whole preserved specimens, histology, and hematoxylin staining), was dependent on specimen condition. The epithelium is very thin (1 – 2 cell layers thick; Fig. 1.14) and easily damaged during collection and handling. Using SEM the skin appeared smooth with

neither cellular boundaries nor microridges, and only a few superficial neuromasts could be located that were in good enough condition to allow determination of hair cell orientation. A more complete picture of neuromast distribution was determined using several *C. microdon* individuals (Fig. 1.15B) revealing ~500 superficial neuromasts on one lateral side of the body with ~6 superficial neuromasts between each of the ventral photophores (those between the pectoral and pelvic fins), for a total of ~66 superficial neuromasts ventrally. Thus, it is estimated that there may be a total of over 1066 neuromasts on both sides of the head and body of a single fish.

Gonostoma elongatum

Examination of whole preserved *Gonostoma elongatum* specimens and µCT images revealed the presence of partially ossified cranial lateral line canals and numerous, small, white dots (= putative superficial neuromasts) covering the head and body.

The cranial bones appear thin and needle-like, and the only bony canal pores were found in the supracleithrum (Fig. 1.16). Bilaterally symmetrical, longitudinal bony ridges extend dorsally from the frontal bones. Rostral to the orbit, each ridge is separated into two ridges, which then merge into a single ridge at the level of the anterior edge of the orbit (Fig. 1.16C; 17B). A trough in the preopercle is interpreted as a partially ossified PO canal (St. 3; Fig. 1.16B). In addition, lateral line canal pores in the epithelium in whole preserved specimens, indicate the presence of SO, PO, IO canals as well as what appear to be OT, PT, and ST canals continuing caudally from the SO canal (Table 4; Fig. 1.17). The SO has seven canal pores and starts rostral to the orbit with the rostral-most canal pore at the level of the anterior naris. The next canal pore sits at the level of the

posterior naris, medial to the longitudinal ridges in the frontal bone. The third SO pore also sits medial to the longitudinal ridges. A single pore is present medial to the single, fused longitudinal bony ridge (at the level of the orbit). Caudal to the orbit, three more canal pores are found lateral to the longitudinal ridge. Two groups of pores were seen indicate the presence of canals at the posterior margin of the skull (OT, PT, and ST canals). Three pores indicate the presence of a PO canal, which is partially ossified (St. 3) as indicated by the presence of a bony trough in 3-D µCT reconstructions. Three canal pores are found ventral to the orbit, suggesting the presence of an IO canal (rostral to the preorbital photophore, ventral to the orbit at the level of the lens, and caudal to the orbit, level with the vertical midline of the eye). No canal pores are visible along the lower jaw, suggesting the absence of a MD canal in the dentary or angular-articular bones.

White dots, similar to those identified as superficial neuromasts in *Argyropelecus* and *Cyclothone*, are found on the head and body of *Gonostoma elongatum* (Fig.1.18). They are domed, circular structures that stand out against the darkly pigment skin, are visible under low magnification on a dissecting microscope, and appear to be innervated. They are smaller than those in *Argyropelecus* and *Cyclothone* (~30 – 40 µm in diameter), but have a similar distribution and are found around the nares, on the opercular region, in rows along the upper and lower jaws, and in vertical lines caudal to the orbit (Fig. 1.17B). On the trunk, they are found in vertical lines that run around the circumference of the body, with approximately one vertical line per body segment (defined by the myomeres; Fig. 1.18D) located in between the major lateral and ventral photophores, as in *Cyclothone* spp. (Fig. 1.18C). These are interpreted as superficial neuromasts. They were not visible in specimens clearly damaged during collection. Instead, lines of concave,

circular, depressions were found in locations where superficial neuromasts would be expected, and occasionally, lines of superficial neuromasts were interspersed between the depressions.

As in *Argyropelecus* and *Cyclothone*, an assessment of the distribution of the superficial neuromasts was dependent on specimen condition. In the best-preserved *Gonostoma elongatum* specimen examined (50 mm SL), approximately 499 superficial neuromasts (white dots) were found on the left side of the head, 366 were found on the left side of the trunk, and 144 white dots were found ventrally on the trunk. There appear to be approximately 72 superficial neuromasts (in vertical lines) per body segment circling the trunk, in body segments between the pectoral fin to the pelvic fin (in ~11 body segments). Fewer are found per body segment caudal to the pelvic fins, as the body tapers towards the caudal fin. Approximately 30 superficial neuromasts per body segment are found in the next 15 body segments (from the pelvic fin to midway through the anal fin), but it was difficult to determine numbers of superficial neuromasts per segment for the remainder of the ~12 body segments. Thus, there could be more than 612 superficial neuromasts on one side in *Gonostoma elongatum*.

Family Phosichthyidae

Species in the seven phosichthyid genera are elongate with lateral and ventral series of photophores with a body form similar to that of the gonostomatids (Nelson et al., 2016).

Ichthyococcus ovatus

The cranial osteology of *Ichthyococcus ovatus* was observed using µCT reconstructions only, which revealed both fully and partially ossified cranial lateral line canals (Table 1.4). *Ichthyococcus* has broad, flat bones (opposed to the needle-like bones in *Cyclothone* and *Gonostoma*), but they are still thin and are difficult to differentiate from soft tissue in µCT. An obvious longitudinal bony ridge extends dorsally from the frontal bone as in *Argyropelecus* (Fig. 1.7C; 1.12A). Canal pores are not present in the frontal bone, but a longitudinal bony ridge suggests the presence of an enclosed, but partially ossified SO canal (likely St. 3); but this was not revealed in µCT images. A weakly ossified, but enclosed MD canal (St. 4) appears to be present. The PO canal is ossified along its rostro-caudal length (St. 4) with a single, prominent pore towards the base of the preopercle, but as it turns to run dorso-ventrally, the canal appears as an open trough (St. 2 or 3; µCT 3D volume rendering) or as a weakly ossified, but fully enclosed canal (St. 4; µCT cross-section).

Family Stomiidae

The barbeled dragonfishes of the family Stomiidae are diverse, with approximately 286 species in 27 genera (Nelson et. al., 2016). Most have an elongate body, a mental barbel, and ventral and lateral photophore series in addition to numerous minute photophores on the head and body. Lateral line morphology is described here in representatives of 14 genera based on examination of whole preserved specimens, histology, and/or µCT imaging.

Aristostomias tittmani

The cranial osteology of *Aristostomias tittmani* was observed in µCT reconstructions only, revealing SO, MD, and PO canals (Table 1.4; Fig. 1.19). An obvious, and mostly ossified SO canal is present and a longitudinal bony ridge, with which the SO canal appears to be associated, extends dorsally from the frontal bone (Fig. 1.12C, 1.19A – B). The rostral portion of the SO canal is represented by a trough in the nasal bone (St.3), but the SO canal in the frontal bone is well ossified (St. 4) and is located medial to the longitudinal bony ridge (Fig. 1.19 B). Caudal to the orbits, the SO canal moves laterally through the bony ridge (so that a canal pore sits lateral to the ridge). The canal appears to be rather narrow, yet the canal pores in the bone are relatively large. In the lower jaw, canal pores were found in the rostral portion of the dentary bone (St. 4), but the canal is in the form of an open trough in the caudal portion of the dentary bone (St. 2b/3; Fig.1. 19C). The preopercle houses a hollow tube with pores at either end, interpreted as a fully ossified PO canal (St. 4; Fig. 1.19B).

Astronesthes spp.

Examination of whole preserved specimens (*Astronesthes niger*), µCT reconstructions (*A. gemmifer*), and histology (*A. niger*) revealed the presence of SO, PO, MD, and IO canals, a canals extending caudally from the SO canal (likely OT, PT, and ST canals; Table 1.4), and a proliferation of superficial neuromasts.

Astronesthes spp. have two sets of longitudinal ridges extending dorsally from the frontal bone on the dorsal surface of the head (Fig. 1.12E). In contrast to *Gonostoma elongatum* (Gonostomatidae), *Echiostoma barbatum* (Stomiidae) and *Eustomias hulleyi*

(Stomiidae), both ridges extend caudal to the orbit and never fuse into a single longitudinal ridge. The SO canal, which runs in close association with these ridges, has seven pores and begins rostrally with pores at the level of the anterior and posterior nares. The next pore sits just rostral and medial to where the inner longitudinal ridge starts. The third SO pore sits medial to the orbits and is the only SO pore that is medial to the inner longitudinal ridge. Caudal to the orbit three more pores sit lateral to the outer longitudinal ridge, indicating that the SO canal moves through the outer longitudinal ridge (from medial to lateral). The SO canal appears to be enclosed and fully ossified (St. 4) as the majority of the lateral line pores are resolved in µCT reconstructions. Interestingly, the SO canal pores medial to the inner longitudinal ridge (the third pore in the SO series) was not resolved in µCT reconstructions, suggesting that the anterior portion of the SO canal is enclosed and either incompletely ossified (St. 3) or weakly ossified (St. 4). Histology confirmed that the SO canal neuromasts lateral to the outer longitudinal bony ridge is enclosed and ossified (St. 4, Fig.1. 21F, H), but histology was not available for the rest of the SO canal. The mean diameter of the SO canal neuromasts was 101 µm (range = 78 – 128 µm, n = 3 neuromasts) but they vary in both length and width within the canal.

In whole preserved specimens nine canal pores were visible in the skin at posterior margin of the skull. They appear to be in three different series (the first with three pores in a longitudinal row visible laterally, the next with three pores forming a triangle, and the posterior most series with three pores running in a vertical line, caudal to the operculum) indicating one (or more) canals caudal to the SO canal. In whole specimens, these canals appear to be enclosed and fully ossified (St. 4) and some of the pores could be resolved in µCT reconstructions, indicating that at least portions of these

canals are fully ossified. Nine canal pores are visible in the epithelium over the lower jaw of whole preserved specimens, indicating the presence of an MD canal. Most, but not all, of these canal pores were visible in µCT reconstructions suggesting that the MD canal is mostly well ossified (St. 4), but may be enclosed and incompletely ossified (St. 3), or enclosed and weakly ossified more caudally (St. 4). The MD canal appears to be contiguous with the horizontal arm of the PO canal. Three pores are visible on the ventral portion of the preopercle and µCT reveals that the PO canal is fully ossified (St. 4) in µCT reconstructions. A single pore is found rostral and ventral to the orbit in whole preserved specimens, indicating the presence of an IO canal. Histology revealed that the IO canal is enclosed but incompletely ossified (St. 3; Fig. 1.20E), and contains a neuromast of ~80 µm wide (n = 1 neuromast). The IO canal was not resolved in µCT reconstructions, however, indicating that the infraorbital bone is thin and does not easily differentiate from soft tissue. All canals appeared to be narrow and bony lateral line canal pores (in µCT images) were large while epithelial pores (in whole preserved specimens) were smaller.

Numerous superficial neuromasts were visible in histological material (Fig. 1.20A – D, G). These were smaller than canal neuromasts and densely placed, with multiple superficial neuromasts (morphologically distinct from photophores) sitting side by side in a vertical line (Fig. 1.22A, C). Caudal to the orbit, as many as 13 superficial neuromasts were found in a vertical line in a single histological section. The analysis of sequential histological sections suggests that they are found in discrete vertical lines. A layer of pigment is found below the neuromasts and the basement membrane and pigment appear as depressions in the epithelium below the superficial neuromast. In whole preserved

specimens, white dots were not seen on the skin (in contrast to *Argyropelecus* spp., *Cyclothone* spp., and *Gonostoma elongatum*), but brown depressions in the skin were present (like those described in *G. elongatum*) in the same locations as superficial neuromasts seen in histological material. These were found in discrete vertical lines on the head as well as on the trunk. They had a distribution like that in *G. elongatum* (Gonostomatidae), with one line running around the circumference of the trunk in each body segment. Thus, brown depressions are interpreted as superficial neuromasts that were damaged in handling or otherwise removed.

Bathophilus filifer

Canal and neuromast morphology was described in one preserved *Bathophilus filifer* specimen that was subsequently used for SEM and histological analyses. Canal pores were visible in the skin, indicating the presence of SO, PO, MD canals and a canal in the posterior portion of the head (likely the OT canal; Table 1.4). These canals are fully enclosed and either partially (St. 3) or fully ossified (St. 4). Five SO pores are found on the dorsal surface of the head. The SO canal starts rostral to the orbit, and medial to the nares. In contrast to other taxa, a longitudinal bony ridge was not found extending from the frontal bone (Fig. 1.12B). Two SO pores are found in close proximity, at the level of the anterior and posterior nares. Three more SO pores are found dorsal and caudal to the orbit. An additional two pores are visible laterally (slightly ventral to the SO pores), indicating the presence of a canal(s) caudal to the SO canal (likely the OT canal). Three pores are visible along the opercular flap (one dorsally, one ventrally, and one midway along the operculum), indicating the presence of a PO canal. Five pores are

found ventrally along the lower jaw (three located rostrally, one approximately midway along the length of the lower jaw, and the fifth at the posterior end of the jaw) indicating the presence of a MD canal. No pores were found ventral to the orbit that would have suggested the presence of an IO canal.

Small, circular, brown depressions in the epithelium are found on the head and trunk, running in vertical lines around the circumference of the trunk (Fig. 1.21B). These appear similar to those seen in other species (e.g. *Gonostoma elongatum*, Gonostomatidae and other stomiids). Histology revealed no distinguishing characteristics of these structures and SEM revealed that the skin is very thin and smooth, without microridges and cellular boundaries, observed in other fish taxa. The brown depressions could be clearly distinguished from photophores**,** which are convex and rise above the surrounding epithelium (Fig. 1.21C). The majority of the depressions were covered by debris (Fig.1. 21C – D), but others were entirely clear of surface details with no identifying characteristics (Fig. 1.21E). Thus, it appears that the brown depressions are not superficial neuromasts, but likely represent the locations of superficial neuromasts that were damaged and removed during handling.

Echiostoma barbatum

Examination of a single whole preserved *Echiostoma barbatum* specimen and 3-D μCT reconstructions of three specimens revealed lateral line canal pores in the epithelium and bones, respectively (Table 1.4). The cranial bones appear thin and a longitudinal bony ridge extends dorsally from the frontal bones. Rostral to the orbit, the ridge is separated into two ridges (inner and outer), which then merge into a single ridge at the

level of the orbit (as in *Gonostoma elongatum*, Fig. 1.12D). The SO canal is associated with the longitudinal bony ridge (Fig.1. 22A), and has seven pores. The SO canal begins rostral to the orbit with the rostral-most pores at the level of the nares and rostral to the start of the longitudinal bony ridges. Another pore sits medial to the two bony ridges, rostral to the orbit. These rostral-most pores were not visible in µCT reconstructions (Fig. 1.22A) suggesting that this portion of the canal is in the form of a trough in the frontal bone (St. 3). Medial to the orbits, a single pore is found medial to the fused longitudinal bony ridge. Caudal to this pore, three additional pores are found lateral to the bony ridge. All four of these pores were resolved in µCT reconstructions, indicating that this portion of the SO canal is enclosed and fully ossified (St. 4). A trough is found caudal to the SO canal and there appear to be groups of pores indicating the presence of canals caudal to the SO canal (likely OT, PT, and ST canals; St. 3). The first series of pores is comprised of two pores running in a rostro-caudal series (OT). Caudally, a second group of four pores runs rostro-caudally with one of the four pores sitting dorsal to the middle pore in the series, forming an upside down t-shaped group of pores (ST and PT canals). The MD canal has six epithelial canal pores. Five sit in the more rostral portion of the dentary bone where the canal is fully enclosed and ossified (St. 4; Fig. 1.22B). More caudally a trough in the dentary and an elongate epithelial canal pore suggests the continuation of the MD canal as an incompletely ossified, but enclosed canal (St. 3). The PO canal has three pores and appears to be fully ossified ventrally (St. 4; Fig. 1.22C), but the PO canal is in the form of a trough in the dorsal portion of the preopercle, suggesting an incompletely ossified, but fully enclosed canal (St. 3; Fig. 1.24).

Eustomias hulleyi

One whole preserved specimen of *Eustomias hulleyi* was available for study. Small canal pores in the epithelium indicate the presence of several cranial lateral line canals (Table 1.4). A longitudinal bony ridge extends dorsally from the frontal bone. Rostral to the orbit, this ridge is separated into two ridges (inner and outer), which merge into a single ridge at the level of the orbit (as in *Gonostoma elongatum and Echiostoma* barbatum; Fig. 1.12D). The rostral-most pore of the SO canal is rostral to the orbit and medial to the ridges, at the level of the posterior naris. The next three pores are evenly spaced, medial to the fused longitudinal ridge and dorsal to the orbit. Caudal to the orbit, the most posterior SO pore sits lateral to the longitudinal ridge, suggesting that, the SO canal moves laterally through the ridge (from medial to lateral, as in *Argyropelecus* and other stomiids). A pore sits caudal to the SO canal, and is visible laterally, suggesting an additional canal(s) at the posterior margin of the skull (likely only an OT canal). Three small canal pores are visible in the epithelium on the lower jaw, indicating the presence of an MD canal in the dentary bone. Two canal pores are found in the epithelium in the opercular region (one ventrally towards the base of the operculum and the other towards the dorsal edge of the operculum) indicating the presence of a PO canal. All of the canals appear to be narrow and are enclosed by soft tissue (St. 3) or are fully ossified (St. 4).

Flagellostomias boureei

One whole preserved specimen of *Flagellostomias boureei* was available for study. Canal pores in the epithelium indicate the presence of several lateral line canals that appear to be narrow (Table 1.4). A bony longitudinal ridge extends dorsal from the

surface of the frontal bone. The pores of the SO canal, found medial to the ridge, suggest an association between the longitudinal ridge and the SO canal. Two pores caudal to the end of the SO canal are visible on the lateral side of the head, suggesting the presence of a canal extending caudally from the SO canal (likely the OT canal). Three pores are visible along the rostral portion of the lower jaw, indicating the presence of a MD canal in the dentary bone. Caudal to the posterior end of the MD canal, a PO canal with three pores is found in the opercular region and a single pore is found near the dorsal portion of the opercular flap. Two canal pores are in the epithelium rostral and ventral to the orbit, suggesting the presence of an IO canal. All canals are fully enclosed and likely partially (St. 3) or fully ossified (St. 4).

Idiacanthus antrostomus

Examination of two whole preserved specimens revealed the presence of lateral line canals (Table 1.4) and numerous small, domed white dots (= superficial neuromasts) on the head and trunk (Fig. 1.23**)**. The presence of small canal pores in the skin suggests the presence of canals that are either enclosed and partially (St. 3) or fully enclosed and ossified (St.4).

The SO canal runs in close association with a longitudinal bony ridge extending dorsally from the frontal bone (Fig. 1.12C). The SO canal appears to start rostral to the orbit, about at the level of the posterior naris. Three SO pores are found medial to the ridge in the frontal bone, and medial to the orbit, the canal moves laterally through the bony ridge, so that the next three SO canal pores sit lateral to the bony ridge. Caudal to the end of the SO canal, two smaller epithelial pores appear to be associated with a canal

at the posterior portion of the head (likely the OT canal). Two pores sit ventral to the orbit, indicating the presence of an IO canal. Four MD pores were found on the rostral portion of the lower jaw, indicating the presence of a MD canal in dentary. Pores were not visible in the opercular region, suggesting that a PO canal is not present.

White dots were visible over the head and trunk of a single well-preserved specimen and are interpreted as superficial neuromasts. They are numerous, small (30 – 40 µm in diameter), appear as white, domed, circular structures that stand out against darkly pigment skin, and are found in similar locations to those seen in other taxa in other families (i.e. around the nares, along the upper jaw, in vertical lines on the head caudal to the orbit and in vertical lines running around the circumference of the trunk, approximately one line per body segment). Occasionally, in areas where the epithelium appears to be abraded, brown depressions (as in *Bathophilus* and *Gonostoma*) were found where white dots were expected to be based on their distribution in other trunk segments. On one side of the body, ~32 white dots were found in a single vertical line (in body segments between the pectoral fin and the pelvic fin). As the body tapers towards the caudal fin, fewer white dots are in each body segment. Additionally, ~250 white dots were counted on the head (72 dorsally, both sides, and 178 laterally, on one side). Given these counts, it is likely that there are ~2,000 superficial neuromasts on one side of the head and body.

Malacosteus sp.

Two specimens of *Malacosteus* sp. were used to generate µCT reconstructions and revealed the presence of partially (St. 2b or 3) and fully (St. 4) ossified lateral line

canals (Table 1.4). The cranial bones are very thin and could not be easily differentiated from the surrounding soft tissue (3-D volume rendering; Fig. 1.24). A SO canal with two bony pores is located rostral to the orbit and appears to terminate caudal to the orbits (Fig. 1.24A). A trough is found in the rostral portion of the dentary bone, which is interpreted as a partially ossified MD canal (St. 2b or 3, Fig. 1.24B). A trough is also present in the preopercle, which is interpreted as a partially ossified PO canal (St. 2b or 3; Fig.1. 24A).

Neonesthes spp.

Two specimens of *Neonesthes* spp. were used to generate µCT reconstructions which revealed obvious, fully ossified cranial canals (St.4; Table 1.4; Fig. 1.25). A SO canal, with four canal pores, begins rostral to the orbit (Fig. 1.25A). The rostral portion of the MD canal is well ossified and has five or six bony canal pores (Fig. 1.25C). More caudally, the canal is represented by a trough, indicating that the more caudal portion of the MD canal is not fully ossified (St. 2b or 3). The PO canal has three or four pores with two or three located ventrally on the preopercle and one or two pores located more dorsally and is interpreted as being fully enclosed and ossified (St. 4; Fig. 1.25B). Pores in the bone caudal to the SO canal, suggest that a partially ossified canal extends in the posterior portion of the head (St. 2b or 3). All of the canals appear to be narrow, but have large bony canal pores, similar to those in *Aristostomias*.

Opostomias micripnus

Examination of one whole preserved *Opostomias micripnus* revealed the presence of canal pores in the epithelium (Table 1.4). As in *Astronesthes,* two longitudinal bony ridges (inner and outer) extend dorsally from the frontal bone and both extend caudal to the orbit but never fuse (Fig. 1.12E). The SO canal is closely associated with these two ridges, and the three most anterior SO pores sit medial to the two ridges. The fourth SO canal pore is medial to both bony ridges and more caudally, another three pores are found medial to the two ridges. The canal then appears to move through the bony ridges so that the next two pores sit lateral to the outer longitudinal bony ridge. Caudal to the end of the SO canal, three canal pores indicate the presence of canals caudal to the SO canal (likely OT, PT, and ST canals). Seven canal pores are found in the skin of the lower jaw (covering the dentary bone) indicating the presence of a MD canal. Three epithelial pores visible ventrally on the opercular region indicate the presence of a PO canal. Three pores were found in the epithelium ventral to the orbit, suggesting the presence of an IO canal. All canals are enclosed, and either partially (St. 3) or fully ossified (St. 4) and appear to be narrow based on the small size of canal pores in the skin.

Pachystomias spp.

Three specimens of *Pachystomias* spp. were used to generate µCT reconstructions, which revealed well-developed canals with obvious canal pores (Table 1.4). A longitudinal bony ridge extends dorsally along the length of the frontal bone (Fig. 1.12C), with which the SO canal is closely associated. The SO canal starts rostral to the orbit and is located medial to the bony ridge. Medial to the orbit, a trough in the frontal

bone indicates that the rostral portion of the SO canal is not completely ossified (St. 2b or 3). Caudal to the orbit, the SO canal is fully ossified (St. 4; Fig. 1.26A) with two bony pores (one on each end of the bony tube of this segment). In contrast to other stomiids, the SO canal remains medial to the bony ridge along its entire length (it does not move lateral to the ridge). A trough indicates the presence of an incompletely ossified MD canal in the dentary bone (St. 2b or 3; Fig. 1.26C). The PO canal has two pores and appears well-ossified, but the canal is incompletely ossified dorsally and is represented by a trough (St. 2b or 3). Dorsal to the PO canal and caudal to the termination of the SO canal, an ossified canal with two pores is visible indicating the presence of a canal caudal to the SO canal (Fig. 1.26A – B). All of the canals in *Pachystomias* appear to be narrow with small pores.

Rhadinesthes decimus

A single *Rhadinesthes decimus* specimen was used to generate μCT reconstruction, which revealed several cranial canals. Bones were very thin and did not resolve well in 3-D volume rendering; nevertheless 2-D cross-sections indicate there are several cranial canals (Table 1.4). The SO canal originates rostral to the orbit, has four pores, and terminates caudal to the orbit. A fully ossified MD canal (St. 4) is present, but the number of pores is unclear. The PO canal is fully enclosed and ossified (St. 4) ventrally, but dorsally, a trough in the preopercle suggests that the canal is only partially ossified (St. 2b or 3).

Tactostoma macropus

One whole preserved *Tactostoma macropus* was examined, revealing the presence of several cranial canals (Table 1.4) and numerous small, white dots (= superficial neuromasts) on the head and trunk. A longitudinal bony ridge extends dorsally from the frontal bone along the length of the bone with which the SO canal is associated (Fig. 1.12C). The SO canal originates rostral to the anterior naris and medial to the bony ridge. More caudally a SO pore is found medial to the posterior naris and two more pores are found dorsal to the orbit and medial to the bony ridge. The SO canal appears to move through the bony ridge so that three pores caudal to the orbit sit lateral to the bony ridge. The SO canal appears to be completely ossified. Caudal to the last SO canal pore, two smaller pores sit slightly ventral to the SO canal, indicating the presence of a canal caudal to the SO canal (likely the OT canal), which appears to be partially ossified (St. 3). A very high number of MD pores (ten) are quite obvious in the lower jaw. They extend half way down its length, indicating that an enclosed and fully ossified canal (St. 4) is present rostral. More caudally the canal is represented by a trough indicating a partially ossified (but unenclosed) portion of the MD canal (St. 2a). Four pores in the opercular region indicate the presence of the PO canal, with three located ventrally and the fourth located more dorsally. It appears that the PO canal is fully ossified (St. 4) and the ventral portion of the canal continues dorsally as either an ossified (St. 4), or partially ossified canal (St. 3). Two pores sit rostral and ventral to both the orbit and the prominent preorbital luminescent organs, indicating the presence of an IO canal, which is enclosed and either partially (St. 3) or fully ossified (St. 4).

White dots are visible on the head and body and have a similar appearance and distribution to the superficial neuromasts in *Idiacanthus antrostomus* (Stomiidae), *Gonostoma elongatum* (Gonostomatidae), *Argyropelecus* (Steronoptychidae), and *Cyclothone* (Gonostomatidae). They are small (30 – 40 μm in diameter, similar in size to those in *Gonostoma* and *Idiacanthus*), densely placed, and are seen predominantly around the nares, and in vertical lines on the lateral surfaces of the head. On the trunk, superficial neuromasts are found in vertical lines around the circumference of the trunk, with one line per body segment that run between the major photophores (as in *Cyclothone*, *Gonostoma*, and *Idiacanthus*). A longitudinal row of superficial neuromasts (~ 1 – 3 per body segment) was also found mid-way between the lateral and ventral photophore series. The vertical lines each contain approximately 12-20 superficial neuromasts (smaller numbers are found caudally as the body tapers towards the caudal fin). In addition to these superficial neuromasts on the lateral surface of the body, there are 3 – 5 superficial neuromasts in this line found ventrally (counted from the ventral photophore to mid-ventral) and approximately 4 or 5 dorsally. A total of 1840 superficial neuromasts were counted in the vertical lines along the length of a single side of the specimen, excluding those in horizontal series along the trunk. An additional 446 were counted on the head. Combining these values, there appear to be a total of over 2286 superficial neuromasts (white dots) on one side of the fish.

Discussion

The morphology of the lateral line system was described in 17 genera of stomiiform fishes representing four different families using a combination of methods

(histology, clearing and staining, nerve staining, hematoxylin staining, SEM, and μCT imaging). This is the first description of the lateral line system in seven of those genera, (*Astronesthes, Cyclothone, Gonostoma, Ichthyococcus, Idiacanthus, Opostomias,* and *Neonesthes*). Prior to this study, our understanding of the mechanosensory lateral line system in stomiiform fishes was limited to incidental comments by Marshall (1954; 1979), references or illustrations alluding to the presence of cranial canals based on the presence of pores in cranial bones in several stomiiform taxa (Fink, 1985; Weitzman, 1967; 1974), and a single detailed description of the innervation of the lateral line system in *Argyropelecus hemigymnus* (Handrick, 1901). Here, the use of multiple methods has revealed that the lateral line system is more elaborate than suggested by reports in the literature, consisting of ossified or partially ossified canals and a proliferation of superficial neuromasts.

All but one stomiiform genus (*Cyclothone*) had at least some cranial lateral line canals, which appeared to be narrow (as opposed to widened). The majority of species examined had some, but not all of the cranial canals found in other bony fishes. Only fishes in four genera (*Astronesthes*, *Flagellostomias, Opostomias*, and *Tactostoma*) had SO, MD, PO, and IO canals as well as the canals caudal to the SO canal (OT, ST, and/or PT canals). The IO canal was most frequently absent among genera examined, which could be due to the absence of the infraorbital bones or due to a failure to resolve these bones in μCT images. However, in *Bathophilus, Echiostoma,* and *Eustomias,* the IO canal was clearly absent in whole preserved specimens based on the absence of canal pores in the skin. Partially ossified canals were present in multiple genera.

μCT imaging is a non-destructive method that allowed for the easy determination of the degree of canal ossification as defined by the developmental stage(s) of the canal (defined for shallow water fishes, as per Bird and Webb, 2014, see Fig. 1.6). However, the results obtained using this method should be interpreted with caution to account for decalcification during fixation or storage, or for the possible difficulty in separating low density bones from soft tissue in 3-D reconstructions.

The utilization of other methods in addition to μCT imaging can allow for a more accurate description of the lateral line system. In this study, the interpretation of data from histology, μCT imagining, and examination of whole specimens analyzed in combination-confirmed that the troughs visible in canal-bearing bones (in μCT reconstructions) are partially ossified cranial canals (St. 2b or 3). In the nine genera in which the presence of cranial canals had already been known (based on published osteological descriptions, Table 1.1), this work revealed the presence of additional, fully or partially ossified cranial canals, highlighting the importance of using multiple morphological methods to generate a full and accurate description of lateral line morphology.

The discovery of very large numbers of superficial neuromasts counters the hypothesis based on Handrick (1901) who reported that one species of *Argyropelecus* has a very small number of superficial neuromasts (Table 1.5). First, examination of whole preserved specimens revealed the presence of small, domed, white dots on the head and trunk of several species. These structures had a similar morphology and distribution in all species examined. In detailed analyses of *Argyropelecus aculeatus* and *Cyclothone microdon,* these were determined to be superficial neuromasts. Given the similarity in

their appearance and distribution in all species examined, it is concluded that they are superficial neuromasts.

The superficial neuromasts on the head were densely placed and distributed around the nares, in vertical lines ventral and caudal to the orbit, along the lower jaw, and on the dorsal surface of the head. On the trunk, they were found in association with the photophores, and in discrete vertical lines, approximately at the level of each body segment running around the circumference of the trunk. In some species, additional superficial neuromasts were found in horizontal rows at or dorsal to the horizontal septum. Additionally, they were found extending onto the pectoral and pelvic fins in *Argyropelecus* and *Cyclothone*, a location where superficial neuromasts have not been reported for bony fishes. Little variation in superficial neuromast distribution was seen among species within a genus (*Cyclothone* and *Argyropelecus*) or among genera within a family (Gonostomatidae and Stomiidae). However, examination of additional high quality specimens may reveal species-specific variations in lateral line morphology.

It is important to note that these specimens were fairly small compared to maximum body lengths reported for each species (i.e. *Gonostoma elongatum* max length = 275 mm SL, *Idiacanthus antrostomus* max length = 330 mm SL, *Tactostoma macropus* max length = 343 mm SL; fishbase.org) and it is unknown if the number of superficial neuromasts in each vertical line increases with specimen size (e.g., as trunk diameter increases). This study found that all stomiiform species examined had more than 200 superficial neuromasts on one side of the body. In two well, preserved stomiid specimens (*Idiacanthus antrostomus* and *Tactostoma macropus*), over 2,000 superficial neuromasts were observed on one side of the head and body.

The estimated numbers of superficial neuromasts provided here are conservative, but indicate that these fishes have superficial neuromast numbers comparable to those found in shallow water species described as having a proliferation of superficial neuromasts. For instance, similarly sized gobies (family Gobiidae), known for superficial neuromast proliferation on the head and body (Asaoka et al., 2010, 2011; Sumi et al., 2015), had fewer superficial neuromasts than many stomiiform specimens examined in this study (Table 1.5). Among the gobies, *Rhyacicthys aspro* (47.3 mm SL) had 308 neuromasts (Asaoka et al., 2010), *Pterogobius elapoides* (68 mm SL) had 1,068 neuromasts, and *Odontobutis obscura* (72 mm SL) had 1,598 neuromasts (Asaoka et al, 2011). Even the blind morph of the Mexican blind cavefish, *Astyanax mexicanus* (45.3 mm SL) has a comparable number of superficial neuromasts as some stomiiform fishes, with 2,647 found on one side of the head and body (Sumi et al., 2015). However, representatives of the shallow-dwelling teleost order Salmoniformes, (i.e. *Oncorhyncus mykiss*), thought to be closely related to the Stomiiformes, have very few superficial neuromasts (Montgomery et al., 2003, Cech & Mussen, 2006), suggesting that a proliferation in superficial neuromasts in Stomiiformes is a feature not shared with salmoniforms, and is likely an adaptation to life in the light-limited environment of the deep sea.

Further, comparison of stomiiform fishes to other taxa reveals that they have many features characteristic of larval fishes. In contrast to the broad flat cranial bones of shallow water fishes (e.g., salmonids, Fig.1.27), stomiiforms tend to have a reduced number of thin, needle-like or weakly or incompletely ossified cranial bones, as dramatically illustrated in µCT reconstructions. The partially ossified canals observed in

the stomiiforms have a morphology that resembles early stages of bone canal development as described in larval zebrafish, salmonids, and cichlids (Allis, 1889; Jollie, 1984; Webb & Shirey, 2003; Tarby & Webb, 2003; Bird &Webb, 2014). Additionally, the superficial neuromasts observed in stomiids are small and morphologically similar to the neuromasts in larvae of shallow-dwelling fishes (*Amia calva,* Allis, 1889; *Danio rerio*, Webb & Shirey, 2003; cichlids, Bird & Webb, 2014). Thus, the lateral line system in adult stomiiform fishes appears larval in morphology, adding to the list of larval characteristics that Marshall (1984) reports in these fishes (including eye, swimbladder, kidney, and muscle morphology).

It should be noted that stomiiform fishes are not the only deep-sea taxa reported to have a proliferation of superficial neuromasts. In addition to the taxa referenced earlier that have a reduced canal system (anglerfish: Lophiiformes, snipe eel: Notocanthiformes, and gulper eel: Saccopharyngiformes; Fig. 1.3), it appears that other groups with cranial lateral line canals also have numerous superficial neuromasts. Halosaurids (Notocanthiformes), melamphaids (Stephanoberyciformes), searsiids (Argentiniformes), myctophids (Myctophiformes), evermannelids, ipnopids (Aulopiformes), and macrourids (Gadiformes) are among the groups with well-developed canals (either wide or narrow) that also have a proliferation of superficial neuromasts (Marshall 1979; Marshall and Staiger, 1975; Harold, 2002). Thus, it appears that all deep-sea fishes examined have a fairly well-developed lateral line system with variation in cranial canal morphology (narrow, widened, or reduced [partially ossified]), and a corresponding proliferation of superficial neuromasts. These findings suggest the importance of the lateral line system in the deep-sea fishes.

The condition of specimens was a critical factor in the interpretation of lateral line morphology of these fishes. The similarity in the distribution of the small, brown depressions in the skin of whole preserved fish (*Astronesthes, Bathophilus, Echiostoma, Eustomias, Flagellostomias, Opostomias*) and the co-occurrence of brown depressions and lines of superficial neuromasts (the "white dots" in *Gonostoma, Idiacanthus,* and *Tactostoma*) suggests that the depressions represent the location of superficial neuromasts that have been removed or otherwise damaged. This is supported by the presence of pigment in depressions below the superficial neuromasts of *Astronesthes niger* (Fig. 1.20). In *Argyropelecus* and *Cyclothone,* superficial neuromasts were often visible in the epithelium that had otherwise been damaged, suggesting that superficial neuromasts are easily removed during collection or handling. If this is the case, it makes sense that seemingly well-preserved specimens may have lost the epithelium in which superficial neuromasts would sit, leaving behind only the underlying pigmented tissue that had sat beneath the neuromast. In whole specimens, this pigment stands out as numerous, tightly spaced, depressions in the skin that are a different in color (brown) than the surrounding epithelium. It is therefore concluded that the brown depressions on the head and trunk of stomiiform specimens represent the former locations of superficial neuromasts.

The number and distribution of superficial neuromasts was highly dependent on specimen condition. All specimens examined, even the most pristine, were slightly damaged, so estimates of the distribution and number of superficial neuromasts is fairly conservative. Even with the conservative number of superficial neuromasts reported here, it was found that *Argyropelecus hemigymnus* has over 20 times more superficial neuromasts on the head and body than were previously illustrated (Handrick, 1901),

mostly likely due to the quality of the specimen previously described by Handrick. This work has shown that our ability to accurately describe the morphology of the lateral line system in deep-sea fishes is dependent upon the acquisition and examination of high-quality, well-preserved, intact specimens. The current work was limited by the amount of high quality material available and it is likely that stomiiform fishes have a greater degree of superficial neuromast proliferation than accounted for here. Future studies on a higher number of specimens from a larger number of taxa is needed to determine the total number of superficial neuromasts in these fishes, the nature of inter- and intraspecific variation in lateral line morphology, and to confirm if a proliferation of superficial neuromasts is characteristic of all taxa in the order.

Given the abundance of stomiiform fishes circumglobally and the variation in depth ranges among species (i.e. Marshall, 1954, 1979), these fishes make an interesting study system for examining how lateral line morphology varies both phylogenetically and with environmental conditions in the deep sea. *Cyclothone* is particularly interesting in this regard as morphological differences are correlated with interspecific variation in depth distributions. For instance, *Cyclothone* species share similar superficial neuromast distributions and all lack cranial canals. However, future work is needed to better describe the lateral line morphology in the shallower dwelling *Cyclothone* species (i.e. *C. signata, C. alba, C. braueri,* etc.) in addition to species distributed in deeper waters to determine how variation in lateral line morphology may be correlated with depth and to elucidate possible sensory and behavioral adaptations to light-limited environments.

Furthermore, because of the limited availability of information on the behavior of stomiiform fishes, descriptions of the lateral line morphology may help infer behavioral

and ecological characteristics of these poorly understood fishes. Based on gut content analyses that suggest that *Argyropelecus* and *Chauliodus* feed selectively (Merrett and Roe, 1974) and video of *Argyropelecus* sp. (MBARI) showing them striking at prey (rather than filter feeding), it is likely that these fishes may be using the lateral line system (in addition to other senses) to locate prey. Furthermore, Marshall (1979) suggested that sexually dimorphic taxa (e.g., *Cyclothone* and *Argyropelecus*) may follow flows and chemical concentration gradients back to the source of pheromones produced by potential mates. Additionally, behavioral observations of various stomiiform fishes suggest that they spend most of their time suspended fairly motionless within the water column. This behavior, while possibly a mechanism to reduce metabolic demands, may also be useful for reducing self-generated flows, which may be easily detected by the numerous neuromasts over the head and body. The highly proliferated superficial neuromasts in these fishes, described here for the first time, suggests the importance of the lateral line system for the potential detection of hydrodynamic stimuli from biotic sources such as predators, prey, and mates.

Literature Cited

Allis, E. P. J. (1889). The anatomy and development of the lateral line system in *Amia calva*. *Journal of Morphology*, 11(3), 463 – 566.

Andersen, V. & Sardou, J. (1992). The diel migrations and vertical distributions of zooplankton and micronekton in the Northwestern Mediterranean Sea. 1. Euphausiids, mysids, decapods and fishes. *Journal of Plankton Research*, 14(8), 1129–1154. http://doi.org/10.1093/plankt/14.8.1129.

Angel, M.V. (1997) What is the deep sea? In *Deep-sea Fishes*. (Randall, D. J. & Farrell, A. P., eds). San Diego: Academic Press.

Asaoka, R., Nakae, M. & Sasaki, K. (2014). Innervation of the lateral line system in *Rhyacichthys aspro*: The origin of superficial neuromast rows in gobioids (Perciformes: Rhyacichthyidae). *Ichthyological Research*, 61, 49–58. http://doi.org/10.1007/s10228-013-0373-8.

Asaoka, R., Nakae, M. & Sasaki, K. (2010). Description and innervation of the lateral line system in two gobioids, *Odontobutis obscura* and *Pterogobius elapoides* (Teleostei: Perciformes). *Ichthyological Research*, 58(1), 51–61. http://doi.org/10.1007/s10228-010-0193-z.

Asaoka, R., Nakae, M. & Sasaki, K. (2012). The innervation and adaptive significance of extensively distributed neuromasts in *Glossogobius olivaceus* (Perciformes: Gobiidae). *Ichthyological Research*, 59(2), 143–150. http://doi.org/10.1007/s10228-011-0263-x.

Badcock, J. (1982). A new species of the deep-sea fish genus *Cyclothone* Goode and Bean (Stomiatoidei, Gonostomatidae) from the tropical Atlantic. *Journal of Fish Biology*, 20(2), 197–211.

Baird, R. C. (1971). The systematics, distribution, and zoogeography of the marine hatchetfishes (Family Sternoptychidae). *Bulletin of the Museum of Comparative Zoology* , 142(1), 115–123.

Bird, N. C. & Webb, J. F. (2014). Heterochrony, modularity, and the functional evolution of the mechanosensory lateral line canal system of fishes. *EvoDevo*, 5(1), 21. http://doi.org/10.1186/2041-9139-5-21.

Bigelow, H. B., Cohen, D. M., Dick, M. M., Gibbs, R. H. Jr., Grey, M., Morrow, J. E., Jr., Schultz, L. P. & Walters, V. (1964). *Fishes of the Western North Atlantic* (H. Bigelow, et al. eds.). New Haven: Sears Foundation for Marine Research.

Bond, G. W. & Tighe, K. A. (1974). A diagnostic character for rapid identification of lightly pigmented species of the genus *Cyclothone* (Gonostomatidae) in the North Atlantic. *Copeia*, 1974, 272–275.

Caruso, J. H. (1989). Systematics and distribution of the Atlantic chaunacid anglerfish (Pisces: Lophiiformes). *Copeia*, 1989, 153-165.

Cech, Joseph, Jr. & Mussen, Timothy (2006). Determining how fish detect fish screens and testing potential fish screen enhancements. California Energy Commission, PIER Energy-Related Environmental Research Program. CEC-500-2006-117.

Childress, J. J., Barnes, A. T., Quetin, L. B. & Robison, B. H. (1978). Thermally protecting cod ends for the recovery of living deep-sea animals. *Deep-Sea Research*, 25, 419 – 422.

Coombs, S., Janssen, J., & Webb, J. F. (1988). Diversity of lateral line systems: Phylogenetic, and functional considerations. In *Sensory biology of aquatic animals* (J. Atema, R. R. Fay, A. N. Popper, & W. N. Tavolga, eds.), pp. 553-593. NY: Springer-Verlag.

Coombs, S. & Bleckmann, H. (2014). The gems of the past: A brief history of lateral line research in the context of the hearing sciences. In *The Lateral Line System* (eds. S. Coombs & R. R. Fay), pp. 1-16. New York: Springer. doi:10.1007/2506.

De Busserolles, F., Marshall, N. J. & Collin, S. P. (2014). The eyes of lanternfishes (Myctophidae, Teleostei): Novel ocular specializations for vision in dim light. *Journal of Comparative Neurology*, 522, 1618–1640. http://doi.org/10.1002/cne.23495.

Denton, E.J. & Gray, J.A.B. (1989). Some observations on the forces acting on the neuromasts in fish lateral line canals. In *The Mechanosensory Lateral Line: Neurobiology and Evolution*. (eds. S. Coombs, P. Gorner & H. Munz), pp 229-246. New York: Springer-Verlag.

DeWitt, F. A. J. (1972). Bathymetric distributions of two common deep-sea fishes, *Cyclothone acclinidens* and *C. signata*, off Southern California. *Copeia*, 1972, 88–96.

Dewitt, F.A.J. & Cailliet, G. M. (1972). Feeding habits of two bristlemouth fishes, *Cyclothone acclinidens* and *C. signata. Copeia*, 1972, 868–871.

Douglas, R. H. & Partridge, J. C. (2011). Vision: Visual Adaptations to the Deep Sea. *Encyclopedia of Fish Physiology (Vol. 1)*. Elsevier Inc. http://doi.org/10.1016/B978-0-12-374553-8.00089-7.

Fange, R., Larsson, A. & Lidman, U. (1972). Fluids and jellies of the acusticolateralis system in relation to body fluids in *Coryphaenoides rupestris* and other fishes. Marine Biology, 17, 180-185.

Fink, W. L. (1985). Phylogenetic interraltionships of the stomiid fishes (Teleostei: Stomiiformes). *Miscellaneous Publications Museum of Zoology, University of Michigan no. 171*. (eds. R. R. Miller & C. L. Haven), Ann Arbor: The University of Michigan.

Gagnon, Y. L., Sutton, T. T. & Johnsen, S. (2013). Visual acuity in pelagic fishes and mollusks. *Vision Research*, 92, 1–9. http://doi.org/10.1016/j.visres.2013.08.007.

Grey, M. (1960). A preliminary review of the family Gonostomatidae, with a key to the genera and the description of a new species from the tropical Pacific. *Bulletin of the Museum of Comparative Zoology*, 122(2), 55–126.

Haedrich, Richard L. (1997). Distribution and population ecology. In *Deep-sea Fishes*. (Randall, D. J. & Farrell, A. P., eds). San Diego: Academic Press.

Handrick, K. (1901). Nervensystems und der leuchtorgane von *Argyropelecus hemigymnus*. *Zoologica*, 32(13), 1-69.

Harold, A. S. (1993). Phylogenetic relationships of the sternoptychid *Argyropelecus* (Teleostei : Stomiiformes). *Copeia*, 1993, 123–133.

Harold, A. S. (2002). Order Stomiiformes. In *The Living Marine Resources of the Western Central Atlantic. Vol 2: Bony fishes part 1 (Acipenseridae to Grammatidae*). (Carpenter, Kent, E., ed.)., pp.881-913. FAO.

Harold, A. S. & Weitzman, S. H. (1996). Interrelationships of stomiiform fishes. In *Interrelationships of Fishes* (M. L. J. Stiassny, L. Parenti, & G. D. Johnson, eds.), pp. 333–353. San Diego: Academic Press.

Jakubowski, M. (1974). Structure of the lateral-line canal system and related bones in the berycoid fish *Hoplostethus mediterraneus* Cuv. et Val. (Trachichtyidae, Pisces). *Acta Anatomica*, 87(2), 261–274.

Janssen, J. (1997). Comparison of response distance to prey via the lateral line in the ruffe and yellow perch. *Journal of Fish Biology*, *51*, 921-930.

Kinzer, J. & Schulz, K. (1988). Vertical distribution and feeding patterns of midwater fish in the central equitorial Atlantic. II. Sternoptychidae. *Marine Biology* 99, 261–269.

Lawry Jr., J. V. (1972a). A presumed near field pressure receptor in the snout of the lantern fish, *Tarletonbeania crenularis* (Myctophidae). *Marine Behaviour and Physiology*, 1, 295-303.

Lawry Jr., J. V. (1972b). The trigeminofacial innervation of the cephalic lateral line organs and photophores of the lantern fish *Tarletonbeania crenularis* (Myctophidae). *Marine Behaviour and Physiology*, 1, 285-293.

Marshall, N.B. (1954). *Aspects of Deep-Sea Biology*. London: Hutchinson.

Marshall, N.B (1965). Systematic and biological studies of the macrourid fishes. *Deep-Sea Research*, 12, 299-322.

Marshall, N.B. (1979). *Developments in Deep-Sea Biology*. Poole: Blandford Press.

Marshall, N. B. (1984). Progenetic tendencies in deep-sea fishes. In *Fish Reproduction* (G. W. Potts & R. J. Wootton, eds.), pp. 91 – 100. London: Academic Press.

Marshall, N. B. & Staiger, J. C. (1975). Aspects of structure, relationships and biology of deep-sea fish *Ipnops murrayi* (family Bathypteroidae). *Bulletin of Marine Science*, 25(1), 101–111.

Marshall, N. J. (1996). The lateral line systems of three deep-sea fish. *Journal of Fish Biology*, 49, 239–258.

Maynard, S. D. (1982). Aspects of the biology of mesopleagic fishes of the genus *Cyclothone* (Pices: Gonostomatidae) in Hawaiian waters. University of Hawaii.

McHenry, M.J. & Liao, J.C. (2014). The Hydrodynamics of flow stimuli. In *The Lateral Line System* (S. Coombs & R. R. Fay, eds.), pp. 73-98. New York: Springer. doi:10.1007/2506.

Merrett, N. R. & Roe, H. S. J. (1974). Patterns and selectivity in the feeding of certain mesopelagic fishes. *Marine Biology*, 28(2), 115–126. http://doi.org/10.1007/BF00396302.

Miya, M. (1994). *Cyclothone kobayashii*, a new gonostomatid fish (Teleostei : Stomiiformes) from the Southern Ocean, with notes on its ecology. *Copeia*, 1994, 191–204.

Miya, M. (1994). First record of *Cyclothone parapallida* (Gonostomatidae) from the Pacific Ocean, with notes on its geographic distribution. *Japanese Journal of Ichthyology*, 41(3), 326–329.

Miya, M. & Nemoto, T. (1987). The bathypelagic gonostomatid fish *Cyclothone obscura* from Sagami Bay, Central Japan. *Japanese Journal of Ichthyology*, 33(4), 417–418.

Miya, M. & Nemoto, T. (1987). Reproduction, growth and vertical distribution of the meso-and bathypelagic fish *Cyclothone atraria* (Pisces: Gonostomatidae) in Sagami Bay, Central Japan. *Deep- Sea Research*, 34(9), 1565 – 1577.

Miya, M. & Nemoto, T. (1991). Comparative life histories of the meso- and bathypelagic fishes of the genus *Cyclothone* (Pices; Gonostomatidae) in Sagami Bay. *Deep-Sea Research Part A.*, 38, 67–89.

Miya, M. & Nishida, M. (1996). Molecular phylogenetic perspective on the evolution of the deep-sea fish genus *Cyclothone* (Stomiiformes: Gonostomatidae). *Ichthyological Research*, 43(4), 375–398.

Montgomery, J. C., McDonald, F., Baker, C. F., Carton, G. & Ling, N. (2003). Sensory integration in the hydrodynamic world of rainbow trout. *Proceedings of the Royal Society B, 270,* S195–S197. http://doi.org/10.1098/rsbl.2003.0052.

Montgomery, J., Bleckmann, H. & Coombs, S. (2014). Sensory ecology and neuroethology of the lateral line. In *The Lateral Line System* (S. Coombs & R. R. Fay eds.), pp. 121-149. New York: Springer. doi:10.1007/2506.

Moore, J. (1993). Phylogeny of the Trachichthyiformes (Teleostei: Percomopha). *Bulletin of Marine Science*, 52, 114-136.

Mukhacheva, V. A. (1966). The composition of species of the genus *Cycltohone* (Pices, Gonostomatidae) in the Pacific Ocean. In *Fishes of the Pacific and Indian Oceans Biology and Distribution Vol. 73* (T. S. Rass, ed.). Jerusalem: Academy of Science Israel Program for Scientific Translation.

Nelson, J. S., Grande, T. C. & Wilson, M. V. H. (2016). *Fishes of the World*.5th edition. Wiley.

Nielsen, J. G. & Bertelsen, E. (1985). The gulper-eel family Saccopharyngidae (Pisces, Anguilliformes). *Steenstrupia*, 11(6), 157–206.

Nouvian, C. (2007). *The Deep: The Extraordinary Creatures of the Abyss*. Chicago: University of Chicago Press.

Pothoff, T. (1984). Clearing and staining technique. *In Ontogeny and Systematics of Fishes. Special Publication No. 1.* American Society of Ichthyologists and Herpetologists.

Schwalbe, M. A. B., Bassett, D. K. & Webb, J. F. (2012). Feeding in the dark: lateral-line-mediated prey detection in the peacock cichlid *Aulonocara stuartgranti*. *Journal of Experimental Biology*, 215(Pt 12), 2060–71. http://doi.org/10.1242/jeb.065920.

Shultz, L.P. (1961). Revision of the marine silver hatchetfishes (Family Sternoptychidae. *Proceedings of the United States National Museum*, 112(3449), 587--649.

Smith, K. L. & Laver, M. B. (1981). Respiration of the bathypelagic fish *Cyclothone acclinidens*. *Marine Biology*, 61(4), 261–266. http://doi.org/10.1007/BF00401564.

Song, J. and Parenti, L.R. (1995). Clearing and staining whole fish specimens for simultaneous demonstration of bone, cartilage, and nerves. *Copeia*, 1995, 114-118.

Sumi, K., Asaoka, R., Nakae, M. & Sasaki, K. (2015). Innervation of the lateral line system in the blind cavefish *Astyanax mexicanus* (Characidae) and comparisons with the eyed surface-dwelling form. *Ichthyological Research*, 62, 420-430. http://doi.org/10.1007/s10228-015-0458-7.

Tarby, M. L. & Webb, J. F. (2003). Development of the supraorbital and mandibular lateral line canals in the cichlid, *Archocentrus nigrofasciatus. Journal of Morphology,* 254, 44-57.

Webb, J. F. (1989). Gross morphology and evolution of the mechanosensory lateral line system in teleost fishes. *Brain, Behavior and Evolution*, 33(1), 34–53.

Webb, J. F. & Shirey, J. E. (2003). Post embryonic development of the lateral line canals and neuromasts in the zebrafish. *Developmental Dynamics*, 228, 370 - 385

Webb, J. F. (2014a). Lateral line morphology and development and implications of the ontogeny of flow sensing in fishes. In *Flow Sensing in Air and Water* (H. Bleckmann, ed.) pp. 127–146. Berlin: Springer. http://doi.org/10.1007/978-3-642-41446-6.

Webb, J. F. (2014b). Morphological diversity, development, and evolution of the mechanosensory lateral line system. In *The Lateral Line System* (S. Coombs & R. R. Fay, eds.). pp. 17–72. New York: Springer. http://doi.org/10.1007/2506.

Weitzman, S. H. (1967). The Origin of the stomiatoid fishes with comments on the classification of salmoniform fishes. *Copeia*, 1967, 507–540.

Weitzman, S. H. (1974). Osteology and evolutionary relationships of the Sternoptychidae, with a new classification of Stomatioid families. *Bulletin of theAmerican Museum of Natural History*, 153, 331 – 476.

Table 1.1: Summary of the presence of cranial lateral line canals in stomiiform genera based on presence of canal pores as reported in the literature. Degree of ossification is noted based on Bird & Webb (2014, Fig. 6). "4" = a fully enclosed and ossified canal, "3" = a fully enclosed but partially ossified canal, "2b/3" = the presence of a trough in the bone interpreted as an incompletely ossified unenclosed or enclosed canal, respectively. Numbers in parenthesis after IO canals indicate the number of infraorbital bones in which a canal is present. Canal abbreviations are as follows: supraorbital (SO), mandibular (MD), preopercular (PO), infraorbital (IO), otic (OT), supratemporal commissure (ST). Genera are listed alphabetically within each family. "*" = genera also examined in the present study, see Table 4.

Family	***Genus***	**SO**	**MD**	**PO**	**IO**	**OT**	**ST**
Sternoptychidae (Weitzman, 1974)	*Araiophos*	3					
	Argyripnus	3				4	
	Argyropelecus *	4		4			
	Danaphos	3		3			
	Maurolicus	3		4			
	Polyipnus		4	2b/3			
	Sonoda	4				2b/3	
	Sternoptyx			3			
	Trophos	4		4		2b/3	
	Valencinnellus	4		3			
Phosychthyidae (Weitzman, 1967)	*Polymetme*	4	4		4 (7)	2b/3	
	Vinciguerria	2b/3				2b/3	
Stomiidae (Fink, 1985)	*Aristostomias* *	4				2b/3	
	Bathophilus *	4				4	
	Chauliodus	2b/3					
	Chirostomias		4	4	2b/3 (1)		4
	Echiostoma *	4	4		4 (1)	4	
	Eustomias *	4	4			4	
	Flagellostomias *	4				2b/3	
	Grammatostomias		4				
	Leptostomias		4	4	2b/3 (1)		4
	Malacosteus *	4					
	Melanostomias	4				2b/3	
	Pachystomias *	4	2b/3			2b/3	
	Photonectes	4			4 (1)	4	
	Photostomias	4				2b/3	
	Stomias	2b/3			2b/3 (1)		
	Tactostoma *		4	4	2b/3 (1)		
	Trigonolampa	4	4	4	4 (1)		4

Table 1.2: List of specimens examined. JFW catalogue numbers refer to specimens held in Dr. Jacqueline F. Webb's collection (URI). Abbreviation for net types used to collect fish: IKMT = Isaacs-Kidd midwater trawl, MOCNESS = multiple opening and closing net with environmental sensing system (either 10 or 20 m^2 opening), OCTT = opening and closing Tucker trawl, RMT = rectangular midwater trawl, TTIC = Tucker trawl with a thermally insulated cod end. Mwo = meters of wire out on the net during specimen collection. Species are ordered alphabetically within each family.

Family	Species	Catalogue #	Number of specimens examined	Size range (mm SL)	Identification determined by	Locality	Collection Information
Sternoptychidae	*Argyropelecus aculeatus*	MCZ 159086	n = 9	30 – 40.5	C. Kenaley and K. Hartel	40°10'48 N, 49°12'48 W	27 June 1978; R/V *Atlantis*; 350 mwo
		MCZ 137835	n = 1	unknown	Woods Hole Oceanographic Institute	Atlantic Ocean (32°30' N, 60°23' W)	20 March 1974; R/V *Knorr*38; 0-440 m; 10' IKMT; coll R. H. Backus
		JFW 1162	n = 4	28.5 – 38	A. Marranzino	Northwestern Atlantic	15 Aug 2014; R/V *Endeavor*; 500 m TTIC; coll. N. Hobbs and B. Seibel
	Argyropelecus affinis	JFW 041	n = 1	41	A. Marranzino	Catalina Basin, CA	1988; R/V *New Horizon*; IKMT; coll. J. Webb
		JFW 2118	n = 1	49	A. Marranzino	Eastern Atlantic (32° N 120° S)	2010; R/V *New Horizon*; TTIC; coll. B. Seibel
	Argyropelecus hemigymnus	JFW 042	n = 1	22	A. Marranzino	Catalina Basin, CA	1988; R/V *New Horizon*; IKMT; coll. J. Webb
		MCZ 159085	n = 5	30 – 33	F. M. Posteiro	Northeastern Atlantic (39°41'42" N, 32°19'30" W)	5 June 1978; R/V *Atlantis II* 101; 0 – 350 m; coll C. E. Lea
	Argyropelecus lychnus	JFW 040	n = 14	14- 36	A. Marranzino	Catalina Basin, CA	1988; R/V *New Horizon*; IKMT; coll. J. Webb
		JFW 041	n = 2	12.5 – 14.5	A. Marranzino	Catalina Basin, CA	1988; R/V *New Horizon*; IKMT; coll. J. Webb
		JFW 061	n = 1	18	A. Marranzino	Brown's Bank, Northwestern Atlantic	July 1986; R/V *Westward*; coll. J. Webb

		JFW 1005	n = 6	16 – 31	A. Marranzino	Catalina Basin, CA	1988; R/V *New Horizon*; IKMT; coll. J. Webb
		JFW 1181	n = 3	10 – 29	A. Marranzino	Monterey Bay, CA	10 Sept 2014; 600 m OCTT; coll. S. Haddock
	Argyropelecus sp.	(specimen data unavailable)	n = 2	unknown			
Gonostomatidae	*Cyclothone acclinidens*	JFW 036	n = 2	41 – 48	A. Marranzino	Catalina Basin, CA	1988; R/V *New Horizon*; IKMT; coll. J. Webb
		JFW 039	n = 1	21	A. Marranzino	Catalina Basin, CA	1988; R/V *New Horizon*; IKMT; coll. J. Webb
		JFW 062	n = 1	45.5	A. Marranzino	Catalina Basin, CA	1988; R/V *New Horizon*; IKMT; coll. J. Webb
		JFW 064	n = 2	31 – 33	A. Marranzino	Catalina Basin, CA	1988; R/V *New Horizon*; IKMT; coll. J. Webb
	Cyclothone alba	JFW 039	n = 1	28	A. Marranzino	Catalina Basin, CA	1988; R/V *New Horizon*; IKMT; coll. J. Webb
		JFW 061	n = 1	28	A. Marranzino	Brown's Bank, Northwestern Atlantic	July 1986; R/V *Westward*; coll. J. Webb
	Cyclothone braueri	JFW 2119	n = 2	28 – 29	A. Marranzino	Eastern Atlantic (32° N 120° W)	2010; R/V *New Horizon*; TTIC; coll. B. Seibel
	Cyclothone microdon	JFW 1160	n = 6	44.5 – 56.5	A. Marranzino	Northwestern Atlantic	15 Aug 2014; R/V *Endeavor*; TTIC; coll. N. Hobbs, B. Seibel
		MCZ 89489	n = 1	unknown		Atlantic Ocean (40°10'24" N, 65°0'18" W)	7 Sept 1985; R/V *Endeavor* 133; 0 – 3000 mwo; 10 m RMT; coll. D. Backus
	Cyclothone parapallida	JFW 061	n = 1	33.5	A. Marranzino	Brown's Bank, Northwestern Atlantic	July 1986; R/V *Westward*; coll. J. Webb
	Cyclothone pallida	JFW 061	n = 2	31.5 – 35	A. Marranzino	Brown's Bank, Northwestern Atlantic	July 1986; R/V *Westward*; coll. J. Webb

	Cyclothone pseudopallida	JFW 051	n = 1	22	A. Marranzino	Catalina Basin, CA	1988; R/V *New Horizon*; IKMT; coll. J. Webb
		JFW 061	n = 2	26.5 – 27.5	A. Marranzino	Brown's Bank, Northwestern Atlantic	July 1986; R/V *Westward*; coll. J. Webb
	Cyclothone signata	JFW 039	n = 6	13 – 33.5	A. Marranzino	Catalina Basin, CA	1988; R/V *New Horizon*; IKMT; coll. J. Webb
		JFW 059	n = 5	25 – 33	A. Marranzino	Catalina Basin, CA	1988; R/V *New Horizon*; IKMT; coll. J. Webb
	Gonostoma elongatum	JFW 1173	n = 1	100	A. Marranzino	Northwestern Atlantic	17 Aug 2014; R/V *Endeavor*; TTIC; coll. N. Hobbs, B. Seibel
		JFW 1176	n = 5	50 – 92	A. Marranzino	Northwestern Atlantic	16 Aug 2014; R/V *Endeavor*; TTIC; coll. N. Hobbs, B. Seibel
		MCZ 140857	n = 2	146 - 182	Woods Hole Oceanographic Institution	Atlantic Ocean (38°36'0" N, 72°3'48" W)	25 April 1982; R/V *Oceanus* 118; 250 – 500 m; MOCNESS 20; coll. J. E. Craddock
Phosichthyidae	*Ichthyococcus ovatus*	MCZ 47693	n = 3	unknown		Atlantic Ocean (24°4'N, 93°52'W)	6 June 1996; R/V *Chain* 060; 0 – 460 m; 10' IKMT; coll R. H. Backus
Stomiidae	*Aristostomias tittmani*	MCZ 163949	n = 1	156	C. Kenaley	Atlantic Ocean (31°45'30" N, 64°10'24"W)	27 March 1993; R/V *Oceanus* 225; 0 – 1065 m; MOCNESS 10; coll. J. E. Craddock
		MCZ 149494	n = 1	77	K. Hartel, F. Porteiro	Atlantic Ocean (36°36'36" N, 25°7'6" W)	9 June 1978; R/V *Atlantis II* 101; 0 – 350 m; coll. C. E. Lea
	Astronesthes niger	MCZ 98847	n = 3	25 - 45	J. E. Craddock	Atlantic Ocean (39°N, 72° W)	5 Aug 1976; R/V *Knorr* 58
		MCZ 52847	n = 1	52	K. Hartel	Atlantic Ocean (36°52'48" N, 66°23'0" W)	10 Nov 1977; R/V *Knorr* 71; Neuston net; coll. K. E. Hartel
	Astronesthes gemmifer	MCZ 133451	n = 1	146	R. H. Gibbs	Atlantic Ocean (34°45' N, 15°6' W)	13 July 1972; R/V *Chain* 105; 0 – 480 m, 10' IKMT; coll. R. H. Backus

		MCZ 42864	n = 1	121	R. L. Haedrich	Atlantic Ocean (1°35'N, 27°3' W)	25 Feb 1963; R/V *Chain* 035; 0 – 290 m; 10' IKMT
		MCZ 148312	n = 1	163		Atlantic Ocean (32°0'0" N, 64°0'0" W)	1 Jan 1970; R/V *Trident*
	Bathophilus filifer	JFW 2131	n = 1	46	A. Marranzino	Pacific Ocean	2010; R/V *New Horizon*, 900 m TTIC; coll B. Seibel
	Echiostoma sp.	(specimen data unavailable)	n = 1	unknown			
	Echiostoma barbatum	JFW 2115	n = 1	210	A. Marranzino	Northwestern Atlantic (37°46.142N, 71°11.702W)	Sept 2011; R/V *Endeavor;* 650 m TTIC; coll B. Seibel
		MCZ 148298	n = 3	187 – 248		Atlantic Ocean (28°58'N, 88°18'W)	27 Oct 1960; R/V *Oregon*; 800 – 1000 m
	Eustomias hulleyi	MCZ 100873	n = 1	118	J. E. Craddock	Atlantic Ocean (32°2'54"N, 64°9'54"W)	16 Nov 1992; R/V *Cape Hatteras* 1692; 200 – 401 m; MOCNESS 10; coll. J. E. Craddock, K. E. Hartel
	Flagellostomias boureei	JFW 2109	n = 1	79	A. Bockus	Hawaii	5 June 2012; 500 m TTIC; coll A. Bockus
	Idiacanthus antrostomus	JFW 1182	n = 1	79	A. Marranzino	Monterey Bay, CA	20 Sept 2014; 600 m OCTT; coll. S. Haddock
		JFW 2106	n = 1	41	A. Marranzino	Gulf of California	July 2015; TTIC; coll. B. Seibel
	Malacosteus niger	MCZ 131758	n = 1	110	Woods Hole Oceanographic Institution	Atlantic Ocean (38°31'12"N, 72°23'36"W)	26 April 1982; R/V *Oceanus* 118; 500 – 750 m; MOCNESS 20; coll. J. E. Craddock
	Malacosteus sp.	MCZ (specimen data unavailable)	n = 2	unknown			

	Neonesthes capensis	MCZ 132802	n = 1	147	J. E. Craddock	Atlantic Ocean (39°30’6”N, 64°14’18”W)	30 Sept 1982; R/V *Knorr* 98; 0 – 1007 m; MOCNESS 20
	Neonesthes sp.	(specimen data unavailable)	n = 1	unknown			
	Opostomias micripnus	MCZ 132634	n = 1	270	C. Kenaley, K. Hartel	Atlantic Ocean (36°3’S, 17°7’ E)	30 April 1971; R/V *Atlantis II 060*; 0 – 10 m 10’ IKMT; coll R. H. Backus
	Pachystomias sp.	(specimen data unavailable)	n = 3	unknown			
	Rhadinesthes decimus	(specimen data unavailable)	n = 1	unknown			
	Tactostoma macropus	JFW 1183	n = 1	84	A. Marranzino	Monterey Bay, CA	20 Sept 2014; 600 m OCTT; coll. S. Haddock

Table 1.3: Number of specimens examined using different morphological methods. Size range (in mm SL) of fishes examined is in parenthesis (when available) below the number of specimens examined. Some specimens were used for multiple procedures. Species are ordered alphabetically within each family.

Family	Species	Whole Preserved Specimens	Hematoxylin Staining	Paraffin Histology	Plastic Histology	SEM	Clearing & Staining	Nerve Staining	µCT
Sternoptychidae	*Argyropelecus aculeatus*	n = 11 (26 - 40.5)	n = 4 (26 - 40)	n = 2 (26 - 28.5)	n = 1 (39)	n = 3 (36 - 40)			n = 1
	Argyropelecus affinis	n = 1 (49)						n = 1 (41)	
	Argyropelecus hemigymnus	n = 5 (30 - 33)						n = 1 (22)	
	Argyropelecus lychnus	n = 3 (10 - 29)		n = 1 (16)		n = 2 (12.5-14.5)	n = 13 (14 - 36)	n = 5 (25 - 28.5)	
	Argyropelecus sp.								n = 2
Gonostomatidae	*Cyclothone acclinidens*	n = 2 (31 - 33)					n = 3 (13 - 51)	n = 1 (45.5)	
	Cyclothone alba						n = 1 (28)	n = 1 (28)	
	Cyclothone braueri					n= 2 (28 - 29)			
	Cyclothone microdon	n = 4 (52 - 60)	n = 4 (52 - 60)	n = 2 (52 - 60)	n = 1 (60)	n = 2 (56.5 - 63)		n = 2 (44.5 - 45)	n = 1
	Cyclothone parapallida							n = 1 (33.5)	
	Cyclothone pallida							n = 2 (31.5 - 35)	
	Cyclothone pseudopallida					n = 1 (22)	n = 1 (27.5)	n = 1 (26.5)	
	Cyclothone signata		n = 1 (26.5)	n = 1 (13)		n = 1 (26.5)	n = 5 (25 - 33)	n = 2 (25 - 35)	

	Gonostoma elongatum	n = 6 (50 - 92)							n = 2 (146-182)
Phosichthyidae	*Ichthyococcus ovatus*								n = 3
Stomiidae	*Aristostomias tittmani*								n = 2 (77 - 156)
	Aristostomias sp.								n = 1
	Astronesthes niger	n = 3 (25 - 45)		n = 1 (52)					
	Astronesthes gemmifer								n = 3 (121-163)
	Bathophilus filifer	n = 1 (46)			n = 1 (46)	n = 1 (46)			
	Echiostoma barbatum	n = 1 (210)							n=3 (187-248)
	Echiostoma spp.								n =1
	Eustomias hulleyi								
	Flagellostomias boureei	n = 1 (79)							
	Idiacanthus antrostomus	n = 2 (41 - 79)							
	Malacosteus spp.								n = 2
	Neonesthes capensis								n = 1
	Neonesthes sp.								n = 1

	Opostomias micripnus	n = 1 (270)							
	Pachystomias sp.								n = 3
	Rhadinesthes decimus								n = 1
	Tactostoma macropus	n = 1 (84)							

Table 1.4: Lateral line canal morphology in stomiiform fishes as determined by examination of preserved specimens, histology, and µCT imaging. Degree of ossification of canals noted (as per Bird & Webb 2014; Fig. 6). "4" = fully enclosed and ossified canal, "3" = fully enclosed, partially ossified canal, "3/4" = fully enclosed, but degree of ossification unclear (determined by examination of whole specimens only), "2b/3" = partially ossified and either unenclosed or fully enclosed, respectively (determined by presence of a trough in the bone), "X" = canal absent, "-" = no data available. Degree of canal ossification was sometimes varied within a single individual for a single canal. Changes in the developmental stage are shows by "-" between stage (i.e. 3 – 4 = St. 3 followed by St. 4). For SO, MD, and canals caudal to SO (either OT, PT, and/or SC) these changes are noted from rostral to caudal. For PO canal these are noted from ventral to dorsal. Refer to Table 1.3 for methods and number of specimens used to determine canal morphology.

Family	Genus	SO	MD	PO	IO	Canals Caudal to SO
Sternoptychidae	*Argyropelecus*	3 - 4	3	3	X	X
Gonostomatidae	*Cyclothone*	X	X	X	X	X
	Gonostoma	3	X	3	3/4	3/4 - 4
Phosichthyidae	*Ichthyococcus*	-	4	4	-	-
Stomiidae	*Aristostomias*	4	4 - 2b/3	4	X	X
	Astronesthes	4	4 - 3	4 - 3	3	4 - 3/4
	Bathophilus	3/4	3/4	3/4	X	3/4
	Echiostoma	3 - 4	4 - 3	4 - 3	X	3
	Eustomias	3/4	3/4	3/4	X	3/4
	Flagellostomias	3/4	3/4	3/4	3/4	3/4
	Idiacanthus	3/4	3/4	X	3/4	3/4
	Malacosteus	4	2b/3	2b/3	-	-
	Neonesthes	4	4 - 2b/3	4	-	2b/3
	Opostomias	3/4	3/4	3/4	3/4	3/4
	Pachystomias	2b/3 - 4	2b/3	4 - 2b/3	-	4
	Rhadinesthes	4	4	4 - 2b/3	-	-
	Tactostoma	3/4	3/4	3/4	3/4	3/4

Table 1.5: Estimated numbers of superficial neuromasts ("white dots") on the head and body in stomiiform fishes examined in this study, and in shallow water taxa as derived from the literature. Total counts represent the number of SNs (= white dots) counted on one side (mid-dorsal to mid-ventral) of the specimen's head and trunk. SNs were counted on whole preserved specimens. Data unavailable for neuromast size indicated by "-". References for other taxa are given below the table.

Family	Species	SL (mm)	# Examined	SN size (μm)	Total # SN
Sternoptychidae	*Argyropelecus aculeatus*		11	~60 – 90	~356
	Argyropelecus affinis	49	1	~50 - 100	~420
	Argyropelecus hemigymnus	30 - 36.5	5	-	~521
	Argyropelecus lychnus	29	1	-	~2,20
Gonostomatidae	*Cyclothone microdon*	52 - 60	4	~50 – 80	~533
	Gonostoma elongatum	50	1	~30 – 40	~1,111
Stomiidae	*Idiacanthus antrostomus*	79	1	~30 – 40	~2,000
	Tactostoma macropus	84	1	~30 – 40	~2,286
[1]Characidae: Characiformes	*Astyanax mexicanus* (blind morph)	45.3	1	-	2,647
	Astyanax mexicanus (eyed morph)	55.2	1	-	2,900
	Gymnocorymbus ternetzi	20.8 – 26.4	3	-	2,471
	Hasemania nana	21.1	1	-	485
	Hyphessobrycon herbertaxelrodi	20.4 – 21.9	2	-	1,477
	Hyphessobrycon megalopterus	24.9 – 26.8	3	-	1,565
	Inpaichthys kerri	25.9 – 28.4	3	-	467
	Paracheirodon innesi	12.8	1	-	787
[2]Zenarchopteridae: Beloniformes	*Zenarchopterus dunckeri*	84.1	1	-	1,449
[3,4] Gobiidae: Perciformes	*Pterogobius elapoides*	68	1	-	1,068
	Glossogobius olivaceus	82	1	-	4,828
[3]Odontobutidae: Perciformes	*Odontobutis obscura*	72	1	-	1,598
[5]Rhyacicthyidae: Perciformes	*Rhyacichthys aspro*	47.3	1	-	308

[1] Sumi et al., 2015
[2] Hirota et al., 2015
[3] Asaoka et al., 2011
[4] Asaoka et al., 2012
[5] Asaoka et al., 2010

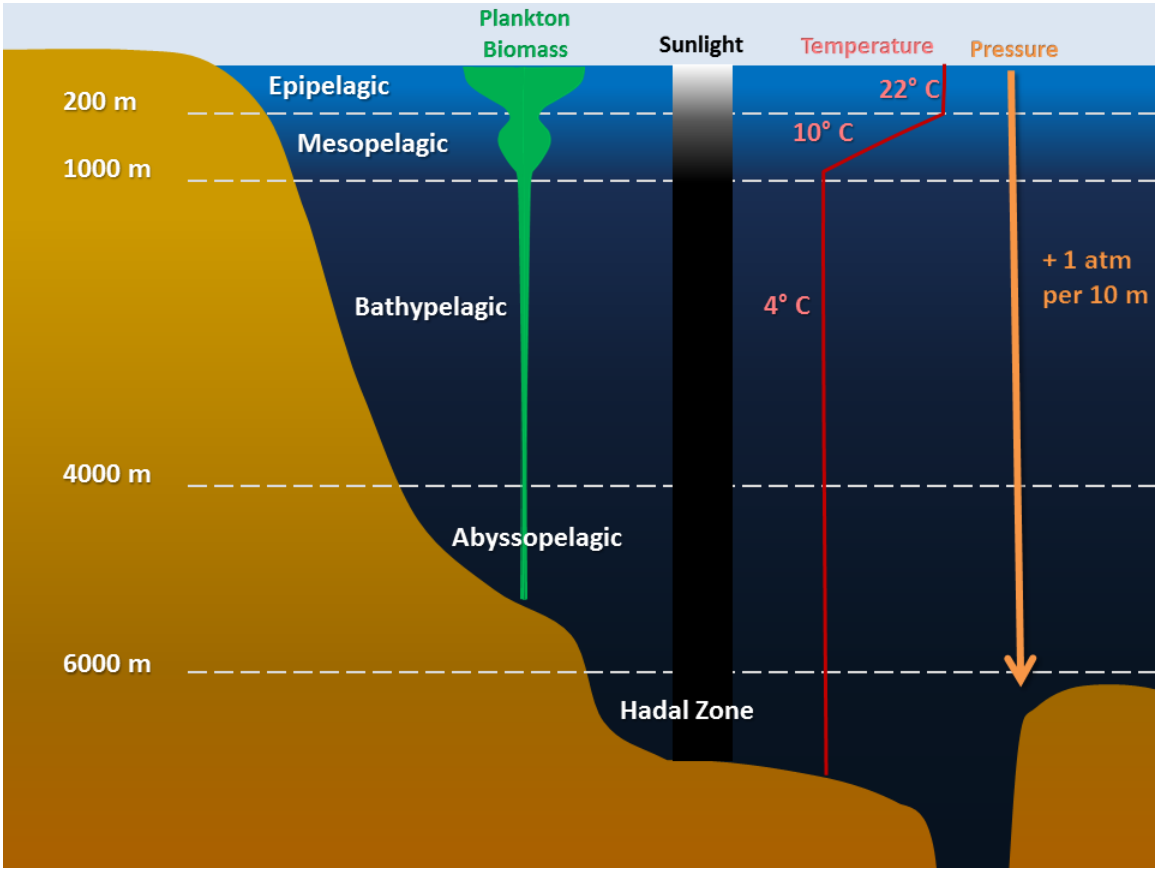

Figure 1.1: Environmental factors in the deep sea. A generalized depth profile showing the different depth zones of the ocean and how environmental factors change through the water column.

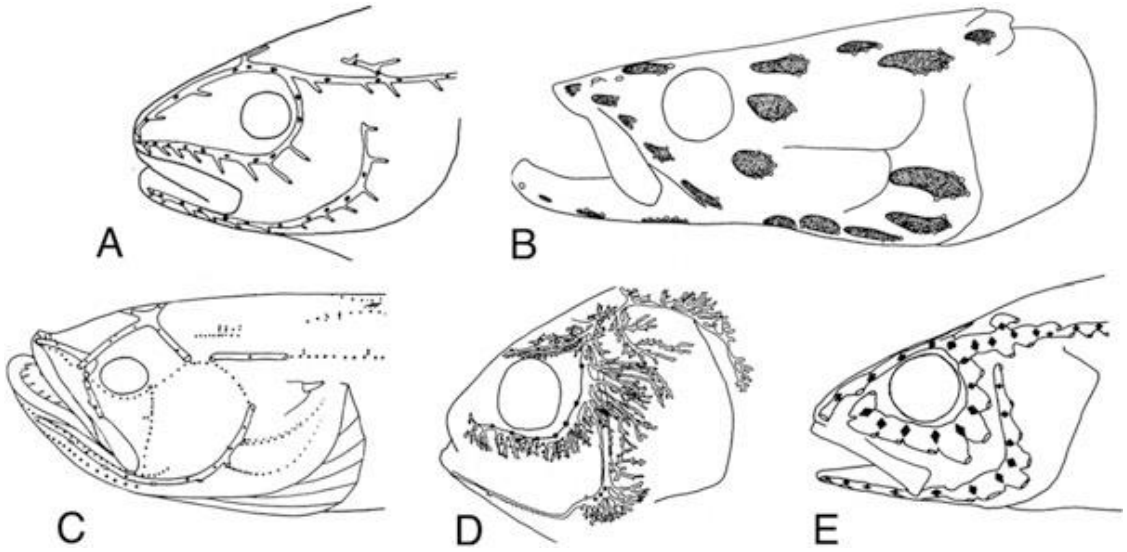

Figure 1.2: Five cranial canal phenotypes found among teleost fishes. A) narrow canal system (*Pollachius virens*), **B)** Narrow canals with widened tubules (*Arapaima*), **C)** Reduced cranial canals with rows of superficial neuromasts (dots; *Porichthys notatus*), **D)** Branched canals (*Brevoortia tyrannus*), and **E)** Widened canals with large neuromasts (diamonds; *Percarina demidoffi*). From Webb, 2014b.

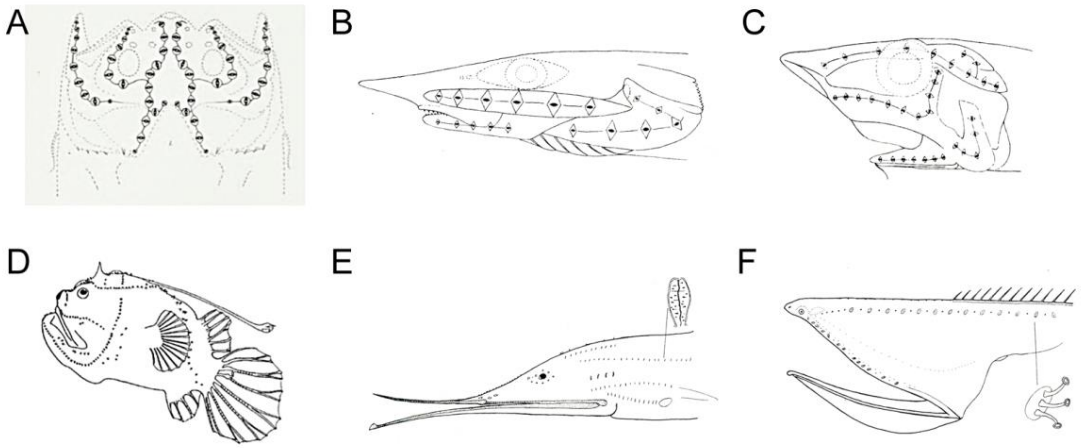

Figure 1.3: Lateral line morphology of deep-sea fishes. Widened lateral line canals with large canal neuromasts (diamonds with black centers) shown in **A)** *Leucicorus lusciosus* (Ophidiiformes; Garman, 1899), **B)** a halosaurid (*Aldrovina* sp.; Marshall, 1979), and **C)** a macrourid (*Coelorhynchus* sp; Marshall, 1979). A reduction of lateral line canals with a proliferation of superficial neuromasts (black dots or open circles) shown in **D)** *Phyrnichthys weldi* (Lophiiformes, from Marshall, 1996), **E)** bob-tailed snipe-eel (*Cyema atrum*; Marshall, 1954), and **F)** gulper eel (*Eurypharynx peacanoides*; Marshall, 1954).

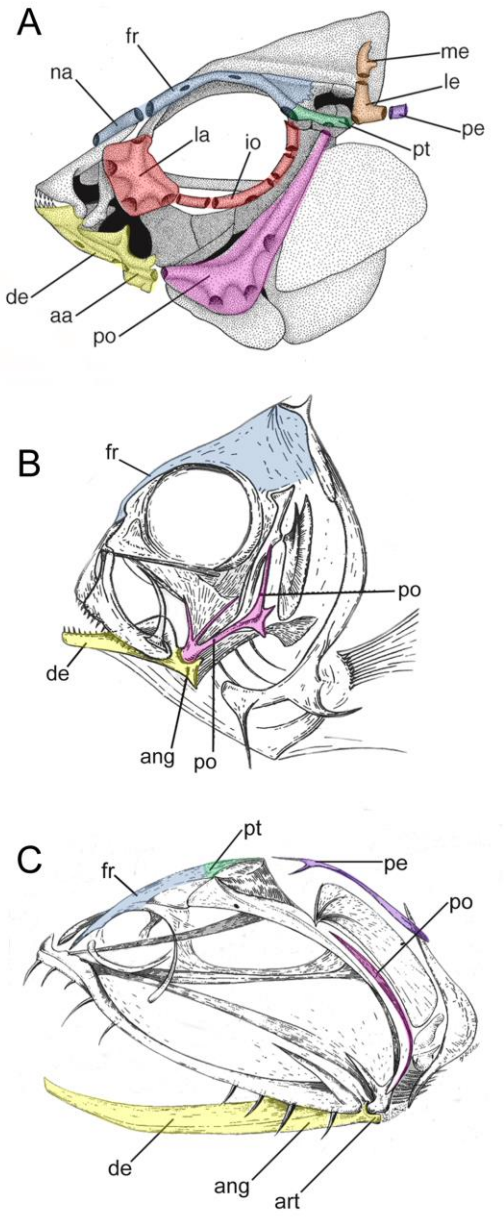

Figure 1.4: Lateral line canal-bearing cranial bones. A) Lateral line canal-bearing bones in a fresh water teleost, the convict cichlid (*Amatitlania nigrofasciata = Archocentrus nigrofasciatus*, Cichlidae, Perciformes; from Tarby & Webb, 2003). **B)** *Argyropelecus* sp. (Sternoptychidae, Stomiiformes). **C)** *Gonostoma elongatum* (Gonostomatidae, Stomiiformes). Images in B-C are from Gregory (1933).Canals color-coded: supraorbital (SO) canal = blue, infraorbital (IO) canal = red, mandibular (MD) canal = yellow, preopoperular (PO) canal = pink, otic (OT) canal = green, supratemporal commissure (ST) = orange, post-otic (PT) canal = purple. Bones containing canals: nasal (na), frontal (fr), lacrimal (la), infraorbital series (io), preopercle (po), pterotic (pt), lateral extrascapular (le), medial extrascapular (me), posttemporal (pe), dentary (de), and angular-articular (aa) or unfused angular (ang) and articular (art). Also see µCT images in Fig. 1.7, 1.16.

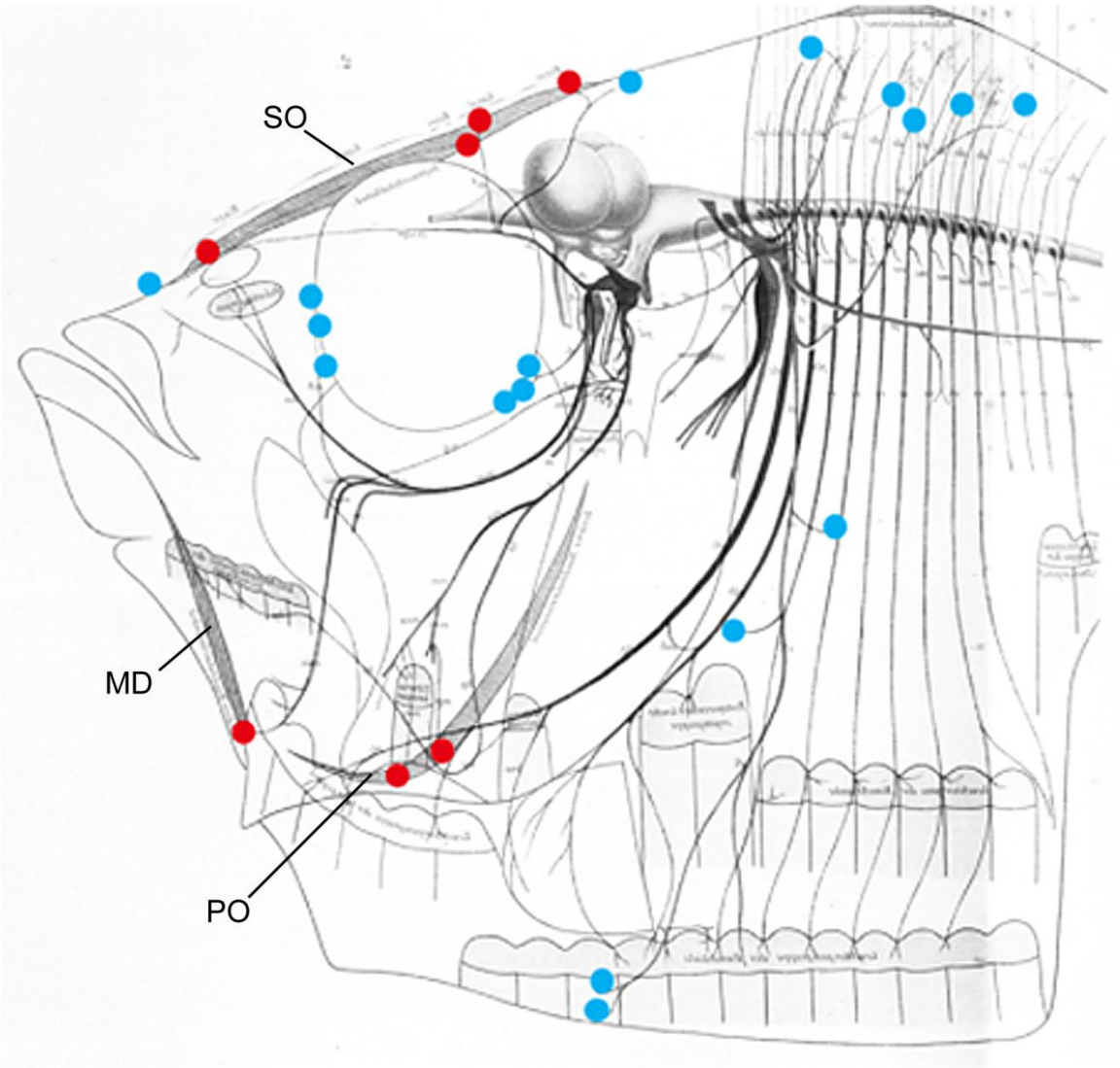

Figure 1.5: Neuromasts and lateral line canals in *Argyropelecus hemigymnus* (Sternoptychidae, Stomiiformes) showing supraorbital (SO), mandibular (MD), and preopercular (PO) lateral line canals and the innervation of a few canal (red circles) and superficial (blue circles) neuromasts (enlarged for emphasis). Note that only 24 neuromasts are illustrated. Modified from Handrick (1901).

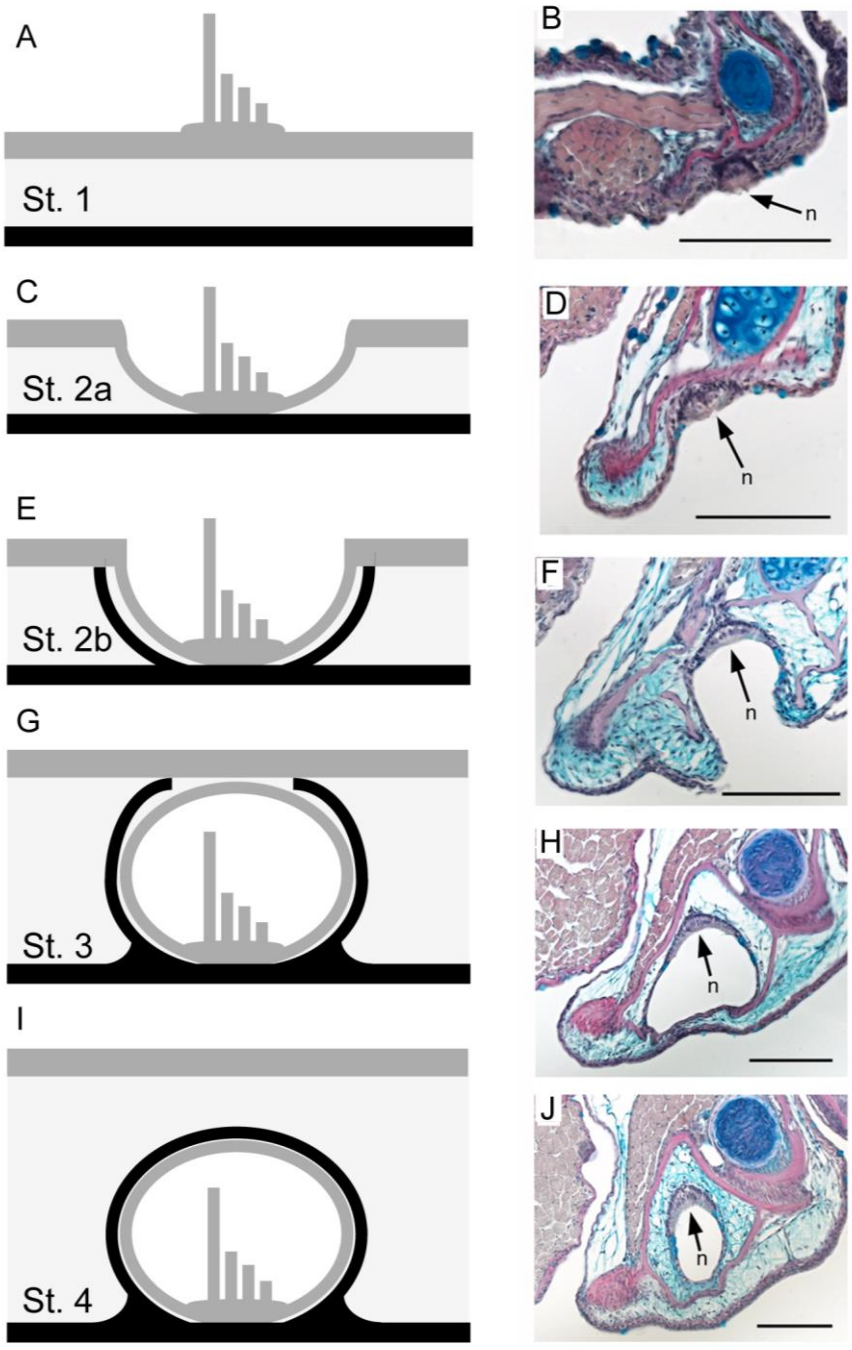

Figure 1.6: Stage in the development of lateral line canal segments in teleost fishes. A, C, E, G, I) Stages in canal segment development as defined in Bird and Webb (2014). Bone = black, epithelium = dark grey, neuromasts with hair cell bungle = dark grey. **B, D, F, H, J**) Representative histological sections of the MD canal in *Tramitichromis* sp. (Cichlidae, Perciformes). Bone (red) and neuromasts (n). Scale bars = 100 µm. Stage 1: a neuromast sits superficially in epithelium (**A, B**). Stage 2a: neuromast sinks into a depression in the skin (**C, D**), Stage 2b: neuromasts sits in a bony trough (**E, F**), Stage 3: neuromast sits in a bony trough and is enclosed by soft tissue (**G, H**), Stage 4: neuromast sits in a canal with ossified roof (**I, J**). From Bird and Webb (2014).

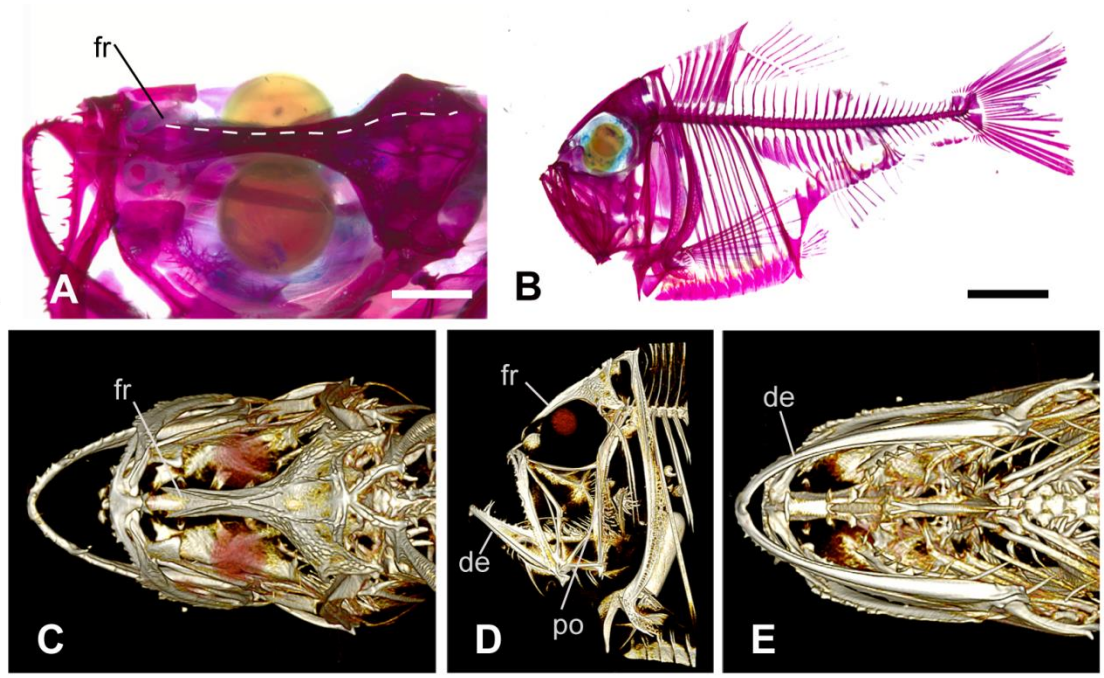

Figure 1.7: Osteology of *Argyropelecus* spp. in cleared and stained specimens (A, B) and µCT imaging (C-E). A) *A. lychnus* cleared and stained (26 mm SL) in dorso-lateral view with right longitudinal bony ridge outlined by white dashed line. Scale = 1 mm. **B)** lateral view of *A. lychnus*. Scale = 5 mm. **C**) 3-D µCT reconstruction of *A. aculeatus* (MCZ 137835, size unknown) in dorsal view, **D)** lateral view, and **E)** ventral view. Bones associated with lateral line canals: frontal (fr), dentary (de), preopercle (po).

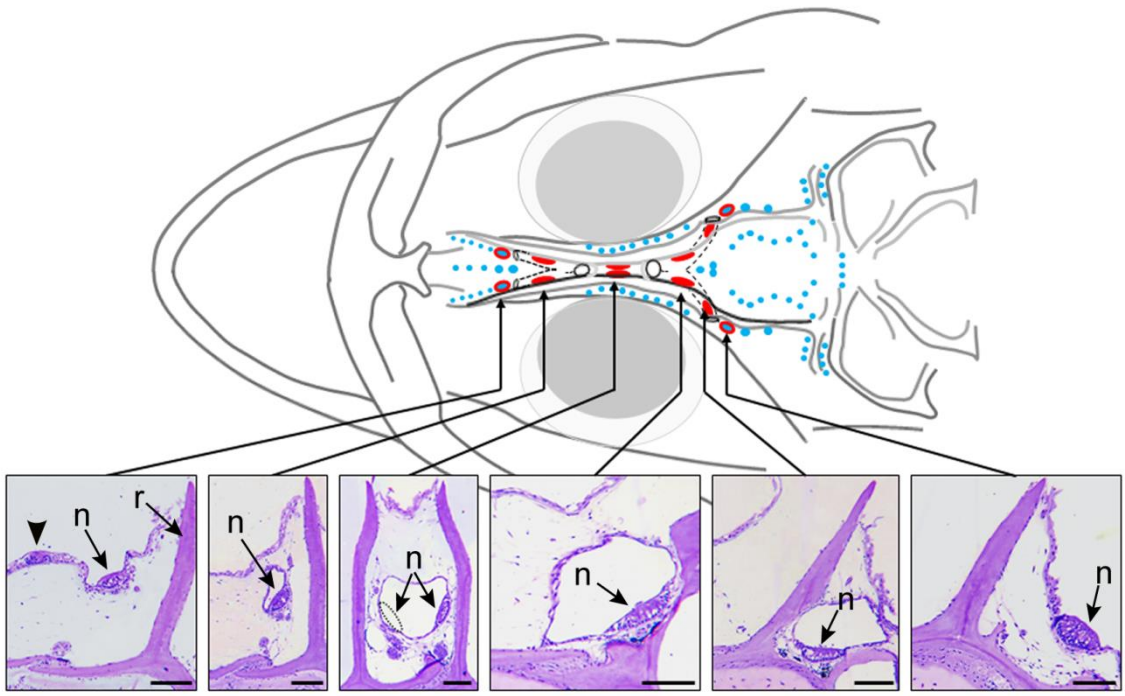

Figure 1.8: Supraorbital canal and neuromast morphology in *Argyropelecus aculeatus*. Line drawing (in dorsal view) derived from a 3-D µCT reconstruction of one specimen (MCZ 137835, size unknown). SO canal and superficial neuromast distributions based on histology (3 individuals) and examination of 11 whole specimens. Superficial neuromasts (blue), canal neuromasts (red), canal neuromast homologues on the skin surface (blue circles with red outline), canal boundaries (black dotted lines), canal pores (black open circles). Representative transverse histological sections of (MCZ 159086, 39 mm SL specimen) at the level of each neuromast (n) from left to right (= rostral to caudal) showing the canal moving from the medial to the lateral side of a bony ridge (r). n = SO canal neuromasts, black arrowhead = superficial neuromasts. Scales = 100 µm.

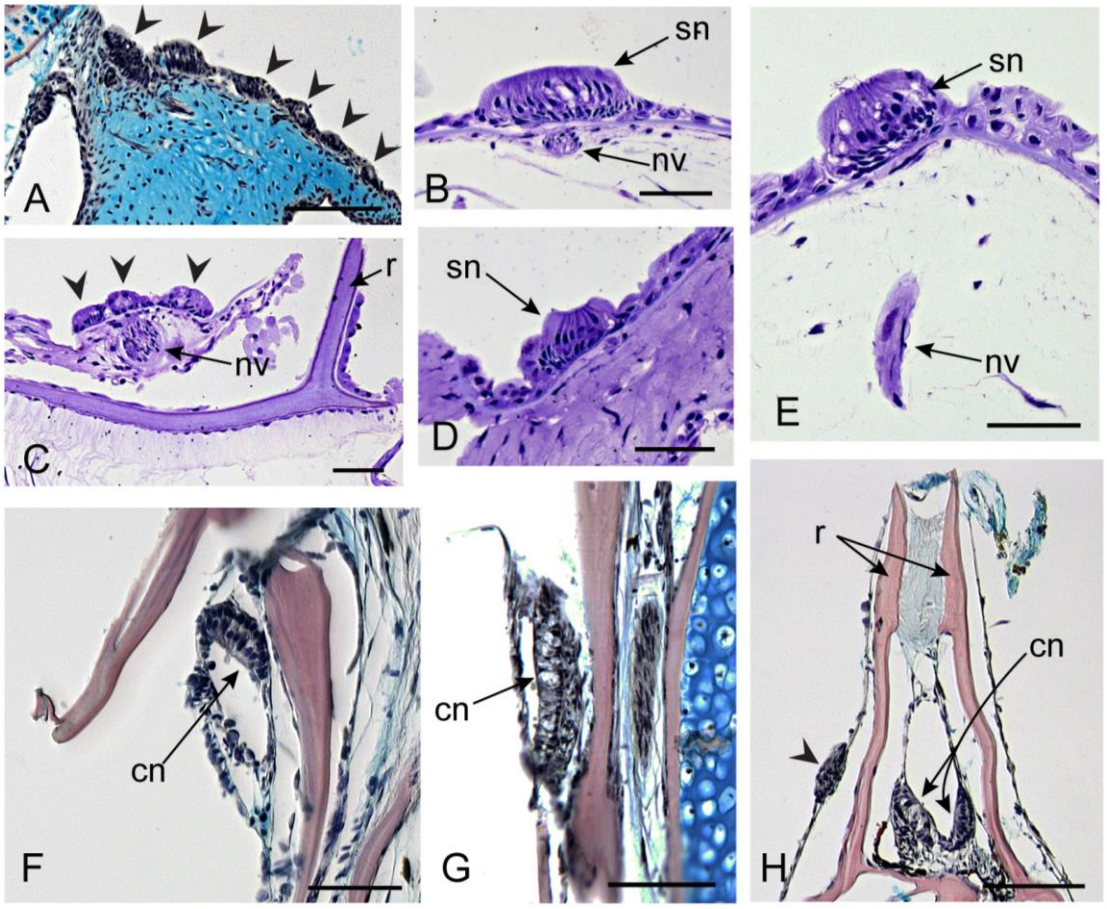

Figure 1.9: Histology of canal and superficial neuromasts in *Argyropelecus aculeatus* (26 – 39 mm SL). A) Six superficial neuromasts (black arrowheads) near the nares. Scale = 100 µm. **B)** Larger superficial neuromast (sn) with nerve (nv) innervation. Scale = 50 µm**. C)** Three superficial neuromasts (black arrowheads) medial to the longitudinal bony ridge in the frontal bone (r),innervated by nerve (nv). Scale = 50 µm. **D)** Superficial neuromast (sn). Scale = 50 µm. **E)** Superficial neuromast (sn) with nerve (nv). Scale = 50 µm. **F)** MD canal neuromast (cn) in partially ossified (St. 3) canal (red). Scale = 50 µm. **G)** PO canal neuromast (cn) in a partially ossified (St. 3) canal, but canal bone forming trough is not visible in this section. Scale = 100 µm. **H)** SO canal neuromasts (cn) sitting side by side in the partially ossified medial canal, medial to the longitudinal bony ridge (r). Superficial neuromast (black arrowhead) sits in the skin lateral to the bony ridge. Scale = 100 µm.

Figure 1.10: Schematic representations of canal and neuromast distribution in *Argyropelecus* spp. (see next page). **A)** *A. aculeatus* based on histology of 3 specimens (26 – 39 mm SL) and 11 whole preserved specimens (26 – 40.5 mm SL); outline from an illustration of a 46 mm SL specimen. **B)** *A. affinis* based on a whole preserved specimen (49 mm SL). Outline from an illustration of a 51 mm SL specimen. **C)** *A. hemigymnus* based on 5 whole preserved specimens (30 – 33 mm SL). Outline from an illustration of a 30 mm specimen. Superficial neuromasts (blue), canal neuromasts (red), canal boundaries (black dotted lines), canal pores (black open circles). Neuromasts enlarged, not to scale. Outlines from Baird (1971).

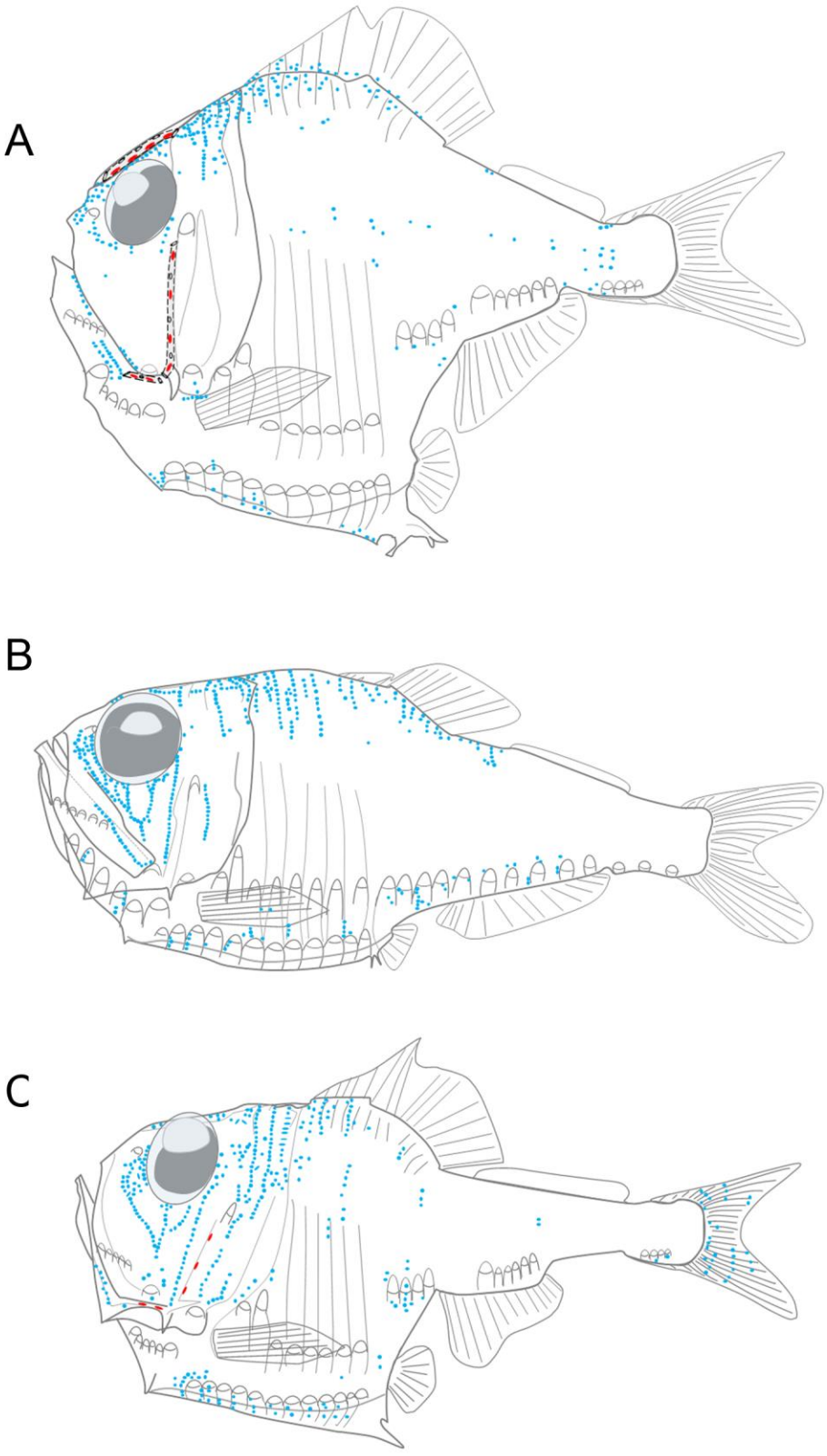
A
B
C

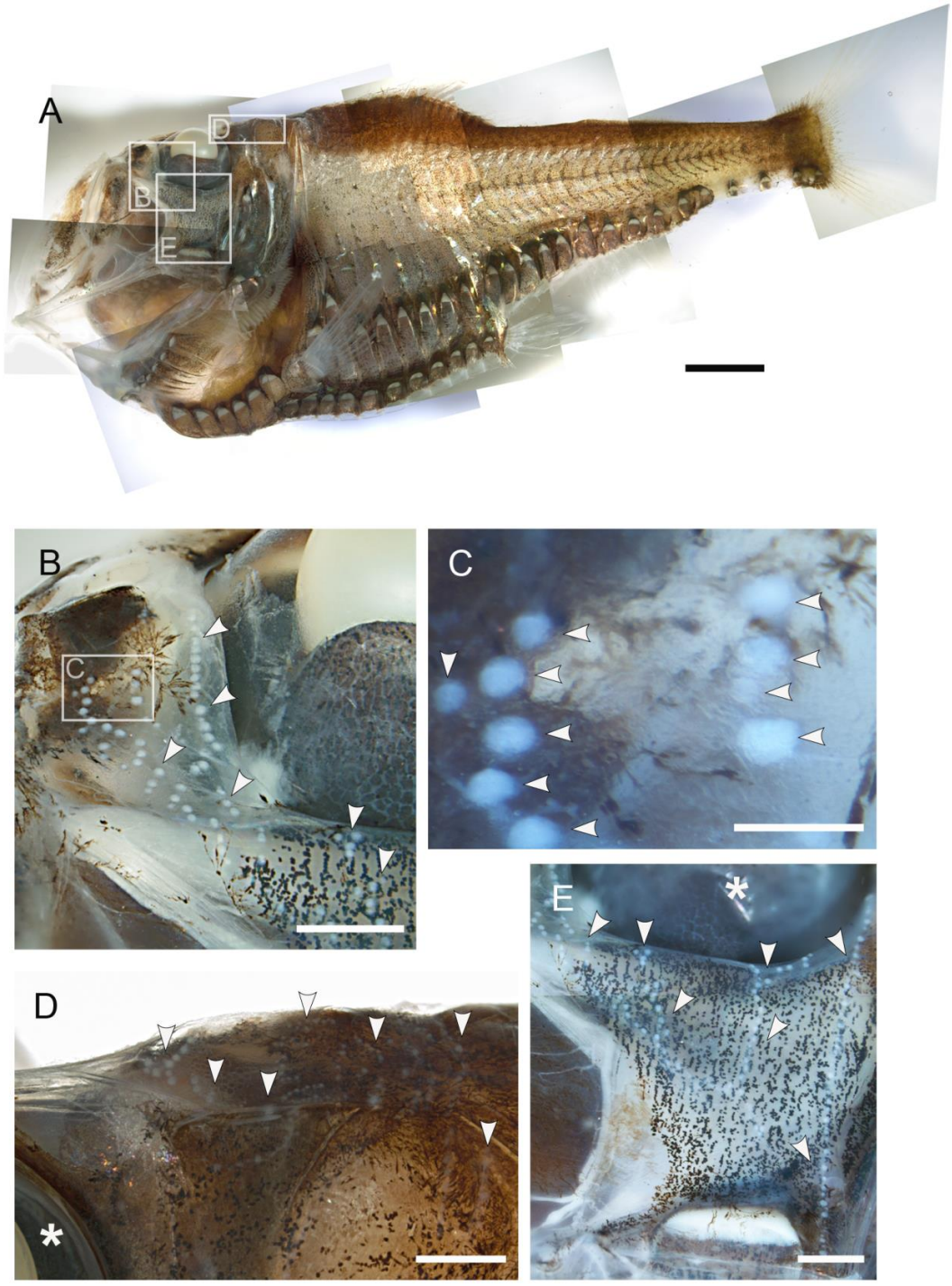

Figure 1.11: Putative superficial neuromasts (= "white dots") on the head of *Argyropelecus affinis*. **A)** Composite image of *A. affinis* (49 mm SL) showing areas enlarged in B, D, and E. Scale = 5 mm. **B)** Close up rostral to the eye (see box B). Scale = 1 mm. **C)** Close up of white dots rostral to eye (see box C). Scale = 0.25 mm. **D)** Close up of white dots dorsal and caudal to eye (see box D, in dorso-lateral view of head medial to the longitudinal bony ridges caudal to the orbit. Scale = 1 mm. **E)** Close up of vertical lines of white dots ventral to the orbit (see box E). Scale = 1 mm. Asterisk = eye in D, E; arrowheads = superficial neuromasts.

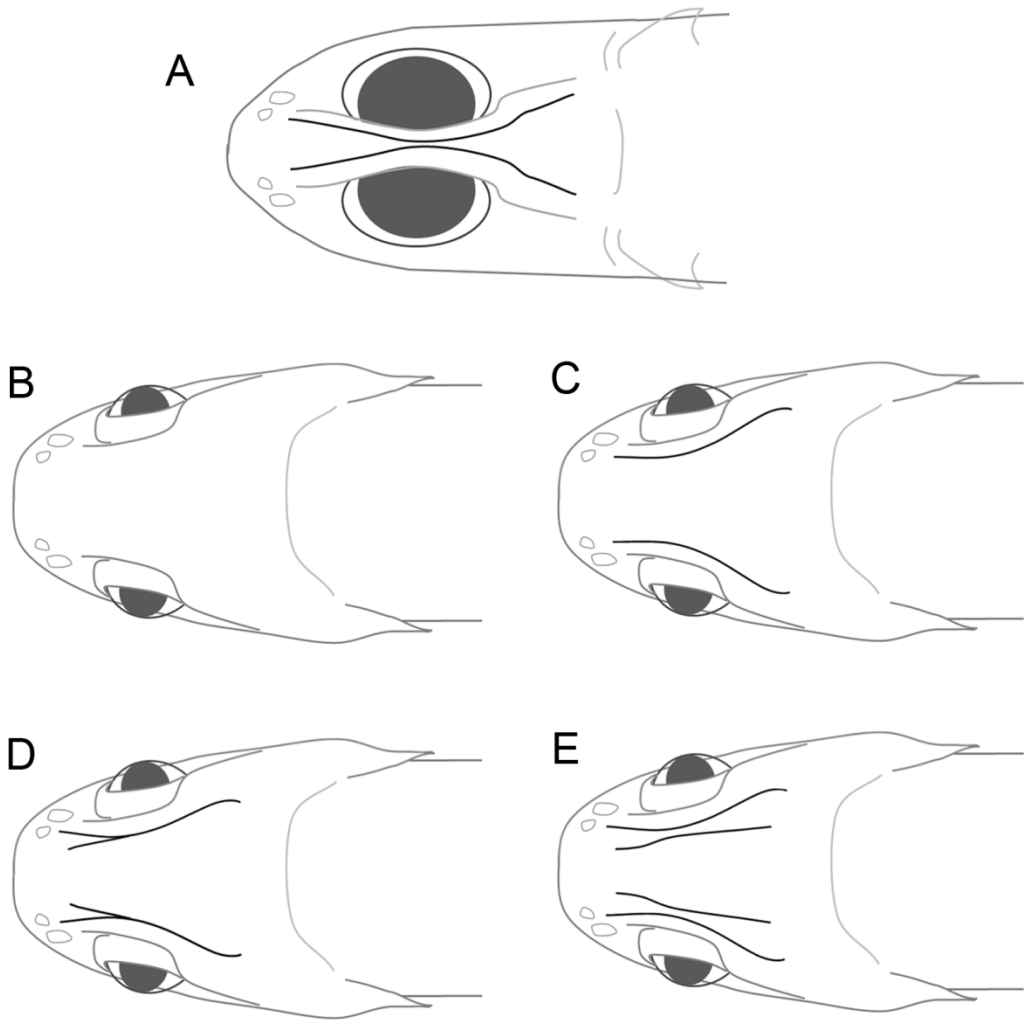

Figure 1.12: Longitudinal bony ridges on the dorsal surface of the head in stomiiform fishes. A) One pair of bilaterally symmeterical longitudinal ridges extends from the right and left frontal bones and meet (but do not fuse) medial to the orbits, as in *Argyropelecus* and *Ichthyococcus.* **B)** No ridge is present in *Cyclothone* and *Bathophilus*. **C)** One pair of longitudinal ridges extends from the frontal bone, but do not meet or fuse medially, as in *Aristostomias*, *Idiacanthus*, *Pachystomias*, and *Tactostoma.* **D)** One pair of longitudinal ridges extends from the frontal bone. Each ridge is split into two separate ridges rostral to the orbit, but fuse into a single ridge as each moves caudally, as in *Gonostoma* , *Echiostoma*, and *Eustomias.* **E)** Two pairs of longitudinal bony ridges extend from the frontal bone, but never meet or fuse medially, as in *Astronesthes* and *Opostomias*.

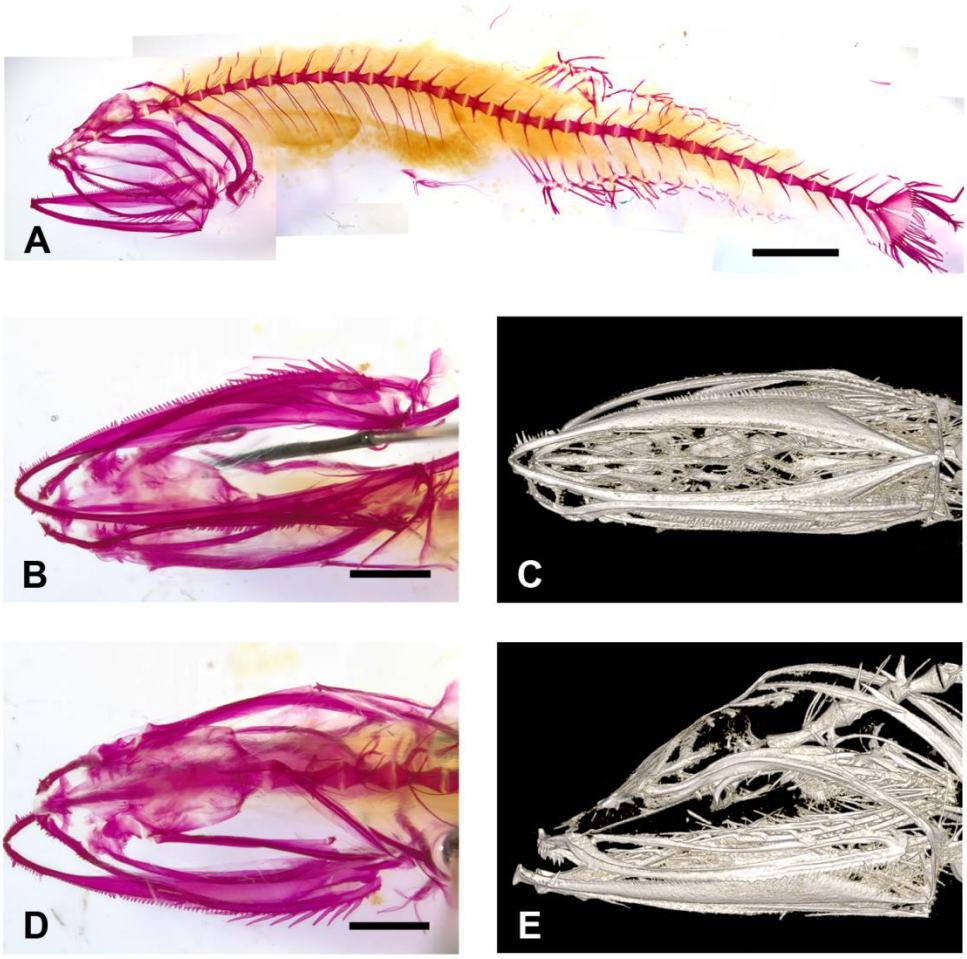

Figure 1.13: Osteology of *Cyclothone* spp. based on cleared and stained specimen and µCT imaging (Gonostomatidae: Stomiiformes). Ossified cranial lateral line canals are completely absent. Cleared and stained *C. acclinidens* (20.5 mm SL; gill arches removed) in **A)** lateral (scale = 5 mm), **B)** ventral (scale = 2 mm), and **D)** Dorso-lateral (scale = 2 mm) views. 3-D µCT reconstruction of *C. microdon* (MCZ 89489) in **C)** ventral and **E)** lateral views.

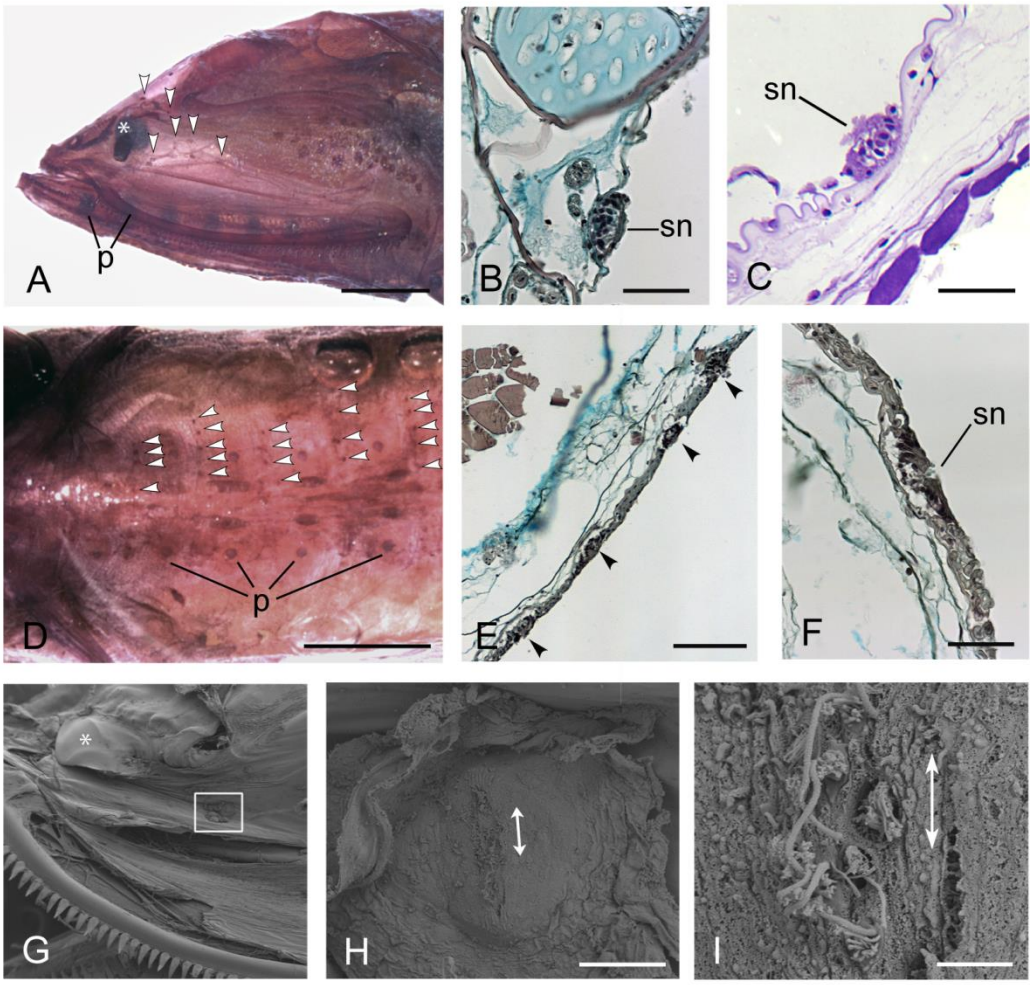

Figure 1.14: Superficial neuromasts in *Cyclothone* spp. A) Lateral view of the head of *C. signata* (26.5 mm SL) stained with hematoxylin. Eye (asterisk), rostral-most photophores (p), stained superficial neuromasts (white arrowheads). Scale = 1 mm. **B)** Superficial neuromast (sn) on the lower jaw of *C. microdon* (52 mm SL). Scale = 50 µm. **C)** Superficial neuromast (sn) on trunk of *C. microdon* (44 mm SL). Scale = 50 µm. **D)** Ventral view of trunk of *C. microdon* (52 mm SL) stained with hematoxylin. Photophores (p), neuromasts (white arrowheads). Scale = 2 mm. **E)** Row of four superficial neuromasts (black arrowheads) ventrally on trunk (*C. microdon*, 52 mm SL). Scale = 100 µm. **F)** Superficial neuromast on trunk (sn) in *C. microdon* (52 mm SL). **G)** SEM of head of *C. braueri* (28 mm SL). Asterisk = eye. **H)** Superficial neuromast in box in G. Double headed arrow = hair cell orientation in sensory strip. Scale = 20 µm. **I)** Close up of the sensory strip in the center of the neuromast in H, showing hair cells. Double headed arrow = hair cell orientation. Scale = 2 µm.

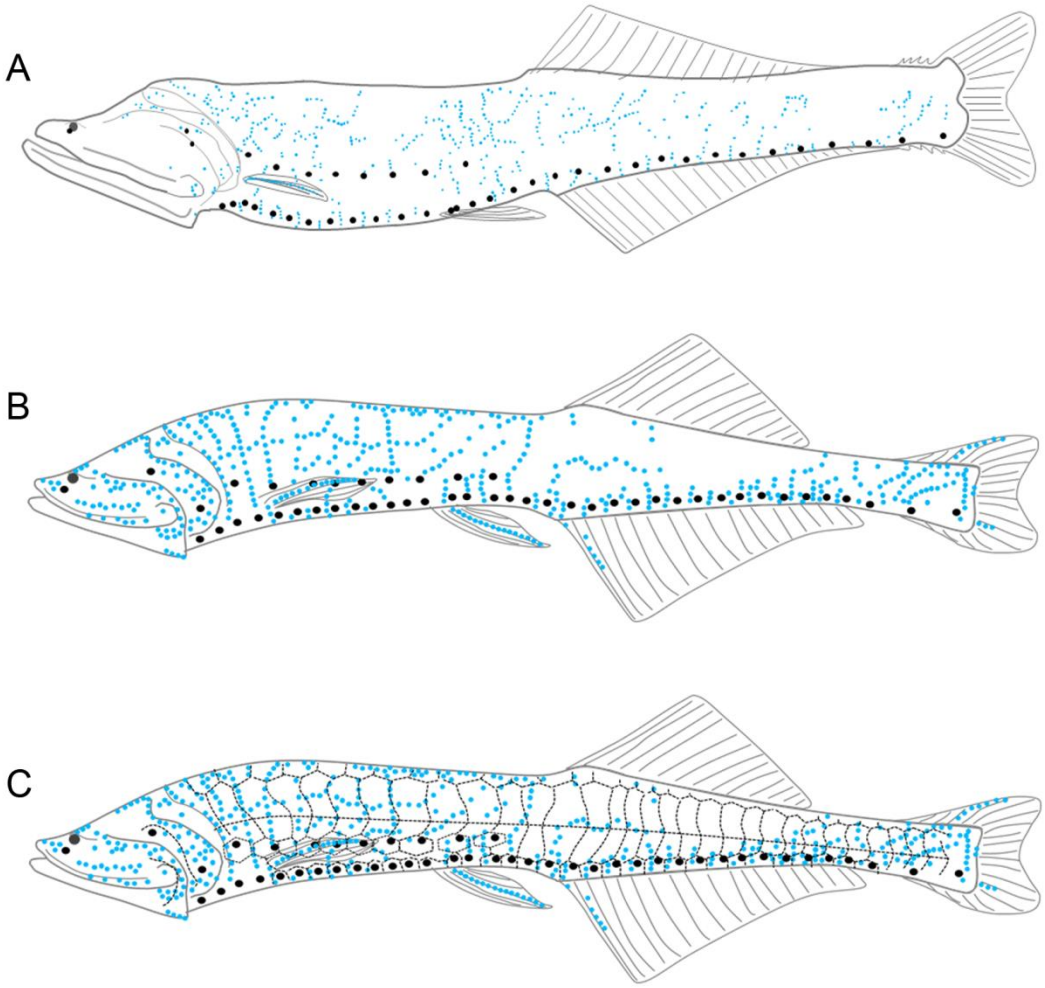

Figure 1.15: Neuromast distribution in *Cyclothone* spp. A) Tracing of *C. microdon* stained with hematoxylin (52 mm SL), **B)** Superficial neuromast distribution based on four *C. microdon* specimens (52 – 60 mm SL). **C)** Composite pattern of SNs with putative nerve branches (dotted black line), based on general distribution and innervation patterns in two *C. acclinidens* (31 – 33 mm SL), two *C. braueri* (28 – 29 mm SL), four *C. microdon* (52 – 60 mm SL) and one *C. signata* (26.5 mm SL). Outlines in B and C from a 34.5 mm SL specimen illustrated in Mucacheva (1966). Blue dots = superficial neuromasts (enlarged, not to scale), black dots = photophores.

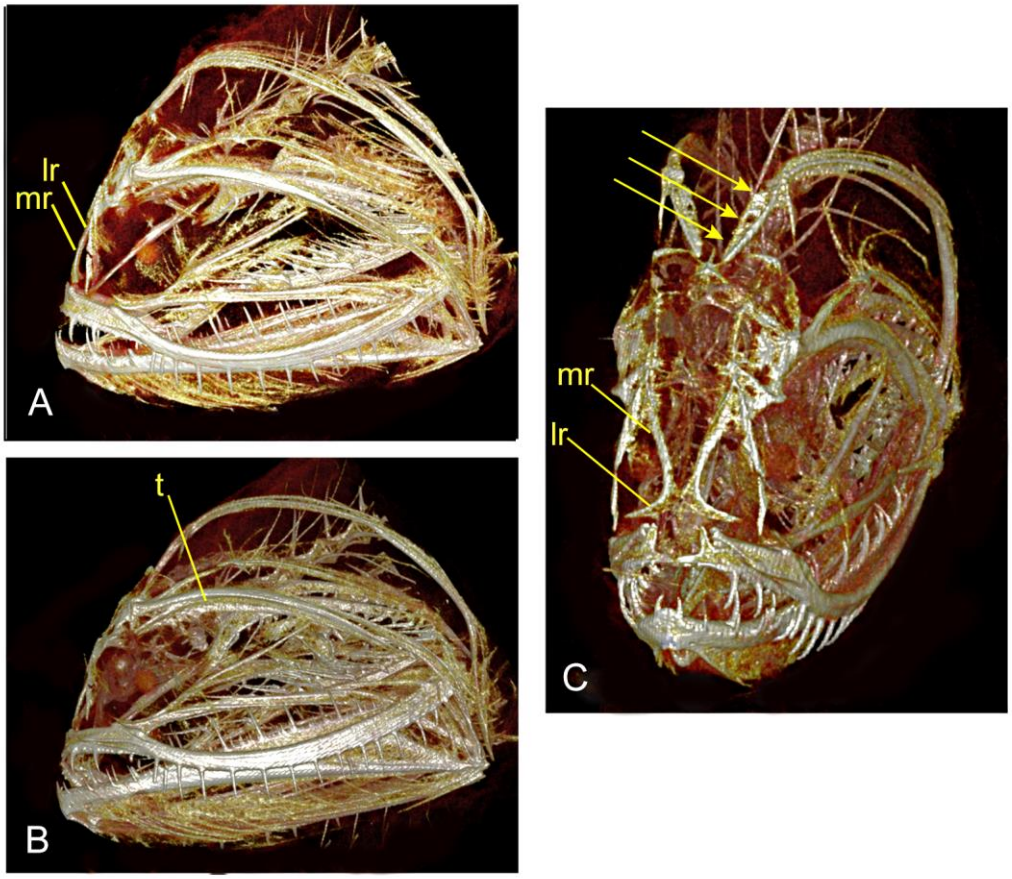

Figure 1.16: Osteology of *Gonostoma elongatum* in µCT reconstruction (Gonostomatidae: Stomiiformes). A) Lateral view showing thin cranial bones and the inner longitudinal ridge (ir) and outer longitudinal ridge (or) extending off the frontal bone. **B)** Ventro-lateral view showing a trough (t) in the preoperculum. **C)** Anterior view showing the inner (ir) and outer (or) longitudinal bony ridges on the frontal bones and bony pores (yellow arrows) associated with a canal in the posterior region of the head. Coloration shows variation in tissue density along a gradient from red (less dense) to white (most dense) tissue.

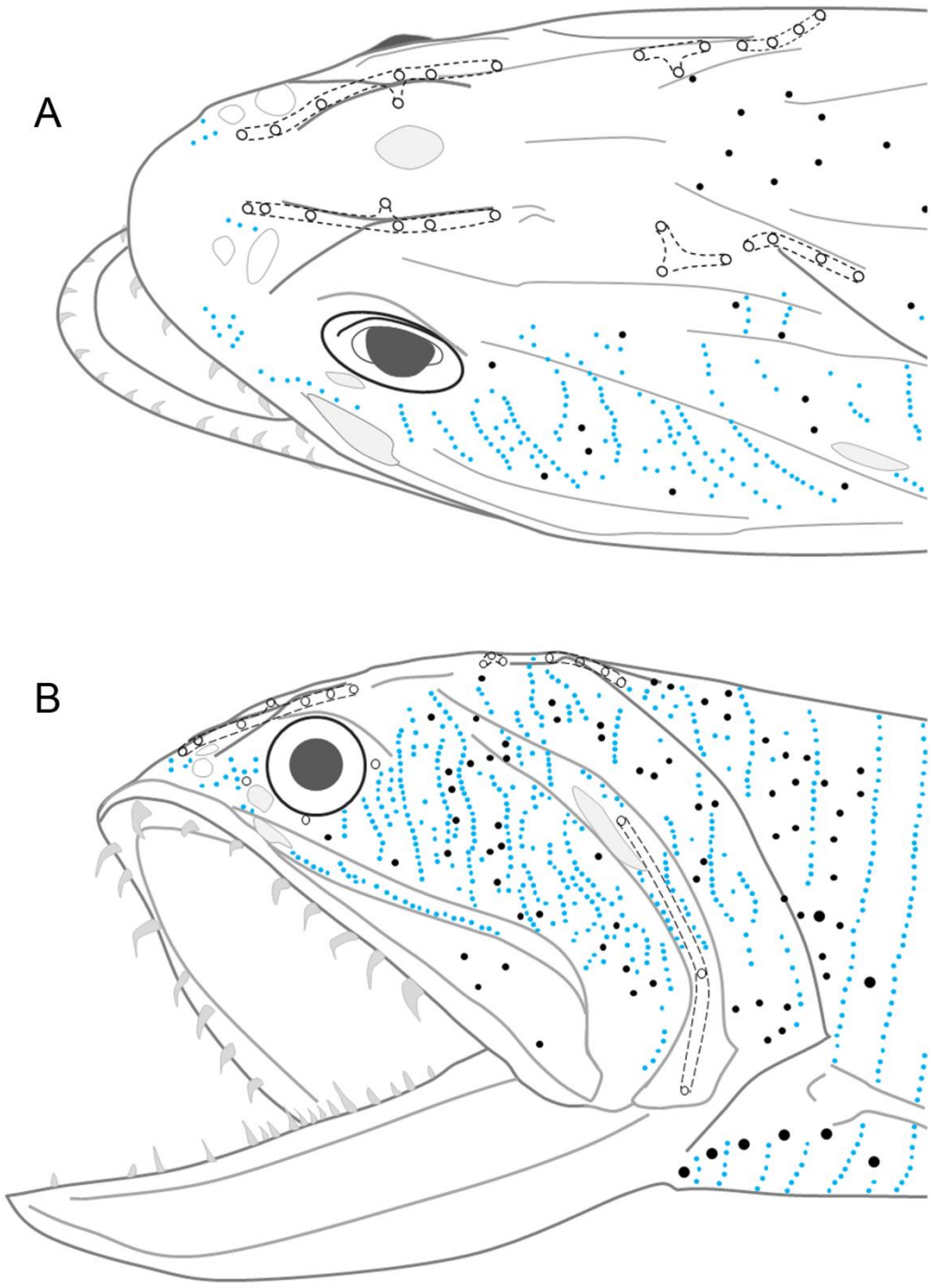

Figure 1.17: Canal and neuromast distribution in *Gonostoma elongatum*. A) Dorso-lateral and **B)** lateral views of *G. elongatum* showing superficial neuromasts (blue dots), and likely locations of lateral line canals (black dotted lines) based on location of pores (open black circles). Prominent luminescent organs = light grey and photophores = closed black circles. Superficial neuromast distribution based on tracing of one specimen (50 mm SL). Pore location based on six specimens (50 - 92 mm SL).

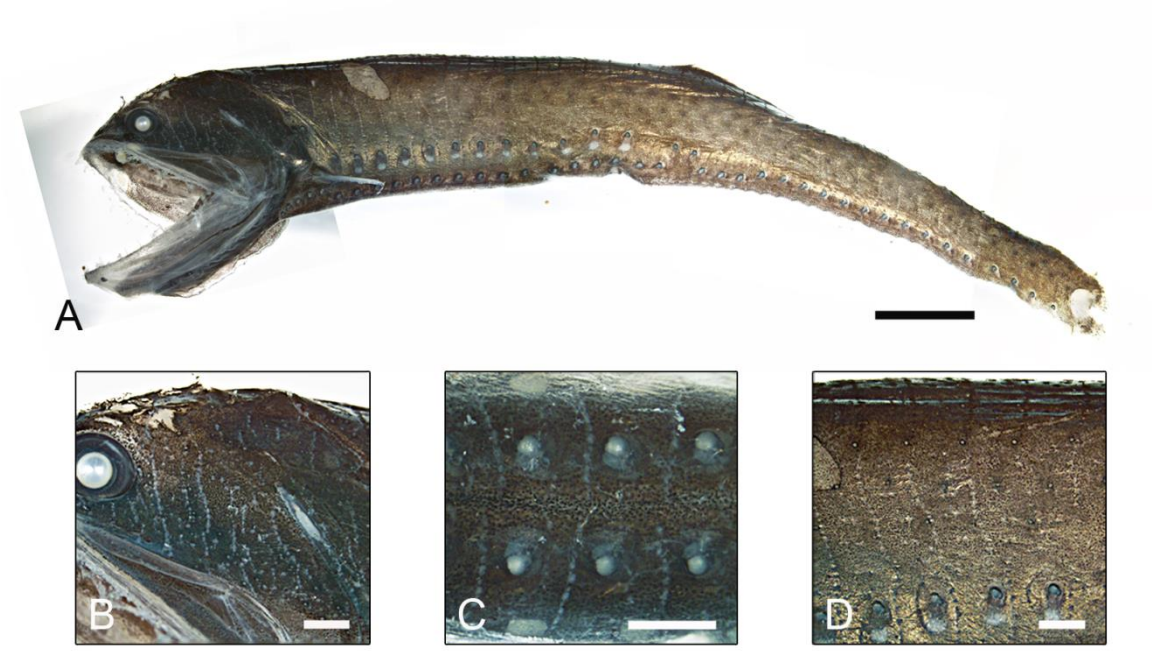

Figure 1.18: Distribution of putative superficial neuromasts in *Gonostoma elongatum* (50 mm SL). **A)** Composite image of specimen. Scale = 5 mm. **B)** Close up of the vertical lines of superficial neuromasts (= white dots) ventral to the eye from box in A. Scale = 1 mm. **C)** Ventral view of the trunk, caudal to the pectoral fins, showing lines of superficial neuromasts between major photophores. Scale = 1 mm. **D)** Close up of the vertical lines of superficial neuromasts and depressions (as in Fig. 1.21) on the trunk in lateral view. Scale = 1 mm.

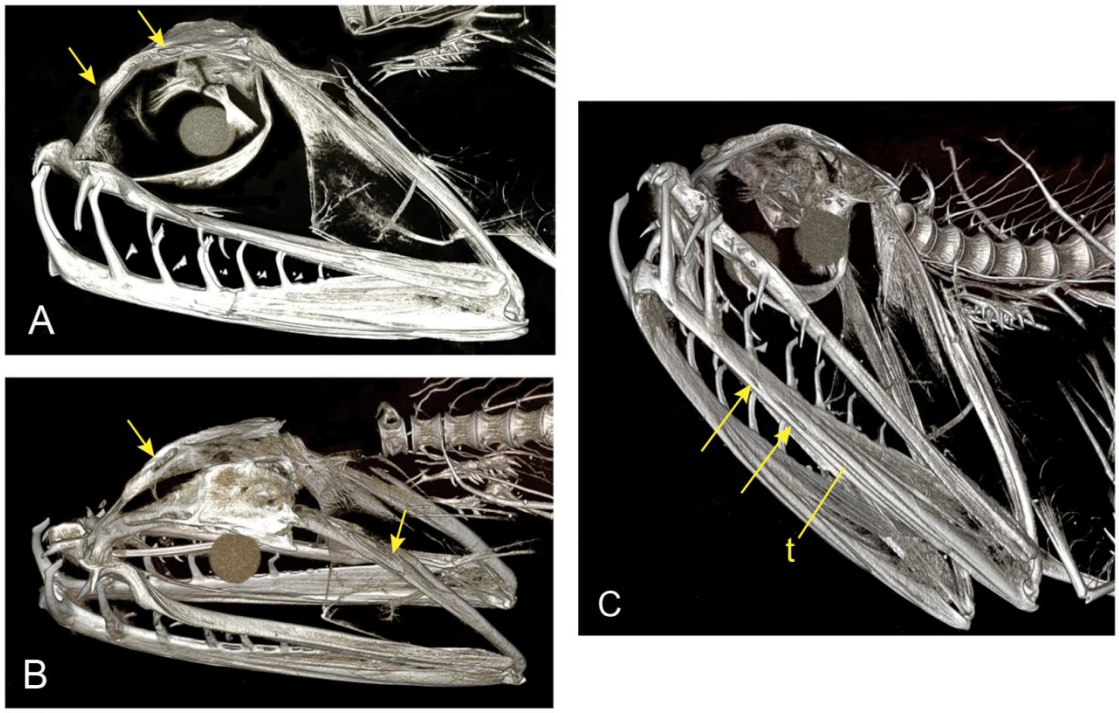

Figure 1.19: Osteology of *Aristostomias tittmani* in µCT reconstructions (Stomiidae: Stomiiformes). **A)** Lateral view with SO canal pores (yellow arrows). **B)** Dorso-lateral view of SO and PO canal pores (yellow arrows) and **C)** Ventro-lateral view showing MD canal pores (yellow arrows) followed by a trough (t) in the dentary, interpreted as a continuation of the MD canal.

Figure 1.20: Transverse histological sections of superficial and canal neuromasts in *Astronesthes niger* (MCZ 52847; 52 mm SL; Stomiidae: Stomiiformes). (see next page). **A)** Row of four superficial neuromasts (black arrowheads) ventral to a minute photophore (p) on the head. Scale = 100µm. **B)** Close up of the superficial neuromasts from A. Scale = 50 µm. **C)** Row of four superficial neuromasts (black arrowheads) rostral to the eye, superficial to photophores (p) that are directed into the eye. Scale = 100 µm. **D)** Row of four superficial neuromasts (black arrowheads). Scale = 50 µm. **E)** IO canal neuromast (cn) in an incompletely ossified canal (St. 3) with two superficial neuromasts (black arrowheads) sitting in the skin. Scale = 100 µm. **F)** SO canal neuromast (cn) in a completely ossified canal (St. 4) showing the nerve (n) innervating the neuromast. Scale = 100 µm. **G)** Close up of a single superficial neuromast. Pigment is visible forming a depression in the tissue underlying the neuromasts. Scale = 40 µm. **H)** Close up of SO canal neuromast (cn) in a fully ossified canal (St. 4). Scale = 50 µm.

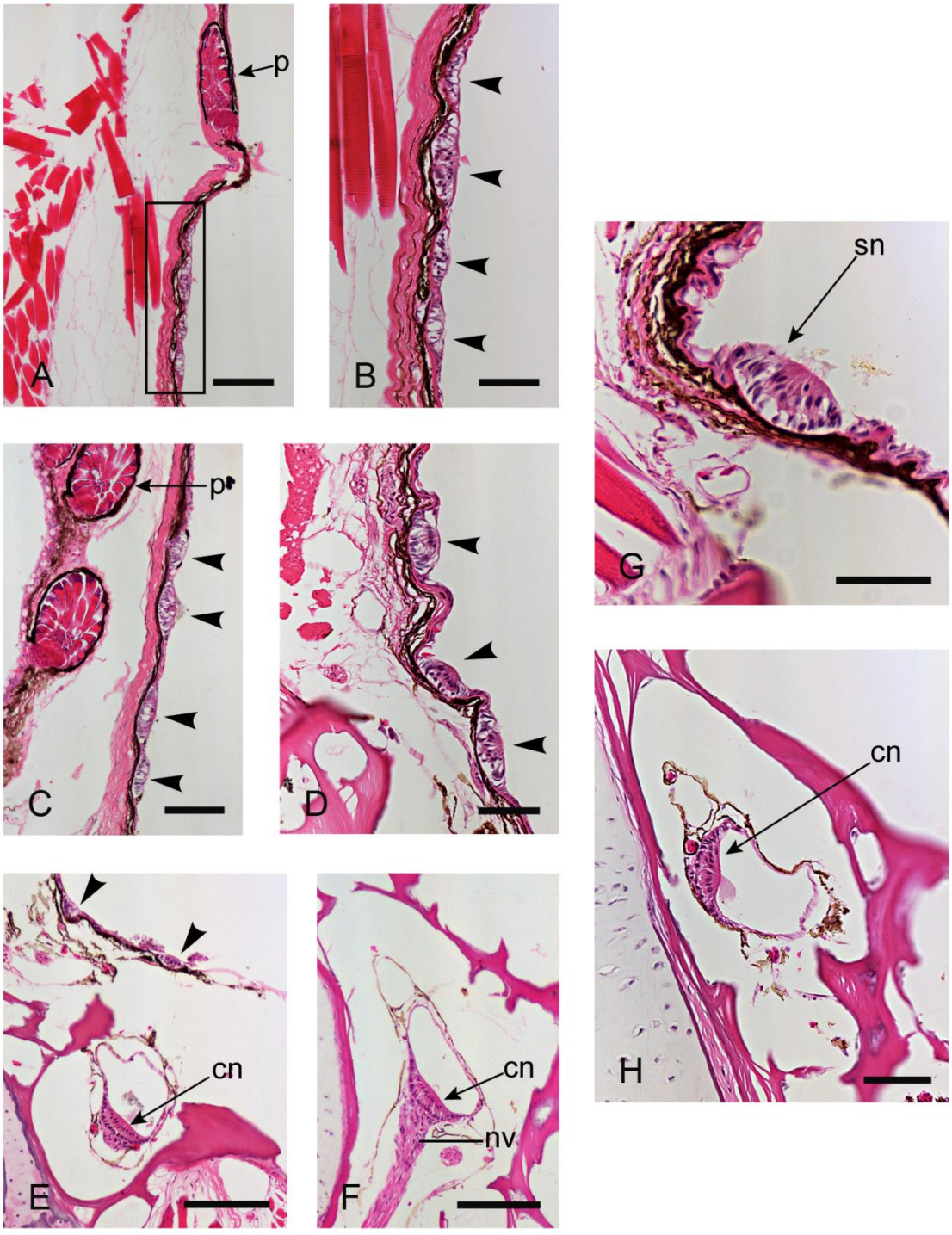
p
A
B
sn
G
p
C
D
cn
H
cn
E
cn
nv
F

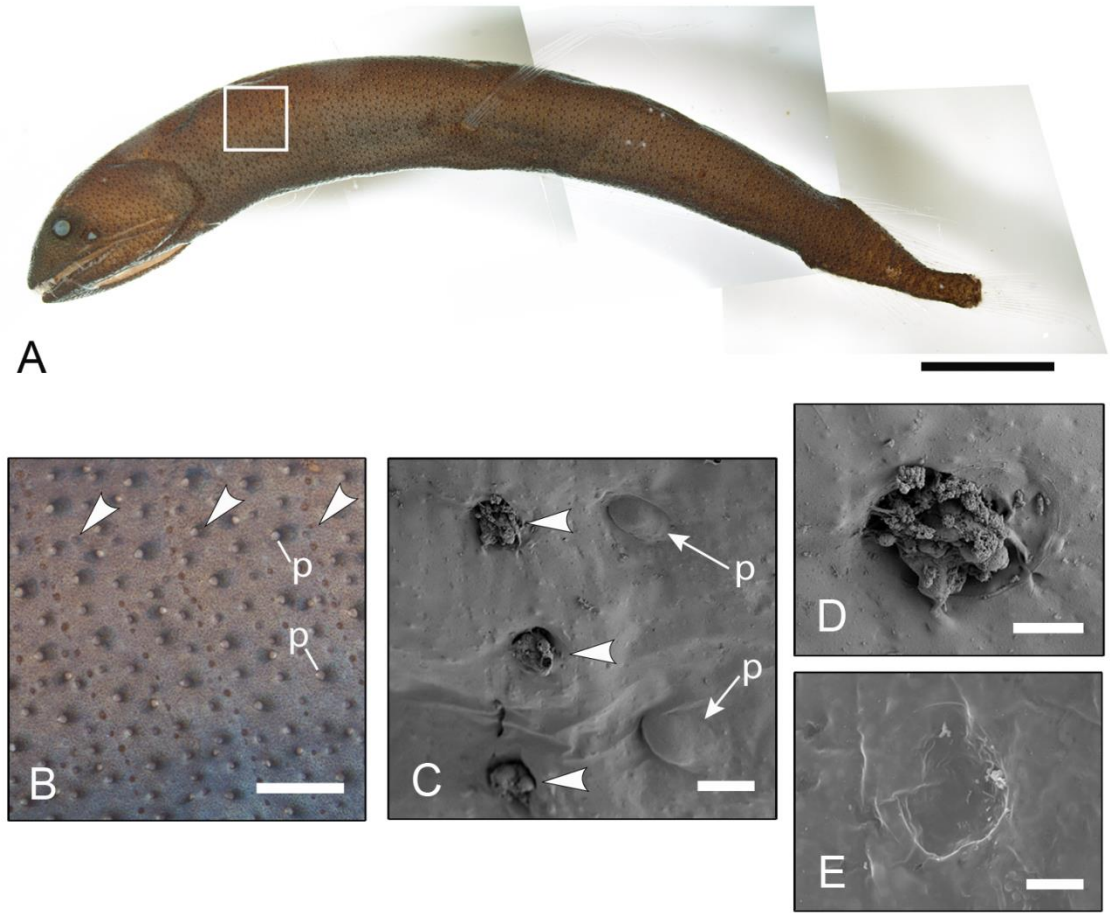

Figure 1.21: Brown depressions in the skin of *Bathophilus filifer* (Stomiidae: Stomiiformes). A) Composite image of a *Bathophilus filifer* specimen (46 mm SL). Scale = 5mm. **B)** Close up of skin (from box in A) showing multiple minute photophores (p) and lines of brown depressions in the skin (white arrowheads). Scale = 0.5 mm. **C)** SEM of skin showing a line of depressions in the skin (arrowheads) and photophores (p). Scale = 20 μm. **D)** Close up of the depressions in the skin shown with debris and **E)** without debris. Scale = 10 μm (D - E).

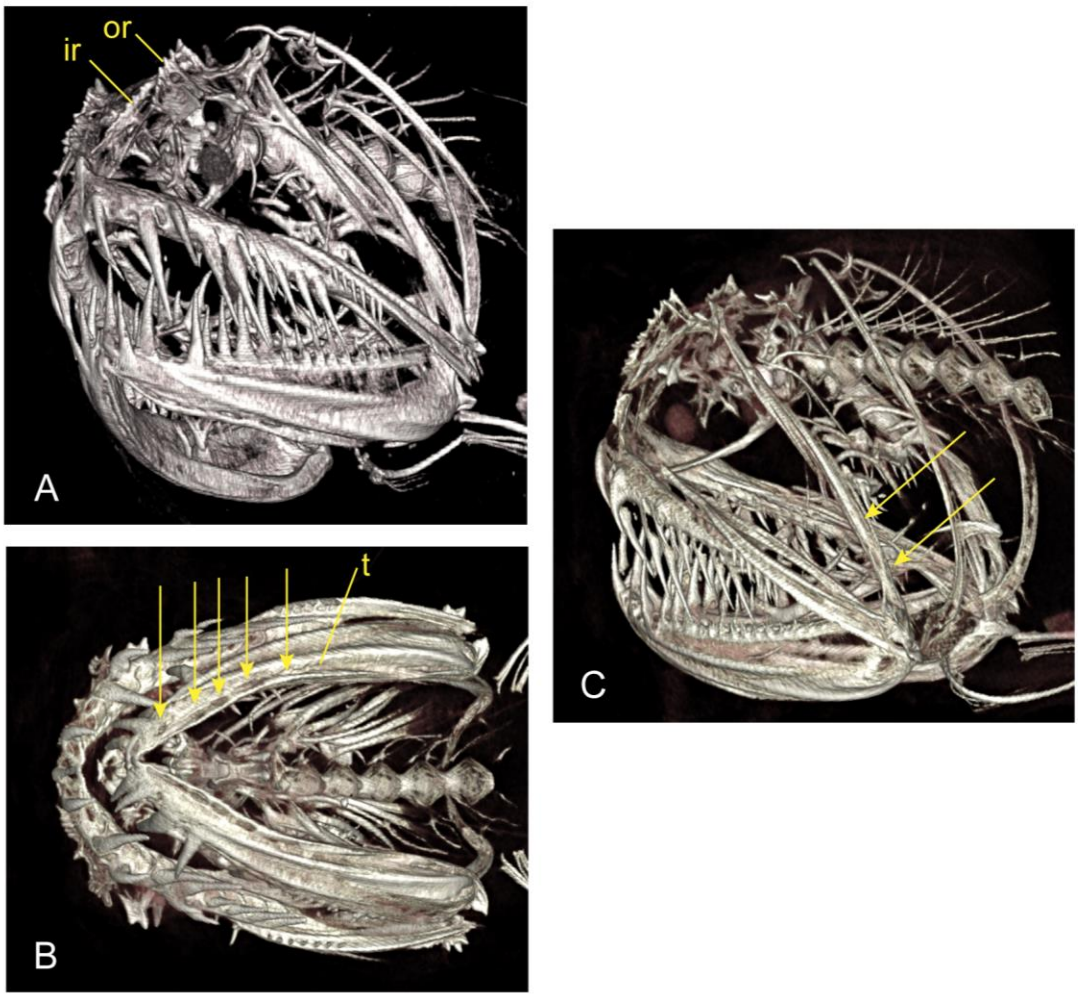

Figure 1.22: Osteology of *Echiostoma barbatum* using µCT 3-D reconstruction (Stomiidae: Stomiiformes). A) anterior view showing the medial (mr) and lateral (lr) bony ridges extending off the frontal bone associated with the SO canal. **B)** Ventral view showing bony MD canal pores (yellow arrows) followed by a trough (t) interpreted as an incompletely ossified continuation of the MD canal. **C)** Lateral view showing bony PO canal pores (yellow arrows).

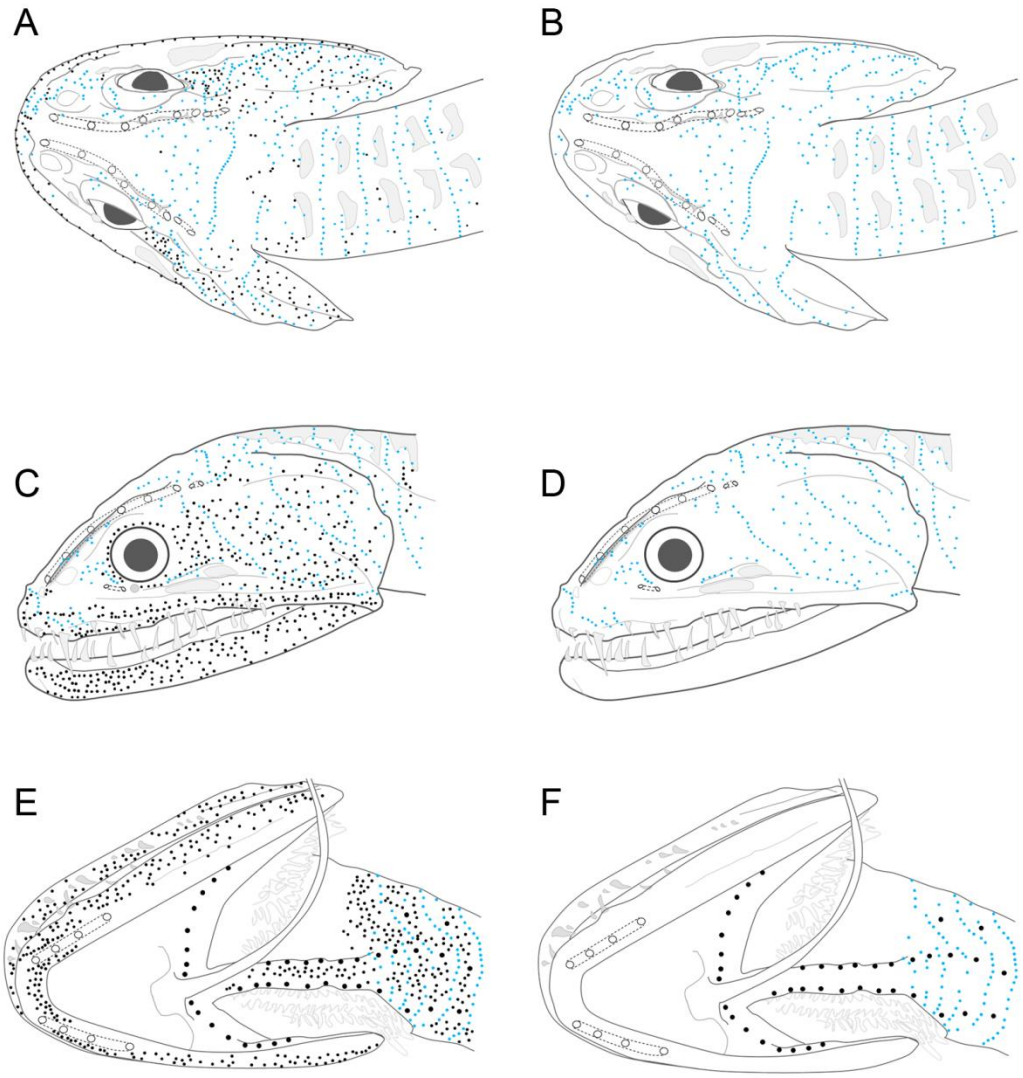

Figure 1.23: **Canal, neuromast and photophore distribution in *Idiacanthus antrostomus* (Stomiidae: Stomiiformes). A-B)** Dorsal **C-D)** lateral, and **E-F)** ventral views of *I. antrostomus* showing superficial neuromasts (blue dots), and likely locations of lateral line canals (black dotted lines) based on location of canal pores in the epithelium (open black circles). Prominent luminescent organs = light grey and photophores = closed black circles. **B, D, F)** Photophores removed (except for the major ventral photophores in F), showing only the lateral line morphology. Superficial neuromast distribution based on tracing of a single specimen (79 mm SL) and pore location (n = 2 specimens, 49 – 79 mm SL).

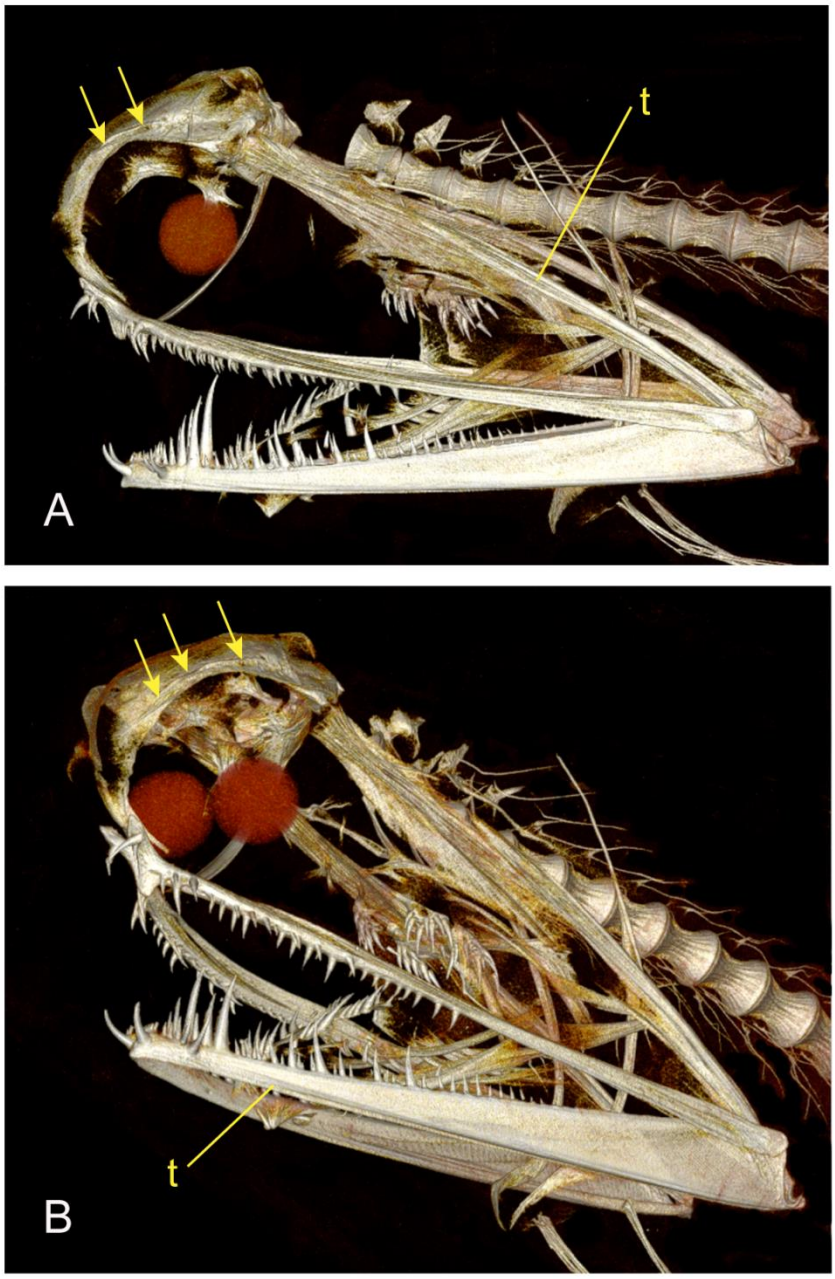

Figure 1.24: **Osteology of *Malacosteus* sp. in µCT reconstruction (Stomiidae: Stomiiformes). A)** Lateral view showing bony pores in the SO canal (yellow arrows) and a trough (t) in the preopercle interpreted as a partially ossified PO canal (St. 2b or 3). **B)** Anterior view showing the bony pores of the SO canal (yellow arrows) and a trough (t) in the dentary interpreted as a partially ossified MD canal (St. 2b or 3).

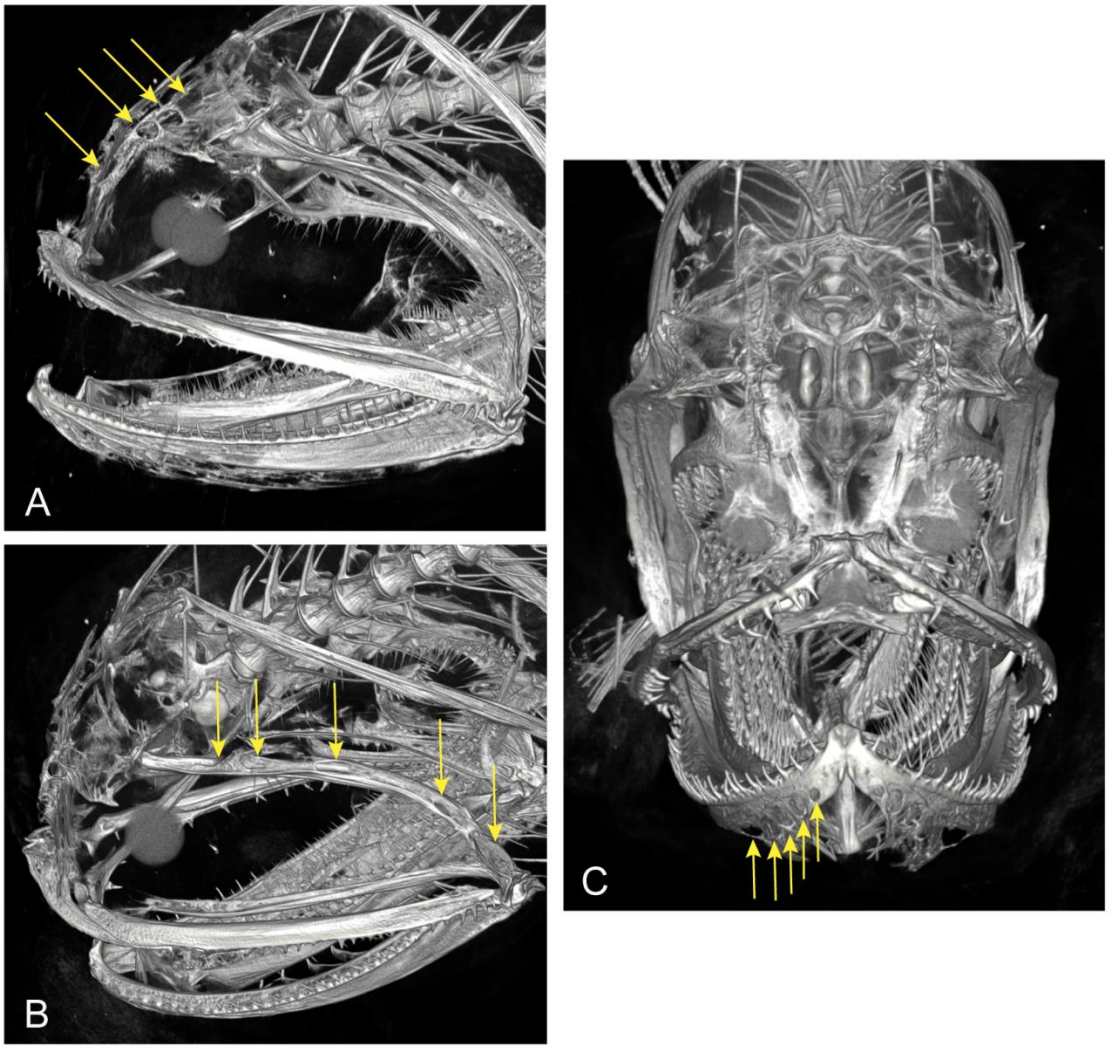

Figure 1.25: Osteology of *Neonesthes capensis* (MCZ 132802; specimen size unknown) in µCT reconstruction (Stomiidae: Stomiiformes). A) Lateral view showing the bony pores of the SO canal, **B)** Dorso-lateral view showing bony PO canal pores, and **C)** anterior view showing the bony pores of the MD canal. Pores = yellow arrows.

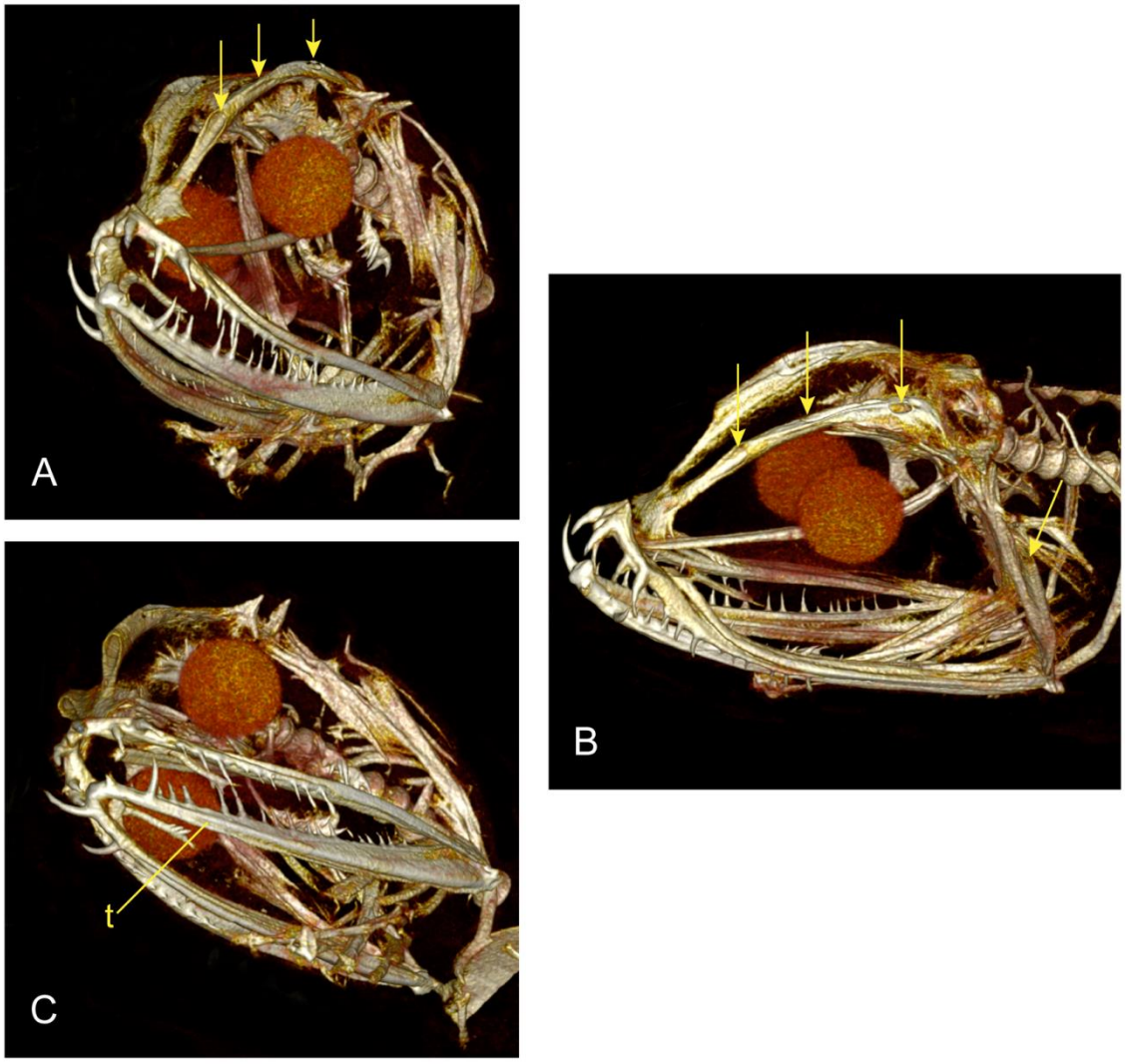

Figure 1.26: Osteology of *Pachystomias* sp. in µCT reconstruction (Stomiidae: Stomiiformes). **A)** Anterior view with visible tube of the SO canal, **B)** Dorso-lateral view showing SO canal pores and evidence of a PO canal, and **C)** Ventro-lateral view showing trough (t) in the dentary interpreted as a partially ossified (St. 2b or 3) MD canal. Canal pores = yellow arrows.

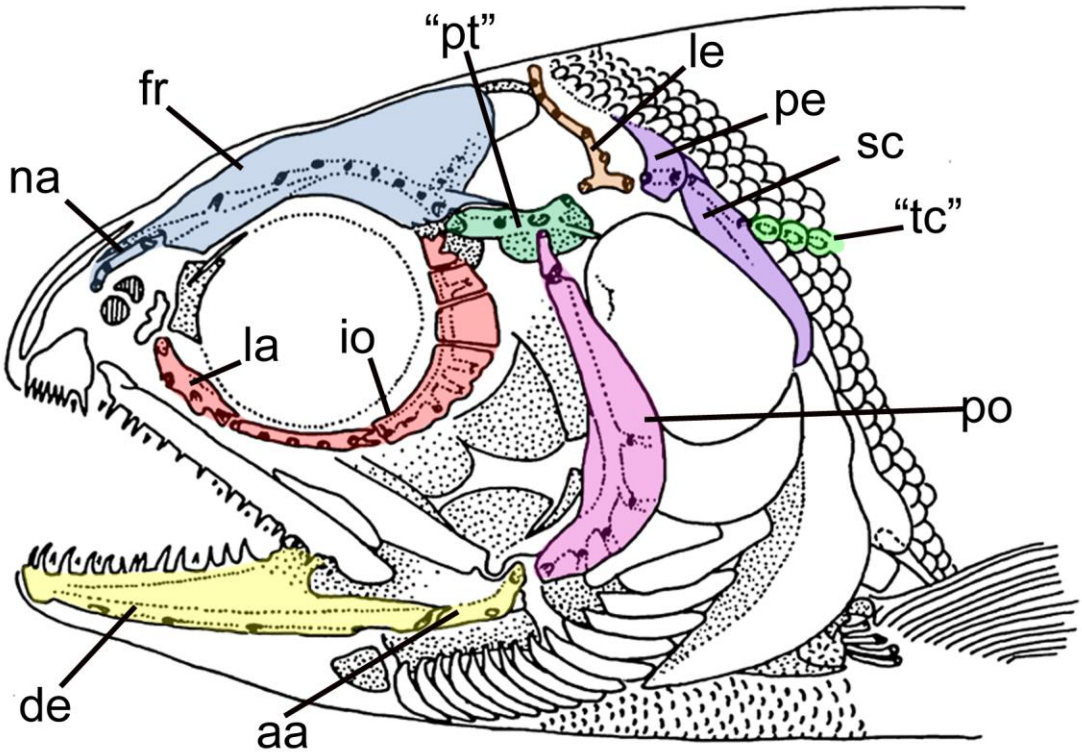

Figure 1.27: Osteology of a salmon (*Oncorhynchus nerka,* Salmoniformes*)*. Modified from Jollie (1984). Based on a 100 mm SL individual. Lateral line canal-bearing bones are color-coded: supraorbital (SO) canal = blue, infraorbital (IO) canal = red, mandibular (MD) canal = yellow, preopoperular (PO) canal = pink, otic (OT) canal = dark green, supratemporal commissure (ST) = orange, post-otic (PT) canal = purple, trunk scales (= "trunk" canal) = light green. Bones containing canals: nasal (na), frontal (fr), lacrimal (la), infraorbital series (io), preopercle (po), intertemporaosupratermporal/ "pterotic" ("pt"), lateral extrascapular (le), medial extrascapular (me), posttemporal (pe),supracleitherum (sc), dentary (de), and angulo-articular (aa), trunk scales ("tc"). Canal names are based on Webb (2014b).

CHAPTER 2

This manuscript has been formatted for submission to the *Journal of Morphology*.

Introduction

Bioluminescence, the production of light by living organisms, is a widespread phenomenon in the poorly lit waters of the deep sea. An estimated 80% of all eukaryotes living in the deep sea are bioluminescent (Davis et al., 2014), including everything from bacteria, to invertebrates and fishes. Bioluminescence has been recorded in 43 families of fishes in 12 orders (including one family of cartilaginous fishes) and has evolved at least 27 times in 14 major clades of teleost fishes (Haddock, 2010; Davis et al., 2014; Davis et al., 2016). Although difficult to study *in situ*, observations of bioluminescence in shallow water fishes (i.e. *Porichthys notatus*) and terrestrial organisms (i.e. fireflies) has led to several hypotheses about the possible functions of bioluminescence in the deep sea (reviewed in Haddock et al., 2010; Widder, 2011). Bioluminescence is thought to play roles in prey location (i.e., lures or illuminating prey), predator avoidance (i.e., eliciting a startle response, creating a burglar alarm, or by using counterillumination for camouflage), and communication (i.e., to attract mates or for use in territorial displays). It is likely that bioluminescence is used for multiple behaviors in any given individual (Copeland, 1991).

In teleost fishes, bioluminescence is produced either by bacterial symbionts (i.e. in anglerfish lures, or subocular organ in flashlight fish) or endogenously in complex photophores or in luminous tissue (Mensinger, 2011; Davis et al., 2014). Photophores come in a variety of sizes, shapes, and morphologies (Mensinger, 2011) and may cover up to 12% of the total body surface of a fish (Cavallaro et al., 2004). Photophores can be simple, made up only of groups of photocytes (photogenic cells), or may be more complex and composed of photocytes grouped inside a photogenic chamber, with a lens

(that concentrates the light and guides it to the external opening of the photophore), a reflector layer (with cells that reflect light emitted by the photocytes towards the lens), and a pigmented layer that surrounds the entire structure (Cavallaro et al., 2004).

Among the fishes in the mesopelagic zone of the deep sea, Myctophiformes and Stomiiformes, are known to have diverse arrangement of photophores. Myctophiform fishes (254 species in 36 genera and 2 families) are known for their species-specific photophore arrangements (found in all but the neoscopelids) and other sexually dimorphic luminous organs. The relatively high speciation rates in Myctophiformes that have species- and sex-specific photophore arrangements, compared to other bioluminescent teleosts in the deep sea, suggests that the observed variation in photophore morphology and arrangements may have driven the radiation of myctophiforms (Davis et al., 2014). Stomiid fishes (Stomiiidae: Stomiiformes) have undergone a similar degree of diversification and are incredibly speciose given the young age of the clade (286 species in 27 genera). This incredible species diversity may be explained by the variety of photophores and species-specific bioluminescent mental barbels driving a radiation similar to that seen in the myctophiforms (Davis et al., 2014; Davis et al., 2016; Nelson et al., 2016).

Fishes in the order Stomiiformes are all characterized by bioluminescence, and those in the family Stomiidae have a particularly diverse assemblage of photophores (Fig. 2.1; Tchernavin, 1953; O'Day, 1973; Haddock et al., 2004). Many species have both large, serial photophores, as well as smaller minute photophores (of varying sizes), and simple luminous tissue (= simple photophores). Both the large, serial photophores and the minute photophores are considered complex photophores, with photocytes arranged in a

photogenic chamber, a pigment layer, and typically, a reflector layer and a lens. Complex photophores have been placed into three different categories based on the morphology of tissues within them. Alpha photophores are characterized by small, spherical or polyhedron-shaped photocytes arranged in one or two chambers and are found in *Argyropelecus*, *Maurolicus*, and *Cyclothone*. Beta type photophores are composed of groups of tubular photocytes with a single collector duct that can be open to the outside (i.e. *Gonostoma*). Gamma type photophores have larger and fewer photocytes that are radially organized within the photophore (i.e. *Vinciguerria, Ichthyococcus,* and *Chauliodus*; discussed in Cavallaro et al., 2014). The simple photophores that are found on the head and body of many stomiids (as well as the gonostomatid, *Gonostoma*) are composed only of groups of photocytes but lack other structures characteristic of complex photophores (i.e. lens, and pigment layer).

Stomiiform photophores have species-specific arrangements (Fig. 2.1 – 2) and many species have sexually dimorphic barbels and/or large, complex antorbital or postorbital photophores (*Aristostomias, Astronesthes ,Bathophilus, Chauliodus, Chirostomias, Echiostoma, Eustomias, Flagellostomias, Grammnatostomias, Idiacanthus, Leptostomias, Malacosteus, Melanostomias, Pachystomias, Photonecthes, Photostomias, Stomias,* and *Trigonolampa*; Herring, 2007). The larger, serial photophores tend to be found in similar locations among all stomiids (i.e. in longitudinal rows positioned laterally and ventrally) and counts of these photophores are used in species identification (Bigelow, 1964; Copeland, 1991; Harold, 2004). However, the minute photophores (when present) are more numerous and their distribution is not as conserved among species. These photophores are rarely described in detail, but appear to have

species-specific distribution (i.e., *Chauliodus* and *Stomias*; Tchernavin, 1953; Bigelow et al., 1964; pers. obs.).

Due to the difficulties of studying bioluminescence in live stomiid fishes, it is hard to determine the functions of these different types of photophores. The incredible diversity of photophores on a single individual further complicates the matter, and many species have numerous simple photophores in close association with the minute complex photophores (Tchernavin, 1953; Nicol, 1960). There are only a few reports of bioluminescence in stomiid fishes kept alive for short periods of time (discussed in Nicol, 1960). Most of these studies describe light produced by the conspicuous, complex orbital photophores. Additional observations in live fishes have described luminescence apparently produced by the simple photophores that cover the head, body, and fins of *Astronesthes*, *Chauliodus*, *Idiacanthus*, and *Stomias* (Nicol, 1960; Bigelow, 1964; Marshall, 1979, O'Day, 1973). In studies describing light produced by the photophores on the trunk, the source of the luminescence was either undetermined or unclear, but the color of the bioluminescence is described as blue, green, or yellowish (Marshall, 1960; Nicol, 1960; Copeland, 1970; O'Day, 1973). Few studies have quantitatively described the emission spectrum of the photophores in stomiid fishes, but they appear to emit light between 460 and 485 nm (with the exception of the red light produced by genera discussed above; reviewed in Herring, 1983). Experiments have shown that the major serial photophores in *Argyropelecus hemigymnus* and *Chauliodus sloani* are capable of producing light that could function in counterillumination based on their angular distribution (ventrally directed light; Denton et al., 1972). Widder (2011) suggests that the numerous simple photophores in *Melanostomias bartobeani* function as a "burglar

alarm" for predator avoidance, but, others suggest only that they do not appear to function in counterillumination (Tchernavin, 1953; Nicol, 1960). Little is known about the distribution or function of the numerous, minute photophores, which highlights the need for additional studies.

A closer examination of these diverse photophores is particularly needed given the new interpretation of superficial neuromast proliferation in these fishes (see Ch. 1). The superficial neuromasts in stomiiform fishes are roughly the same size as some of the minute photophores and are found in close association with photophores (Fig. 2.2). Thus, it is not surprising that the superficial neuromasts have been previously misidentified as minute photophores in some stomiids (Bigelow, 1964). This study uses single wavelength light illumination as a tool to distinguish superficial neuromasts from different types of photophores and other luminous tissue and describes the morphology and distribution of these light-producing structures in several stomiiform fishes.

Methods

Thirty-four species of stomiiform fishes from four families were studied. The general morphology and distribution of photophores in stomiiform fishes was compared to those in other deep-sea fishes of the orders Myctophiformes and Stephanoberyciformes.

Imaging:

Specimens were imaged using discrete wavelengths of light (390, 470, 545 nm) as a tool to characterize the distribution, density, and size of photophores on the head and

body and to differentiate the different types of photophores from one another and from superficial neuromasts. All specimens were imaged using a Nikon SMZ1500 dissecting microscope with a SPOT RT3 25.2 2 MP camera and SPOT 5.2 imaging software (Diagnostic Instruments, Inc.). Images in multiple planes of focus were combined into a single image using Helicon Focus (Helicon Soft LTD.). Specimens were imaged using bright field illumination and when illuminated with three different epifluorescence filter sets (BFP-B excitation $\lambda = 390$ nm; GFP-B excitation $\lambda = 470$ nm; Ds-Red excitation $\lambda = 545$ nm; refer to Table 2.1 for all filter properties).

Histology:

Photophores were examined histologically in four species belonging to three families to further characterize their morphology.

Specimens were decalcified in Cal-Ex (Thermo Fisher Scientific) for 2 hours, dehydrated in ascending concentrations of ethanol and t-butyl alcohol, embedded in Paraplast (Thermo Fisher Scientific), serially sectioned (transverse sections, 8µm thickness), and mounted on slides subbed with 10% albumin in 0.9% NaCl. Sections were stained with a modified HBQ stain (Hall, 1986) and coverslipped with Entellan (Electron Microscopy Sciences). One *Astronesthes niger* was embedded in paraffin and stained with hematoxylin and eosin (H&E) and provided by Dr. Chris Kenaley (Boston College and Harvard University).

Other specimens (or in some cases portions of specimens) were embedded in glycol methacrylate plastic resin (Technovit 7100, Electron Microscopy Sciences) and sectioned at 5µm (on a Leica 4M2265 microtome). Every 3rd section was mounted out of

dH_2O on clean slides, dried on a slide warmer overnight, stained with 0.5% aqueous cresyl violet (5 min, followed by 1 - 2 min tap water rinse), air-dried overnight, and coverslipped with Entellan (Electron Microscopy Sciences).

Five species from the research collection of Dr. J. F. Webb (University of Rhode Island) or from the Museum of Comparative Zoology (Harvard University) were examined: *Astronesthes niger* (MCZ 52847, 52 mm SL, paraffin histology, n = 1), *Argyropelecus aculeatus* (39 mm SL, plastic histology, n = 1; 26 – 28.5 mm SL, paraffin histology, n = 2), *Chauliodus sloani* (180 mm SL, plastic histology, n = 1), *Cyclothone microdon* (60 mm SL, plastic histology, n = 1; 52 – 60 mm SL, paraffin histology, n = 2).

Specimens Examined:

Specimens were collected at sea (in Dr. J. F. Webb's collection at URI, JFW) or were borrowed from either the Museum of Comparative Zoology at Harvard (MCZ) or Scripps Institute of Oceanography (SIO). Specimens were fixed in 10% formalin, stored in either 10% formalin in saltwater (JFW), 70% ethanol (MCZ and SIO). Specimens were illuminated with light of three different excitation wavelengths (390, 470, and 595 nm) unless noted. Between 3 and 24 species were examined that belong to four stomiiform families and compared to one representative species of another bioluminescent deep-sea taxon (*Lampanyctus tenuiformes*, Myctophidae: Myctophiformes) and a non-bioluminescent deep-sea taxon (Melamphaidae: Stephanoberyciformes).

Gonostomatidae:

Cyclothone braueri (JFW 1165, 28 – 29 mm SL, n = 2)

Cyclothone microdon (JFW 1170, 43 – 53 mm SL; n = 4); *C. microdon* (JFW 1169; 56.6; n = 1)

Gonostoma elongatum (JFW 1176; 50 – 89 mm SL; n = 4)

Phosichthyidae:

Ichthyococcus ovatus (MCZ 47693; 31.9 – 51.8 mm SL; n = 3; 470 nm only)

Polymetme thaeocoryla (MCZ 91007; 70.7 mm SL; n = 1; 470 nm only); *P. thaeocoryla* (MCZ 91008; 79.7 mm SL; n = 1; 470 nm only)

Vinciguerria nimbaria (MCZ 151699; 32.5 – 42.9 mm SL; n = 4; 470 nm only)

Sternoptychidae:

Argyropelecus aculeatus (MCZ 150959; 29.5 mm SL; n = 1); *A. aculeatus* (MCZ 159086; 32.5 – 40.5 mm SL; n = 3)

Argyropelecus lychnus (JFW 040; 14 mm SL; n = 1)

Danaphos oculatus (SIO-11-292; 42 mm SL; n = 1)

Stomiidae:

Astronesthes niger (MCZ 52845; 47.9 – 56 mm SL; n = 5; 470 nm only); *A. niger* (MCZ 98847; 25 – 45 mm SL; n = 3)

Bathophilus filifer (JFW 2131; 46 mm SL; n = 1)

Bathophilus flemingi (SIO-10-175; 39 mm SL; n = 1)

Bathophilus metallicus (MCZ 101656; 98.6 mm SL; n = 1; 470 nm only); *B. metallicus* (MCZ 84812; 81.2 – 108.8 mm SL; n = 4; 470 nm only)

Chauliodus sloani (JFW 1174; 105 mm SL; n = 1); *C. sloani* (MCZ 128574; 114.7 mm SL; n = 1; 470 nm only); *C. sloani* (MCZ 128578; 140.4 mm SL;

n = 1; 470 nm only); *C. sloani* (MCZ 128954; 125.9 – 141.8 mm SL; n = 2; 470 nm only)

Chirostomias pliopterus (MCZ 132707; 124.6 mm SL; n = 1; 470 nm only); *C. pliopterus* (MCZ 132708; 105.1 mm SL; n = 1; 470 nm only); *C. pliopterus* (MCZ 59769; 69 mm SL; n = 1); *C. pliopterus* (MCZ 70487; 89.2 mm SL; n = 1)

Echiostoma barbatum (JFW 2115; 210 mm SL; n = 1); *E. barbatum* (MCZ 148300; 54.9 – 157.9 mm SL; n = 4; 470 nm only)

Eustomias hulleyi (MCZ 100873; 147 mm SL; n = 1)

Eustomias schmidti (MCZ 132536; 152.6 mm SL; n = 1; 470 nm only); *E. schmidti* (MCZ 155490; 85.1 mm SL; n = 1; 470 nm only); *E. schmidti* (MCZ 162129; 94 mm SL; n = 1)

Flagellostomias boureei (JFW 2109; 80.5 mm SL; n = 1); *F. boureei* (MCZ 53252; 123.8 mm SL; n = 1; 470 nm only); *F. boureei* (MCZ 70491; 228 mm SL; n = 1; 470 nm only); *F. boureei* (MCZ 70492; 91.2 mm SL; n = 1; 470 nm only)

Grammatostomias dentatus (MCZ 161555; 84.8; n = 1; 470 nm only); *G. dentatus* (MCZ 70497; 141.6 mm SL; n = 1; 470 nm only)

Idiacanthus antrostomus (JFW 1182; 79 mm SL; n = 1)

Idiacanthus fasciola (MCZ 149522; 276.6 mm SL; n = 1; 470 nm only); *I. fasciola* (MCZ 149524; 263.8 mm SL; n = 1; 470 nm only); *I. fasciola* (MCZ 149616; 252.3 mm SL; n = 1; 470 nm only)

Leptostomia gladiator (MCZ 132479; 115.4 mm SL; n = 1; 470 nm only);

L. gladiator (MCZ 89460; 42.3 – 83.6 mm SL; n = 3; 470 nm only)

Melanostomias bartobeani (MCZ 132342; 247.9 mm SL; n = 1; 470 nm only);

M. bartobeani (MCZ 132343; 225.7 mm SL; n = 1; 470 nm only);

M. bartobeani (MCZ 162113; 218.7 mm SL; n = 1; 470 nm only);

M. bartobeani (MCZ 64833; 117.1 mm SL; n = 1; 470 nm only)

Neonesthes capensis (MCZ 132795; 55.9 mm SL; n = 1; 470 nm only);

N. capensis (MCZ 132798; 118.3 mm SL; n = 1; 470 nm only); *N. capensis* (MCZ 41125; 100.3 mm SL; n = 1; 470 nm only)

Pachystomias microdon (MCZ 52356; 170.8 mm SL; n = 1; 470 nm only);

P. microdon (MCZ 58801; 66.5 mm SL; n = 1; 470 nm only); *P. microdon* (MCZ 70579; 66.5 mm SL; n = 1; 470 nm only)

Photonectes margarita (MCZ 132093; 143.6 mm SL; n = 1; 470 nm only);

P. margarita (MCZ 132095; 257 mm SL; n = 1; 470 nm only)

Photostomias goodyeari (MCZ 167549; 85 mm SL; n = 1); *P. guernei* (MCZ 131476; 89.9 – 102.3 mm SL; n = 2; 470 nm only); *P. guernei* (MCZ 131477; 106 mm SL; n = 1; 470 nm only); *P. guernei* (MCZ 131481; 95.7 – 95.8 mm SL; n = 2; 470 nm only); *P. guernei* (MCZ 131488; 94 mm SL; n = 1)

Stomias atriventer (JFW 2083; 129 mm SL; n = 1)

Stomias boa ferox (JFW 1182; 110 mm SL; n = 1); *S. boa ferox* (MCZ 129188; 114.2 – 164.7 mm SL; n = 4; 470 nm only)

Tactostoma macropus (JFW 1183; 84 mm SL; n = 1)

Thysanactis dentex (MCZ 96771; 55 – 85 mm SL; n = 5; 470 nm only)

Myctophidae:

Lampanyctus tenuiformes (JFW 047; 51 mm SL; n = 1)

Melamphaidae:

Melamphus/ Scopelogadus sp. (JFW 083; 53 mm SL; n = 1).

Results

The examination of photophore type (i.e. simple or complex), size (i.e. large or minute), distribution, orientation, and response to different wavelengths of light (390, 470, or 545 nm) in 34 stomiiform taxa revealed that all species had photophores on their head and trunk, but that the diversity of photophores varied among species. Complex photophores (i.e. large serial and minute photophores) and simple photophores, each have distinct morphologies, distributions, and responded differently when exposed to the different wavelengths of light. The superficial neuromasts present in the skin were morphologically distinct from minute photophores and were visible when illuminated by 390 nm and 470 nm wavelengths of light.

Photophore response to illumination at these wavelengths was most obvious in darkly pigmented specimens as the dark epithelium provided a stark contrast to fluorescing structures. In lightly pigmented specimens, the epithelium or underlying muscle reflected light so that photophores did not easily stand out. All of the photophores and neuromasts appeared blue when illuminated with light at 390 nm, appeared green at 470 nm, and appeared red at 545 nm. Storage solution (70% ethanol, 100% ethanol, or

10% formalin in saltwater) did not appear to have an effect on the response of any structures to single wavelength illumination.

Complex Photophores

Large serial photophores were found in all stomiiforms examined and had similar distributions among species. All large serial photophores were directed ventrally and were visible when exposed to all three excitation wavelengths used (390, 470, and 545 nm). A ventral and a lateral series on the trunk were found with approximately 1 per body segment, and a single lateral row, caudal to the origin of the anal fin (as per Harold, 2004).

All stomiiform fishes examined have one or more complex photophores near their eye (Fig. 2.3A, C – D), which reflected light at all three wavelengths as the large serial photophores did (Fig. 2.3). In some species, multiple photophores, including both an antorbital and a postorbital photophore, were present. These two photophores responded differently from one another when illuminated under different wavelengths in some species. In *Tactostoma macropus*, the antorbital photophore was visible when illuminated with 390 and 470 nm light, but emitted only very dim light at 590 nm. The postorbital photophore was much brighter and was visible at all three wavelengths (Fig. 2.4). It is interesting to note that in living or freshly caught specimens, the antorbital and postorbital photophores appear to be different colors and may produce light of different wavelengths (see images in Haddock et al., 2010).

Numerous minute photophores were observed to cover the skin of many stomiid species (Fig. 2.2). Unlike the larger serial photophores, the minute photophores were not

visible to the naked eye in whole preserved specimens. They were variable in distribution, size, and orientation within an individual and between species. In contrast, sternoptychids, phosichthyids, and *Cyclothone* spp. lacked minute photophores. Among the gonostomatids, only *Gonostoma elongatum* had minute photophores. When compared to those in the stomiids, the minute photophores in *Gonostoma elongatum* were less numerous and less diverse, but were all the same size and oriented directly outward (laterally if located on the lateral side of the body, or dorsally if located on the dorsal side of the body).

All species examined appeared to have at least two different sizes of minute photophores. Their distribution varied among species, but appeared to be relatively constant within a species and was found in each body segment on the trunk with more photophores located ventrally rather than dorsally. The photophores located more ventrally tend to be directed ventrally, but several species had some photophores directed ventro-laterally (*Bathophilus metalicus, Chauliodus sloani, Idiacanthus fasciola, Leptostomias gladioator,* and *Stomias boa ferox*). In some species, the minute photophores located dorsally on the trunk had more variable orientation, and were directed dorsally or dorso-laterally (*Eustomias schmidti* and *Flagellostomias boureei*). In most species, minute photophores were visible when illuminated with all three wavelengths (390, 470, and 545 nm; Fig. 2.4). The minute photophores in *Idiacanthus antrostomus* and *Eustomias schmidti* were not visible when illuminated at 545 nm.

The complex photophores all appear to respond similarly when illuminated by the three different excitation wavelengths (Fig. 2.4). All complex photophores appeared brightest when illuminated with light at 470 nm. Photophores appeared the next brightest

at 545 nm (if visible at all) and appeared much dimmer at 390 nm. Photophore type (i.e alpha, beta, or gamma) did not appear to correlate with visibility when illuminated at the three different wavelengths. Species with small photophore diameter (i.e. *Cyclothone microdon*) appeared dimmer (Fig. 2.4), which seems to be more a factor of the size of the photophore (reducing light emission) rather than photophore type.

Simple Photophores

In addition to the numerous complex photophores, many stomiids (and the gonostomatid *Gonostoma*) have simple photophores on their head and trunk, but these were not present in sternoptychids or phosichthyids. These light producing tissues lack a ring of dark pigment, are smaller, and have a less defined shape, appearing occasionally globular in shape, and are located more superficially in the skin compared to the complex photophores. They appear whitish in color and have previously been described as "fatty-appearing material" (in *Astronesthes niger*, Bigelow et al., 1964, pp. 380; Fig. 2.4C). They are often found in groups, either densely placed in well-defined areas or found more diffusely over the head and trunk, on fin rays, and around the anal and genital openings in many species. The arrangement of simple photophores appears to be species-specific. Although lacking numerous discrete simple photophores as seen in *Gonostoma* and the stomiids, some *Cyclothone* species appeared to have a luminous organ along the cheek and at the base of both the dorsal and anal fins. *Gonostoma* and all stomiids appeared to have some type of simple photophore, with more elaborate distributions found in the stomiids.

Simple photophores responded differently than complex photophores when illuminated by the three different wavelengths of light (Fig. 2.4 – 7). All simple photophores were visible when illuminated by 390 and 470 nm light, but none were visible when illuminated by longer wavelength, 545 nm light. In contrast to the complex photophores, the simple photophores appeared brightest at 390 nm, and were the brightest of the visible structures at this wavelength.

In some species, there are other tissues that appear to be luminescent and are likely simple photophores with different morphologies. Simple photophores appear to be suspended within a gelatinous coating in *Chauliodus* and *Stomias* and a luminous "gland" was seen in *Cyclothone* spp. Each of the structures will be described separately.

Gelatinous coatings in *Stomias* spp. and *Chauliodus sloani*

Among stomiids, two genera (*Chauliodus, Stomias*) are reported to have a thick gelatinous coating covering their head and/or body (i.e. Bigelow et al., 1964), which is fragile, easily damaged during collection, and shrinks when specimens are placed in ethanol. The gelatinous coat was observed in specimens of well-preserved *Chauliodus sloani* (105 mm SL, n = 1) and *Stomias boa ferox* (110 mm SL, n = 1). These are the only two stomiiform genera with this gelatinous coat and which are both characterized by hexagon – shaped scales (Fig. 2.1; i.e. Bigelow, 1964).

The gelatinous coat of *Chauliodus sloani* is not present on the head, but begins on the trunk, caudal to the gills, becomes thicker caudally, and then narrows towards the caudal fin. At its thickest point, it appears to make up almost a quarter of the diameter of the trunk and is transparent so that complex photophores in the skin are visible through

the gelatinous coat using bright field illumination and single wavelength illumination (as described above, Figs. 2.6, 2.9).

Small, spherical structures are suspended within the gelatinous coat and appear to be innervated (Fig. 2.4 – 7). These appear to be simple photophores based on reports of their luminescence (Tchernavin, 1953; Nicol, 1960; O'Day, 1973). In specimens in which the gelatinous coating was missing, these structures are found collapsed against the skin surface, falling into neatly clumped areas between groups of complex ventral photophores in the skin (Fig. 2.7C – D). Plastic resin histology revealed that these structures are morphologically distinct from both the large and minute complex photophores in the skin (Fig. 2.6A – D). Compared to the complex photophores, these simple photophores are not surrounded by pigment and appear to be made up only of photocytes. Additional simple photophores were found between the nares and orbits on the dorsal surface of the head, and along the lower jaw (Fig. 2.7B). They are small, flat (not domed), opaque circles that resemble the simple photophores of other stomiids. These structures suspended within the gelatinous coat and those on the head were visible with illumination at 390 and 470 nm but not at 545 nm, like the simple photophores in other taxa (Fig. 2.6E – L).

An almost fully intact gelatinous coating was examined in one specimen of *Stomias boa ferox* (Fig. 2.8), which as in *Chauliodus*, does not cover the head, but is present caudal to the gills, becoming thicker caudally, and thinning out towards the caudal fin.

Opposed to the seemingly homogenous gelatinous coating with few simple photophores found in *Chauliodus*, *Stomias* appears to have many more densely placed

simple photophores composing its gelatinous coat. As other simple photophores, these structures are opaque white and “fatty-appearing”. These, however, are more oval-shaped than the spherical simple photophores found in the gelatinous coat of *Chauliodus*. They are found both dorsally and ventrally, but not on the lateral surface of the trunk. They appear loosely connected to the skin and move easily when disturbed by fluid motion. When the internal structure of the gelatinous coat is visible (on areas of the specimen where the superficial layer of the gelatinous coating was damaged), these elongate simple photophores appear to point away from the surface of the trunk so that they resemble microvilli emerging from the surface of the epithelium. A very thin layer of tissue sits superficial to the simple photophores, connecting these numerous structures. When observed in ventral or dorsal view, they are only visible through the superficial epithelial layer of the gelatinous coat as small, opaque circles that obstruct the visibility of the underlying complex photophores in the skin.

Nerves or blood vessels can be seen running to these structures and extend through the gelatinous coat. Similarly, darkly pigmented nerves running from the surface of the skin through the gelatinous coat have been observed in other *Stomias* species (C. Kenaley, personal communication). On the lateral surface of the trunk (where simple photophores are absent) the gelatinous coat appears transparent and thread-like structures that appear to be nerves are visible running from the surface of the scales but do not appear to run to any obvious structures. In several cases, these appear to extend beyond the gelatinous covering into the external environment and may be free nerve endings. They were only seen on the second horizontal row of scales (counting from dorsal to ventral).

In well-preserved specimens that lacked an intact gelatinous coat, the simple photophores were still visible, but were collapsed into a longitudinal row mid-ventrally (observed in *S. atriventur*, n = 5; *S. boa ferox*, n = 1). When not connected to the gelatinous coating, they fall flat and do not stand upright as they did in the intact gelatinous coat and appear similar to the collapsed circular simple photophores in the *Chauliodus* specimens that lacked an intact gelatinous coat.

Additional simple photophores are also found dorsally between the nares and orbits, and extend onto the pectoral and pelvic fins, in areas not enveloped by the gelatinous coating. These appear similar to those seen in *Chauliodus sloani*. More caudally on the head, they gradually become more elongate, eventually becoming confluent with the gelatinous coat caudal to the gills. All of the simple photophores in the gelatinous coat were visible when illuminated by 390 and 470 nm light. With 545 nm light, the simple photophores were not visible but obscured the glow of the underlying complex photophores in the skin (Fig. 2.8).

Other "Luminous" Tissue in *Cyclothone* spp.

All thirteen species of *Cyclothone* are morphologically similar in appearance and *Cyclothone* spp. can be found in all major oceans. Species found in the same geographic range are often distributed vertically. Deeper dwelling species of *Cyclothone* (i.e. *C. acclinidens, C. atraria, C. microdon*, and *C. pallida*) are described as having white, "fatty-appearing" tissue in a winding pattern along the cheek and on the trunk at the base of the dorsal and anal fins. These structures have been described as "luminous glands" (Mukhacheva, 1966), however there is no evidence that these structures emit light.

These “luminous glands” were examined in *Cyclothone microdon, C. acclinidens,* and *C. pallida* using nerve staining (Sudan Black, 31.5 – 45.5 mm SL, n = 1 – 2 individuals/species; see Table 1.3 for details), hematoxylin staining (*C. microdon* 52 – 60 mm SL, n = 4), and paraffin or plastic histology (*C. microdon* 52 – 60 mm SL, n = 2). These structures stained positively with Sudan Black B (a lipid stain) in all three *Cycothone* species. They also stained positively with hematoxylin (a nuclear stain) in both whole specimens and in histological material, confirming that the “luminous glands” are cellular in nature. In cross-section, they appear to have a highly nucleated circumference but an empty center with no apparent nerve innervation.

Superficial Neuromasts

Superficial neuromasts were found on the head and trunk of all stomiiform species examined (see Chapter 1). These neuromasts have distinct morphological characteristics that differentiate them from both simple and complex photophores (Fig. 2.2). They are much smaller than the larger serial, complex photophores, but are sometimes similar in size to the minute complex photophores. Superficial neuromasts appear as white, circular, domed structures. In contrast, the minute photophores are surrounded by a thick line of dark pigment, do not form a dome above the surrounding epithelium, and have a more defined circular structure than is seen in superficial neuromasts. Additionally, the complex photophores are more deeply anchored within the epithelium than the superficial neuromasts.

Simple photophores are not always circular as is the case for the complex minute photophores and the superficial neuromasts (see Chapter 1). Nevertheless, the color and

shape of the superficial neuromasts makes it difficult to differentiate them from the simple photophores when they occur at high densities on the skin. However, the distribution of superficial neuromasts in discrete vertical lines can help differentiate them from the more broadly distributed simple photophores. Additionally, the neuromasts are distinguished from both complex and simple photophores because they respond differently when illuminated by different wavelengths of light than either type of photophore. Superficial neuromasts are visible when illuminated at 390 and 470 nm (Fig. 2.5E – H). Like photophores, they appear brightest at 470 nm, but in contrast to the complex photophores, superficial neuromasts are not visible at 545 nm light. Unlike the simple photophores, they are only faintly visible at 390 nm, making them easily distinguishable from the simple photophores, which are brightly illuminated at this wavelength.

Discussion

The complement of photophore types found among stomiiform fishes was made much more apparent when illuminated with different wavelengths of light. This study found that photophore types respond differently when illuminated with different wavelengths of light and that superficial neuromasts respond differently than both simple and complex photophores. The morphology and distribution of photophores were described in 34 species of stomiiform fishes.

Illumination of specimens with different wavelengths of light proved to be a useful tool in the differentiation among types of photophores and other luminous tissue in stomiiform fishes. Under illumination at 390 nm, complex and simple photophores and

superficial neuromasts were visible, but simple photophores were the brightest of these structures. At 470 nm, simple and complex photophores and superficial neuromasts were all visible. At 545 nm, only complex photophores were visible. While different complex photophore types (alpha, beta, or gamma) were not distinguishable from one another using the methods in this study (Fig. 2.4), some preorbital and antorbital photophores appeared to have variable responses to different wavelengths of light. Furthermore, the photophore lens was sometimes difficult to distinguish from surrounding tissue under brightfield illumination, but it was very distinct under illumination at 470 nm, for example.

Stomiiformes are found from the upper mesopelagic into the bathypelagic and many species migrate upwards into the epipelagic at night (discussed in Marshall, 1960). These oceanic zones show considerable variation in light conditions (intensity and spectrum) and likely affect the evolution of bioluminescence. A comparative study of the size of different photophores in species found throughout the water column will begin to allow us to use the Stomiiformes as a model to further determine ecological significance of bioluminescence in a variety of oceanic habitats.

This study revealed an impressive variety of minute photophores, which are more diverse than the larger photophores currently used for identification of stomiiforms. A more detailed study of these photophores may reveal patterns that can be used in species identifications, as is currently done for only *Chauliodus* and *Stomias* (i.e. Bigelow, et al., 1964). The larger serial photophores are likely used for counterillumination and are known to produce intensities of light capable of this function (Tchernavin, 1953; Denton, et al., 1972; O'Day, 1973). However, given the variation in size, distribution, and

orientation of the minute photophores, it is possible that they serve one or more different functions. A more detailed examination of variation in their density, distribution, and orientation may elucidate the behavioral and ecological significance of these structures. For instance, there appears to be a higher density of photophores on the ventral surface of the fish (noted in Bigelow et al., 1964; Harold, 2004). Their ventral orientation would suggest a role in counterillumination, while the laterally and dorsally directed photophores are less likely to be used for this purpose and may function in communication, as hypothesized in myctophids.

Particularly interesting, perhaps, is the function of the simple photophores found in diverse patterns among stomatiiforms. As observed in some species, these produce a constant blueish glow around the fish. It seems unlikely that they aid in counterillumination (Tchernavin, 1953; Nicol, 1960; O'Day, 1973). This is especially true when considering the high density of simple photophores found extending onto dorsal side of the head and trunk, which do not seem likely to aid in counterillumination and those extending onto the pelvic and anal fins and around the anal/genital region, which may act more as a signal for mating. It is possible that the unique arrangements of simple photophores serve for species recognition. Simple photophores were absent in basal stomiids (i.e. sternoptychids and less elaborate in the gonostomatids; personal observation), which are also less speciose groups. The elaboration of both simple and complex photophores in the speciose stomiids suggests that there may be a connection between the number, distribution, and diversity of photophores and the radiation of these fishes in the deep sea.

It is important to note that illumination of photophores using single wavelength illumination, as revealed in this study does not mean that the tissues are necessarily bioluminescent or auto-fluorescent; therefore, results from this method should be interpreted with caution (Johnsen, 2006; Haddock et al., 2010). Although not directly examined here, epifluorecence imaging may provide insights into tissue compositions of different photophore types based on the differential reflectance of tissues under illumination at different wavelengths. It is possible that orbital photophores which emit different wavelengths of light, such as the well documented red light produced in some species (i.e. *Aristostomias, Malacosteus,* and *Pachystomias;* Douglas & Partridge, 2011; Kenaley et al., 2014) would react differently when illuminated by different wavelengths of light, as reported here for *Tactostoma*. Although not examined here, the variable responses of the orbital photophores in some individual as well as the different responses of simple and complex photophores when illuminated by different wavelengths of light may suggest a difference in the composition of photophores. This may warrant additional, in depth investigations of the structure, composition, and function of these different luminescent tissues.

Finally, this study provided some of the first detailed descriptions of structures within the gelatinous coats of *Chauliodus* and *Stomias*. Because of its delicate nature, the gelatinous coat has only been described in a few freshly caught specimens (Tchernavin, 1953; Nicol, 1960; O'Day, 1973; Schnell & Johnson, 2012). Observations of live specimens confirm what appear to be simple photophores in the gelatinous coat that produce a bluish glow (Tchernavin, 1953; Nicol, 1960; O'Day, 1973). In this study, histological sections through the simple photophores of *C. sloani* provide a comparison

of the differences between the simple photophores suspended within in the gelatinous coating and the complex photophores in the epithelium composing the skin (Fig. 2.6A – D); however, additional investigation is necessary to fully determine the structural and functional differences among these different groups of photophores. It is also interesting that *Chauliodus* and *Stomias* are the only two stomiid genera which are reported to have a gelatinous coat and are also the only two genera with obvious scales. It is unclear what the function of the gelatinous coat is, but it seems as if the sole function cannot be to house the simple photophores, as both genera have additional simple photophores arranged on their head and fins as seen in other stomiids. Certainly, additional investigation is needed to ascertain the function of this intriguing feature found in these two genera.

Literature Cited

Bigelow, H. B., Cohen, D. M., Dick, M. M., Gibbs, R. H. Jr., Grey, M., Morrow, J. E., Jr., Schultz, L. P. & Walters, V. (1964). *Fishes of the Western North Atlantic* (H. Bigelow, et al. eds). New Haven: Sears Foundation for Marine Research.

Cavallaro, M., Mammola, C. L. & Verdiglione, R. (2004). Structural and ultrastructural comparison of photophores of two species of deep-sea fishes: *Argyropelecus hemigymnus* and *Maurolicus muelleri*. *Journal of Fish Biology*, *64*, 1552–1567. http://doi.org/10.1111/j.0022-1112.2004.00410.x.

Cavallaro, M., Battaglia, P., Laur, R., Guerrera, M. C., Abbate, F. & German, A. (2014). The morphology of photophores in the garrick, *Cyclothone braueri* (Family:Gonostomatidae): An ultrastructure study. *Acta Zoologica*, *96*, 296–300. http://doi.org/10.1111/azo.12076.

Copeland, D. E. (1991). Fine Structure of Photophores in *Gonostoma elongatum*: Detail of a dual gland complex. *Biological Bulletin*, *181*, 144–157.

Davis, M. P., Holcroft, N. I., Wiley, E. O., Sparks, J. S. & Smith, W. L. (2014). Species-specific bioluminescence facilitates speciation in the deep sea. *Marine Biology*, *161*, 1139–1148. http://doi.org/10.1007/s00227-014-2406-x.

Davis, M. P., Sparks, J. S. & Smith, W. L. (2016). Repeated and widespread evolution of bioluminescence in marine fishes. *Plos One*, *11*(6), e0155154. http://doi.org/10.1371/journal.pone.0155154.

Denton, E. J., Gilpin-Brown, J. B. & Wright, P. G. (1972). The angular distribution of the light produced by some mesopelagic fish in relation to their camouflage. *Proceedings of the Royal Society B: Biological Sciences*, *182*(1067), 145–158. http://doi.org/10.1098/rspb.1972.0071.

Douglas, R. H. & Partridge, J. C. (2011). *Vision: Visual Adaptations to the Deep Sea*. *Encyclopedia of Fish Physiology* (Vol. 1). Elsevier Inc. http://doi.org/10.1016/B978-0-12-374553-8.00089-7

Haddock, S. H. D., Moline, M. A. & Case, J. F. (2010). Bioluminescence in the sea. *Annual Review of Marine Science*, *2*, 443–93. http://doi.org/10.1146/annurev-marine-120308-081028.

Harold, A. S. (2002). Order Stomiiformes. In *The Living Marine Resources of the Western Central Atlantic Vol. 2: Bony fishes Part 1 (Acipenseridae to Grammatidae)* (Carpenter, K. E., ed.). FAO.

Herring, P. J. (1983). The spectral characteristics of luminous marine organisms. *Proceedings of the Royal Society B: Biological Sciences*, *220*, 183–217.

Herring, P. J. (2000). Species abundance, sexual encounter and bioluminescent signaling in the deep sea. *Philosophical Transactions of the Royal Society of London. Series B, Biological Sciences*, *355*, 1273–1276. http://doi.org/10.1098/rstb.2000.0682.

Johnsen, S. (2012). *The Optics of Life*. Princeton: Princeton University Press.

Kenaley, C. P., Devaney, S. C. & Fjeran, T. T. (2014). The complex evolutionary history of seeing red: Molecular phylogeny and the evolution of an adaptive visual system in deep-sea dragonfishes (stomiiformes: Stomiidae). *Evolution*, *68*(4), 996–1013. http://doi.org/10.1111/evo.12322

Marshall, N.B. (1979). *Developments in Deep-Sea Biology*. Poole: Blandford Press.

Mensinger, A. F. (2011). Bioluminescence in fishes. *Encyclopedia of Fish Physiology: From Genome to Environment* . Elsevier Inc. http://doi.org/10.1016/B978-0-12-374553-8.00160-X.

Nelson, J. S., Grande, T. C. & Wilson, M. V. H. (2016). *Fishes of the World*.5th edition. Wiley.

Nicol, J. A. C. (1960). Studies on luminescence. On the subocular light-organs of stomiatoid fishes. *Journal of Marine Biological Association of the United Kingdom, 39,* 529–548.

O'Day, W. T. (1973). Luminescent silhouetting in stomiatoid fishes. *Contributions in Science, Los Angeles County Museum of Natural History*. Number *246*, pp. 108.

Schnell, N. K. & Johnson, G. D. (2012). Ontogenetic fusion of the third and fourth pharyngobranchial in barbeled dragonfishes (Stomiidae,Teleostei) with a revision of the identity of the single posterior upper pharyngeal toothplate. *Copeia*, *2012*(3), 394–407. http://doi.org/10.1643/CG-11-051.

Tchernavin, V. V. (1953). *The Feeding mechanisms of deep sea fish*. London: The Trustees of the British Museum. 101 pp.

Widder, E. A. (2001). Marine bioluminescence. *Bioscience Explained, 1*(1), 1–9.

Table 2.1: Properties of epifluorescence filter sets used to deliver single wavelength illumination. The range of wavelengths is shows followed by the center wavelength (CLW). Value referred to throughout text is the CLW value for excitation.

Filter Name	Excitation Wavelength (nm)	Dichroic Mirror Wavelength (nm)	Barrier Wavelenth (nm)
BFP-B	379 – 401 (CWL = 390)	420	415 – 485 (CWL = 460)
GFP-B	450 – 490 (CWL = 470)	495	500 – 550 (CWL = 525)
Ds-Red	530 – 560 (CWL = 545)	570	590 – 650 (CWL = 620)

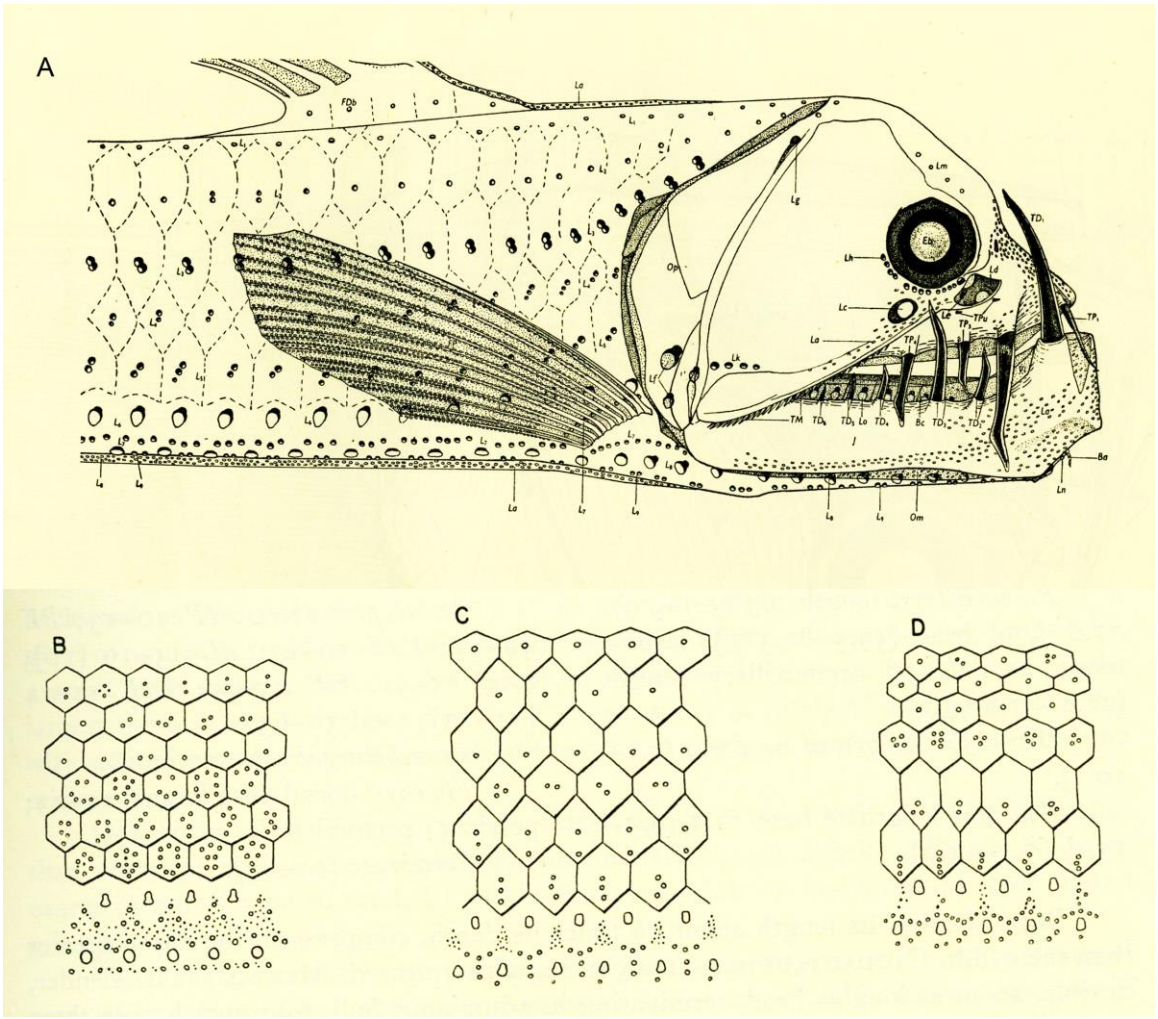

Figure 2.1: **Photophore size and distribution in *Chauliodus* (A; drawings from Tchernavin, 1953) and *Stomias* (B-D; drawings from Migelow et al., 1964). A)** *Chauliodus sloani* showing different sized minute photophores on the lateral surface of the body and larger serial photophores more ventrally. Scale boundaries = dotted lines. **B – D)** Lateral views of scales and photophores in three different species of *Stomias*. **B)** *S. columbrinus*, **C)** *S. affinis*, and **D)** *S. boa ferox.*

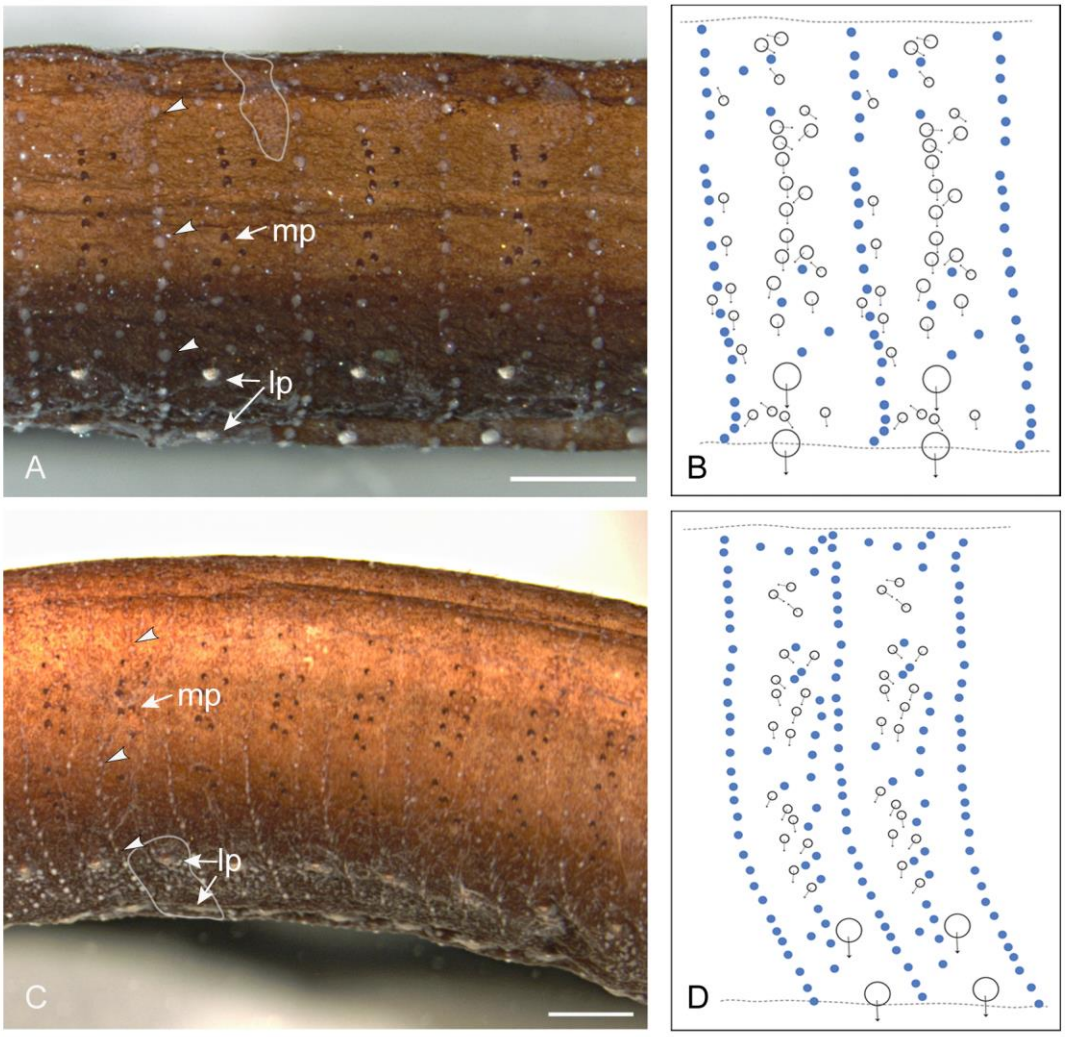

Fig. 2.2: The complex arrangement of photophores and superficial neuromasts on the trunk of *Idiacanthus antrostomus* (A – B) and *Tactostoma macropus* (C – D). A) *Idiacanthus antrostomus* (79 mm SL) trunk showing the regular photophore pattern in four body segments. Scale = 1 mm. **B)** Schematic showing the vertical lines of minute photophores in *I. antrostomus* **C)** *Tactostoma macropus* (84 mm SL) showing a similar photophore pattern in eight body segments. Scale = 1 mm. **D)** Schematic showing the vertical lines of minute photophores in *T. macropus*. In A, C: vertical lines of superficial neuromasts (white arrowheads), minute photophores (mp), large photophores (lp), simple photophores. In B, D: superficial neuromasts (blue dots), photophores (open black circles), angle of orientation (directionality of light, based on the direction opposite the dense pigment in the photophore; arrows). Note the different pattern of photophores between *I. antrostomus* and *T. macropus*.

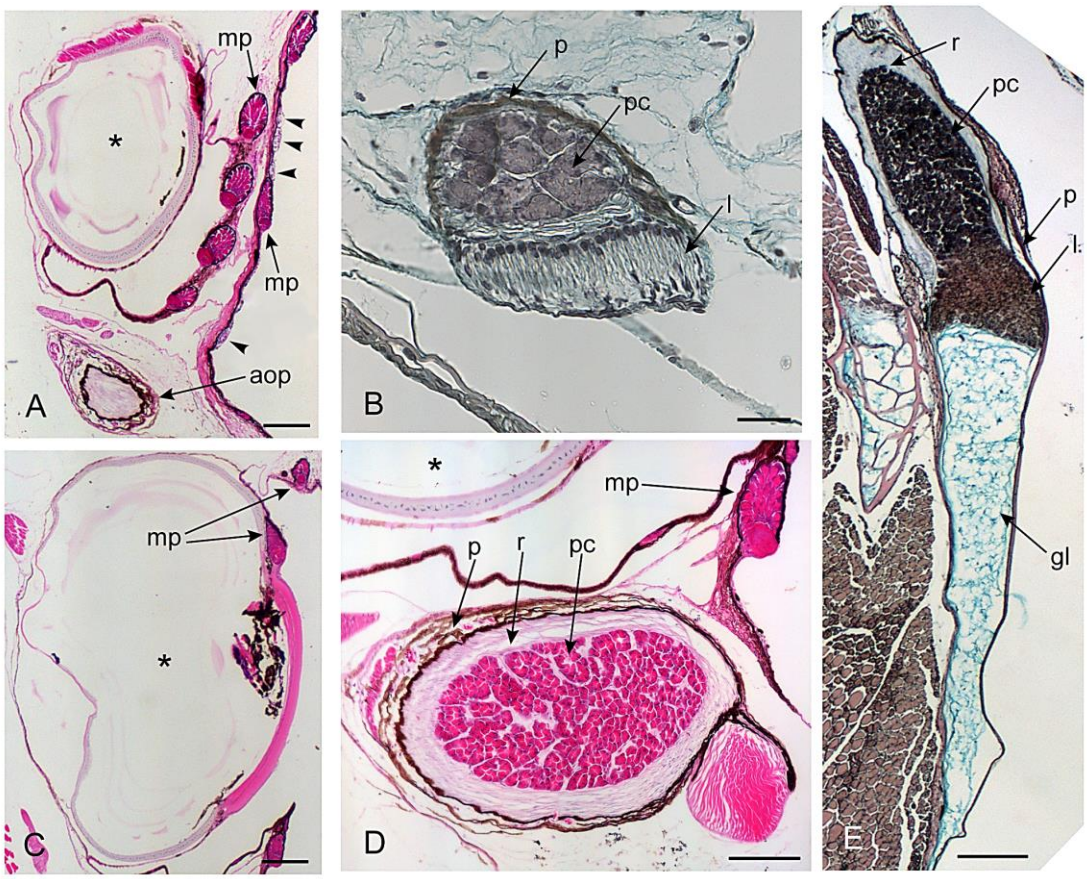

Figure 2.3: Photophores in histological sections in the stomiid *Astronesthes niger* (A, C, E), the gonostomatid *Cyclothone microdon* (B), and the sternoptychid, *Argyropelecus aculeatus* (E). A) Cross section through the orbit of *A. niger* (52 mm SL) showing several minute photophores (mp) on the skin surface as well as a row of them directed at the eye. Minute photophores are interspersed with superficial neuromasts (black arrowheads). The rostral portion of the antorbital photophore (aop) is ventral to the orbit (*). Scale = 200 µm. **B)** A large serial photophore in *C. microdon* (52 mm SL) with visible photogenic chamber (pc), lens (l) and pigment layer (p). Scale = 25 µm. **C)** The eye (*) in *A. niger*, caudal to section in C showing minute photophores (mp) directed into the eye, and one attached to the eye. Scale = 200 µm. **D)** The antorbital photophore in *A. niger* (ventral to orbit [*], same plane of section as in C but at higher magnification). Photogenic chamber (pc), reflector (r), and pigment layer (p) are visible in the antorbital photophore with a smaller minute photophore visible to the right. Scale = 100 µm. **E)** An elongate, complex ventral photophore in *A. aculeatus* (28.5 mm SL) with photogenic chamber (pc), lens (l), reflector (r), pigment layer (p), and gelatinous layer (gl). Scale = 250µm. Histological material courtesy of Christopher P .Kenaley.

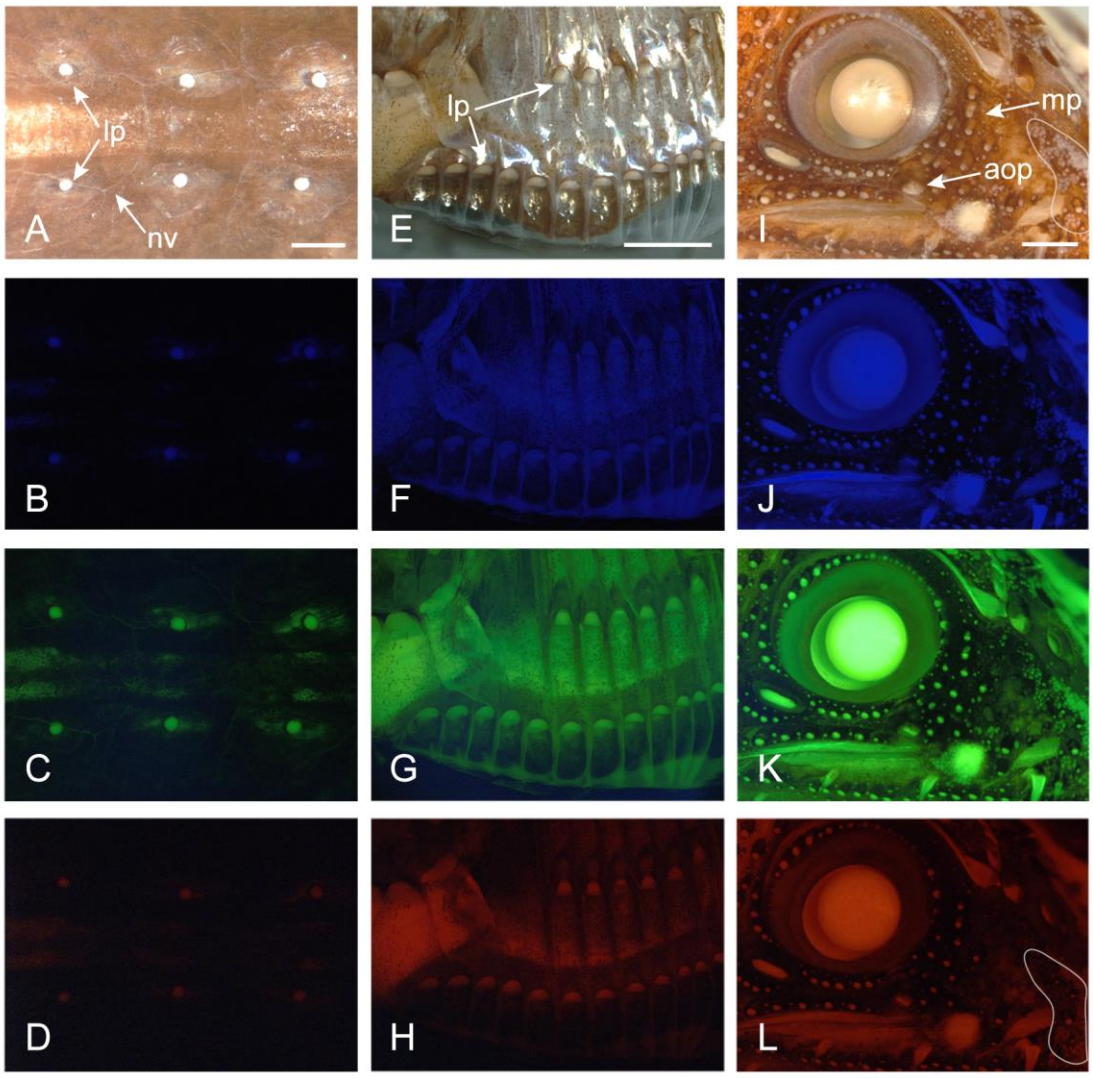

Fig. 2.4: *Cyclothone microdon* and *Argyropelecus aculeatus* and the orbital photophores in *Astronesthes niger* in bright field and illuminated under different wavelengths of light. *Cyclothone microdon* (56.5 mm SL) in ventral view showing three large serial photophores (lp) with thread like nerve (nv) in **A)** brightfield illumination, and under illumination at **B)** 390 nm (blue), **C)** 470 nm (green), and **D)** 545 nm (red). Scale bar (shown only for A) = 0.5 mm. *Argyryopelecus aculeatus* (29.5 mm SL) in lateral view showing ventral and lateral rows of large serial phtotophores (lp) in **E)** brightfield illumination, and under illumination at **F)** 390 nm, **G)** 470 nm, and **H**) 545 nm. Scale (only shown in E) = 2.5 mm. *Astronesthes niger* (39 mm SL) antorbital photophore (aop), numerous minute photophore (mp), and simple photophores (outlined by grey line) under **I)** brightfield illumination and under illumination at **J)** 390 nm, **K)** 470 nm, and **L)** 545 nm. Scale (shown only in I) = 0.5 mm.

Figure 2.5. *Tactostoma macropus* under bright field illumination and illuminated under different wavelengths of light. (see next page). *T. macropus* (84 mm SL) head showing antorbital (aop), suborbital (sop), and postorbital (pop) photophores under **A)** brightfield illumination and illuminated with **B)** 390 nm, **C)** 470 nm, and **D)** 545 nm. Scale (only shown in A) = 2 mm. Trunk in lateral view showing large, serial photophores (lp), minute photophores (mp), simple photophores (area outlined in grey), and vertical lines of superficial neuromasts (white arrowheads) in **E)** brightfield illumination, and illuminated at **F)** 390 nm, **G)** 470 nm, and **H)** 545 nm. Grey outline in D and H show the outline of orbital photophores (D) and simple photophores (H) not visible under 545 nm light. Scale (only shown in E) = 1 mm.

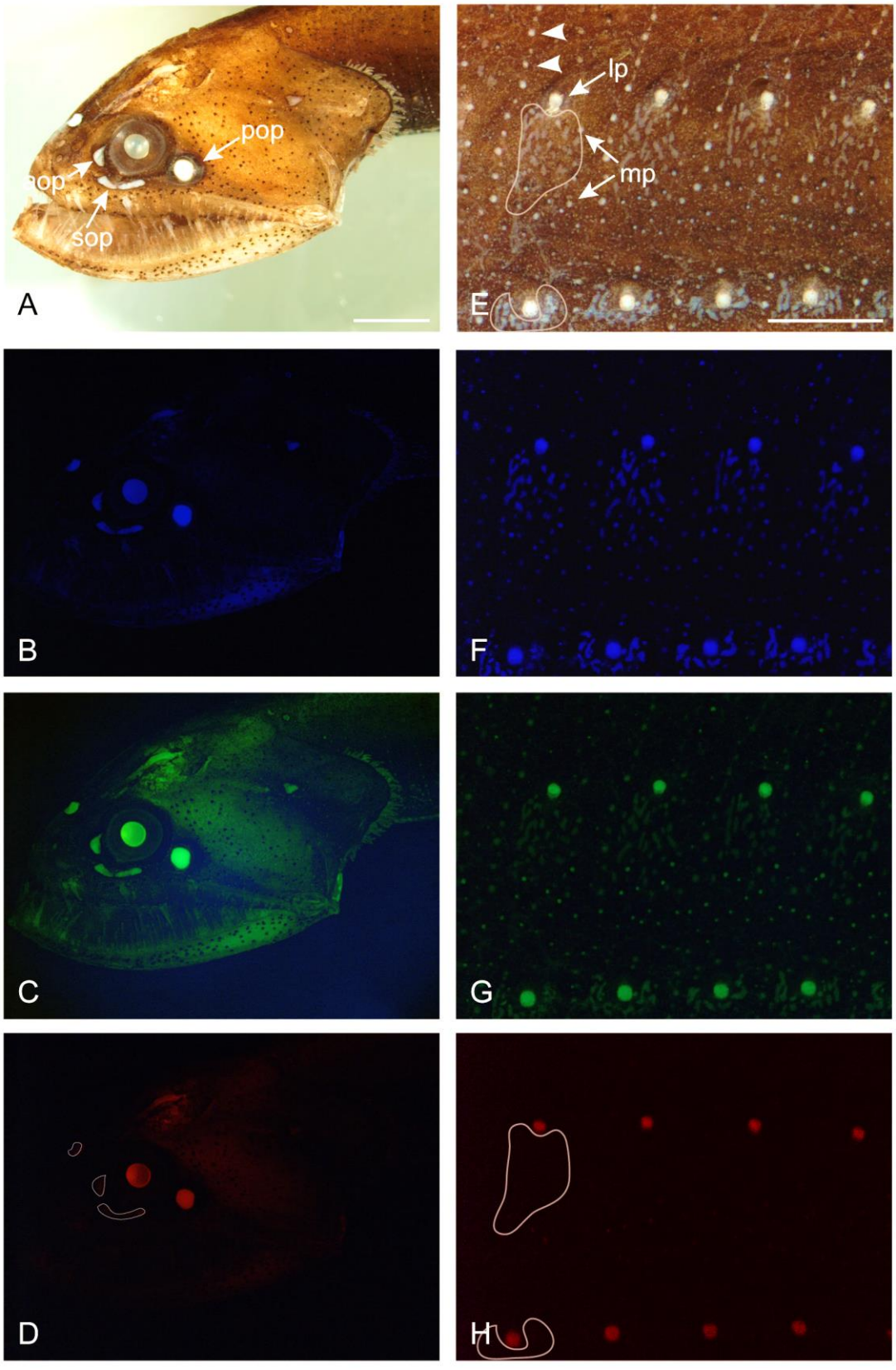
pop
sop
A
lp
mp
E
B
F
C
G
D
H

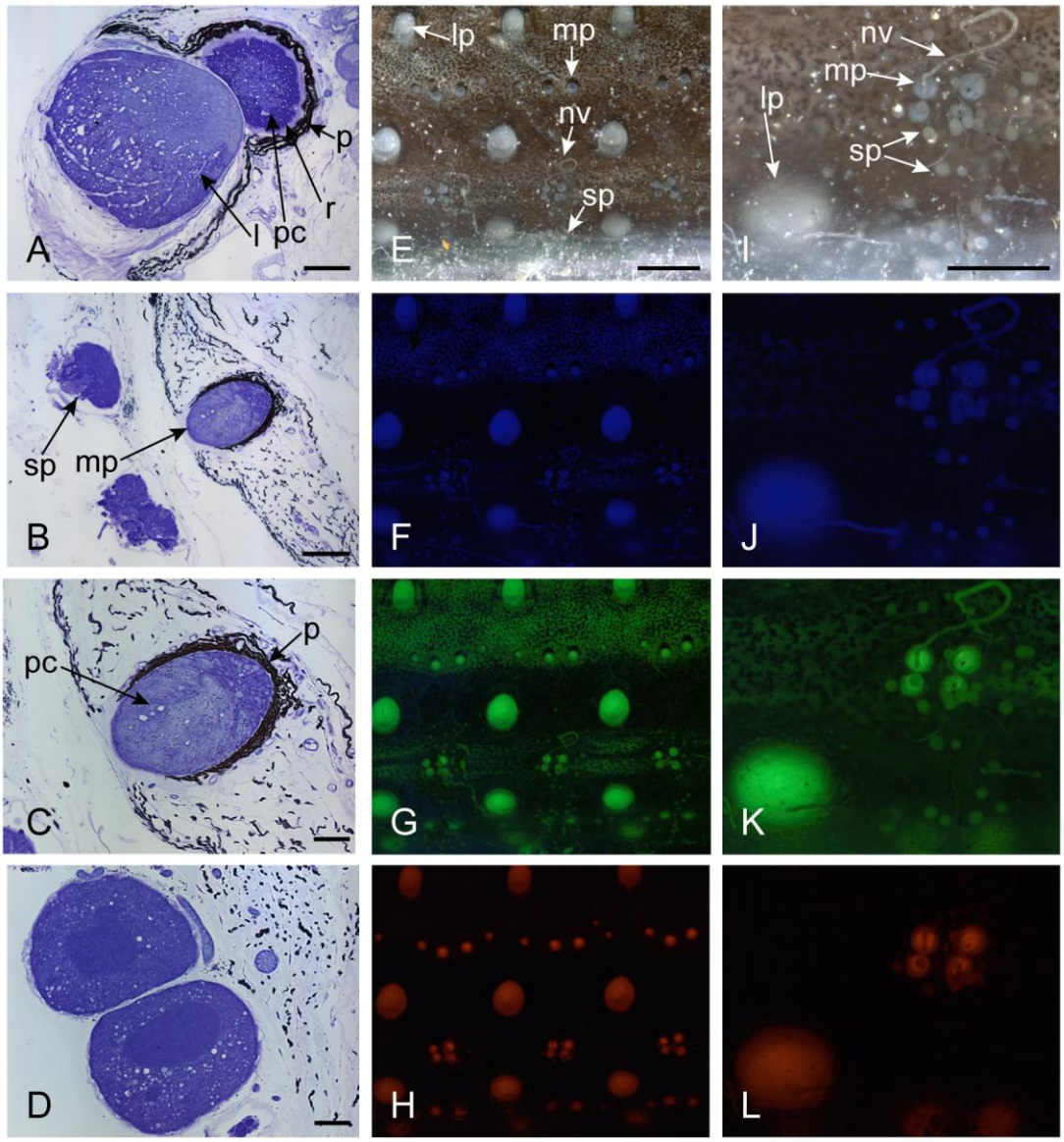

Figure 2. 6. Histology and single wavelengths illumination of complex and simple photophores in *Chauliodus sloani* . Histology of ventral photophores (A-D) in *C. sloani* in which the gelationus coat is not fully intact (see Fig.2.7C-D; 180 mm SL). Ventral is to the left. **A)** Large complex serial photophore showing the photogenic chamber (pc), lens (l), reflector (r), and pigment layer (p). Scale = 100 µm. **B)** Minute complex photophore (mp) and two simple photophores (sp) sitting superficial to the mp. Scale = 100 µm. **C)** Close-up of the minute photophore in B showing visible photogenic chamber (pc) and pigment layer (p). Scale = 40 µm. **D)** Two simple photophores sitting side by side. Scale = 40 µm. Images of a *C. sloani* (130 mm SL) with intact gelatinous coating in brightfield illumination (E, I), 390 nm (F, J), 470 nm (G, K), and 545 nm (H, L). showing the differences in fluorescence by large, complex serial photophores (lp), minute complex photophores (mp), simple photophores (sp) suspended within the gelationus coating, and nerves (nv). E-H shows a body segment with six large complex photophores (lp), and numerous minute complex photophores (mp) visible in all images and multiple simple photophores (sp) visible with 390 and 470 nm illumination only. I – L shows a close up of the same area in which the illumination of the large and minute complex photohpres are obstructed by the gelationus coating. Scale = 1 mm (E – H); 0.5 mm (I – L).

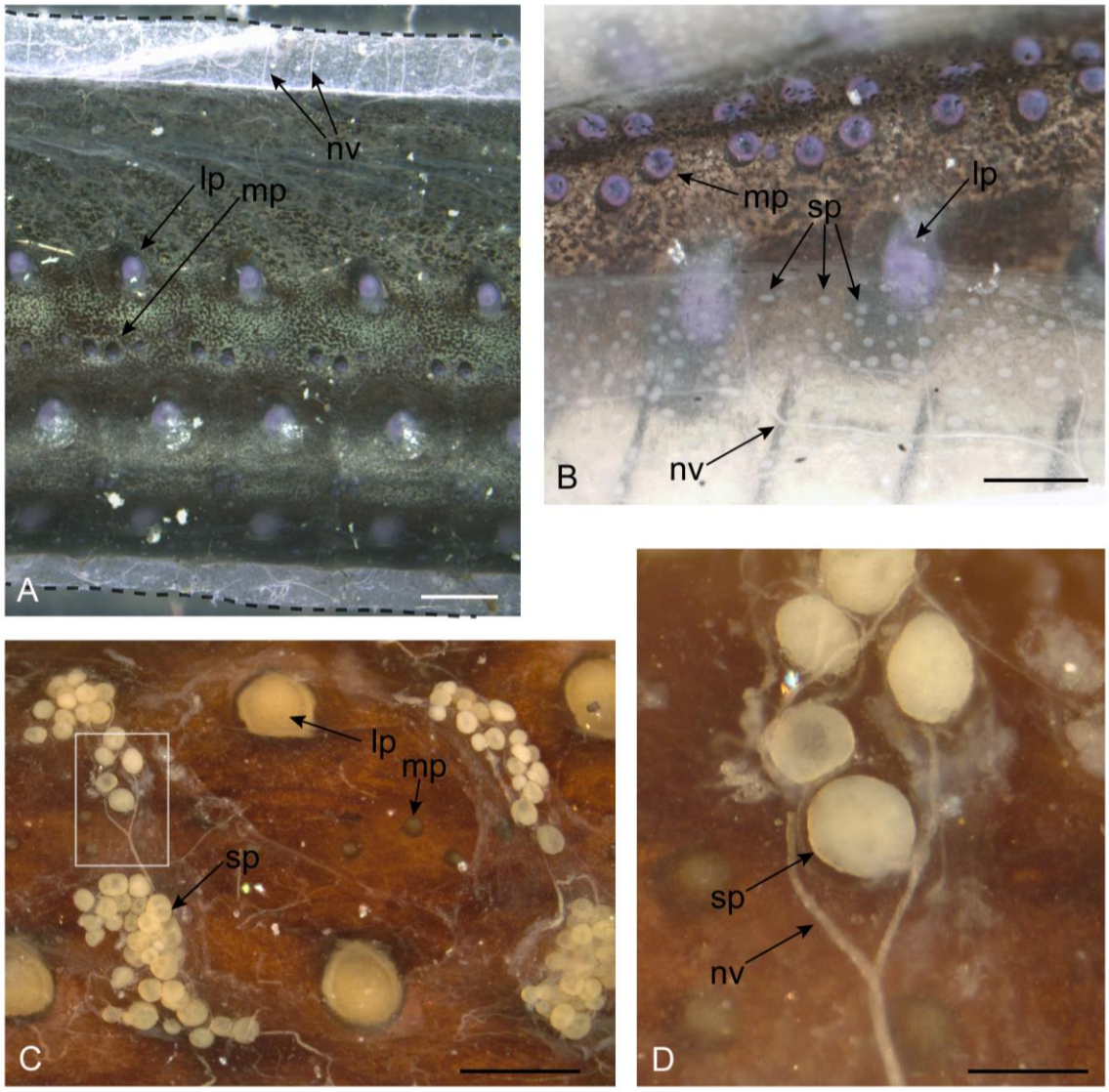

Figure 2.7: Structures within gelatinous coating of *Chauliodus sloani*. A) Intact gelatinous coat on the trunk of *C. sloani* (130 mm SL). Boundary of the unigmented gelationus coat is outlined by black dotted line. Nerves (nv) are visible extending into the gelatinous coating and the underlying large serial photophores (lp) and miute photophores (mp) are visible through the gelatinous coat.Scale = 1mm. **B)** Ventral view of the lower jaw showing the large serial photophores (lp), minute photophores (mp), and numerous simple photophores (sp) which are not in the gelationous coating but are innervated by the visible (nv). Scale = 0.5 mm. **C)** Ventral view of a *C. sloani* specimen with gelatious coating not intact (180 mm SL), leaving beihind the simple photophores (sp) which have fallen in clusters between the large serial photophores (lp), and over the numerous minute photophres (mp). White box shows the location of the close-up in D. Scale = 1 mm. **D)** Close-up of the simple photophores (sp) in C showing with visible nerve (and/or blood vessel; nv) running to the cluster of simple photophores. Scale = 0.25 mm.

Figure 2.8: Gelationus coat of *Stomias boa ferox*. (see next page). Ventro-lateral view of the gelatinous coat in *S. boa ferox* (110 mm SL) illuminated under **A)** brightfield illumination, **B)** 390 nm, **C)** 470 nm, and **D)** 545 nm light. Transparent gelatinous coat (outlined in black dotted line) is filled with numerous, elongate oval simple photophores (sp) overlying the large serial photophores (lp), and numerous minute photophores (mp). Nerves (and/or blood vessels; nv) are visible projecting into the gelatinous coating. Scale (only shown in A) = 1 mm. Closer view of the gelationus coating, which obstructs the illumination of the underlying photophores shown in **E)** brightfield illumination and illuminated by **F)** 390 nm, **G)** 470 nm, and **H)** 545 nm. Scale (only shown in E) = 0.5 mm. Note, the simple photophores are not visible at 545 nm (D, H).

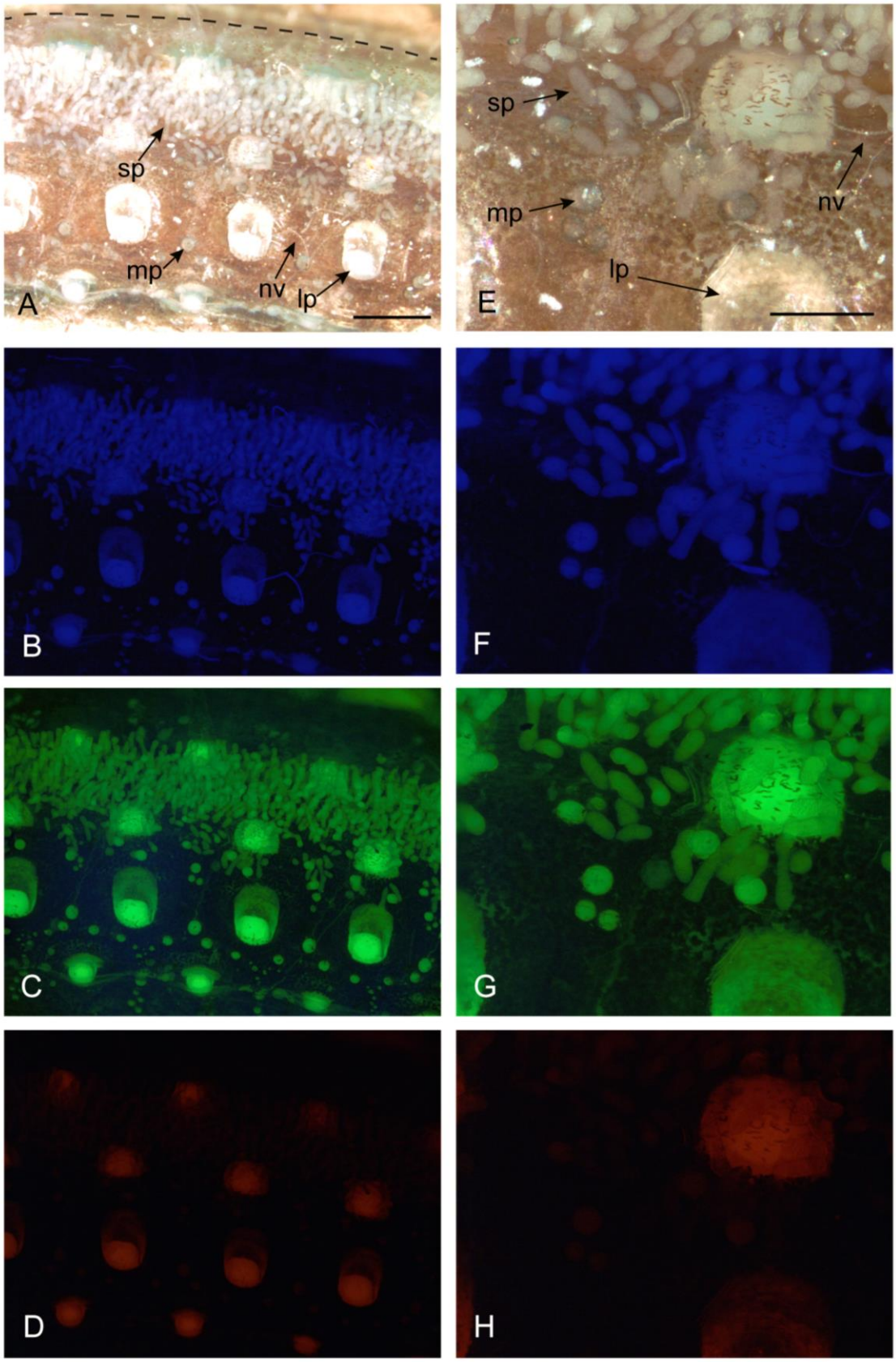
sp
mp
nv
lp
A
sp
mp
nv
lp
E
B
F
C
G
D
H

Appendix 1: *Cyclothone* Identification Character Matrix

There are 13 recognized species of *Cyclothone*. All species are morphologically similar, making it difficult to identify specimens to species. This character matrix can be used to help identify intact *Cyclothone* specimens. Identifying traits for 2 of the 13 *Cyclothone* species (*C. pygmea* and *C. livida*) are not included. Refer to Figure A.1 for abbreviations and locations for photophores. Descriptions are based on a combination of published works. Figures listed next to references refer to the figure number in that publication. References are as follows:

1- Grey (1964)
2- Berry (1965)
3- Mukahcheva (1966)
4- Kawaguchi (1971)
5- DeWitt (1972)
6- Bond & Tighe (1974)
7- Badcock (1982)
8- Miya & Nemoto (1987)
9- Miya & Nishida (1996)

Refer to Supplementary Information to see full character matrix.

Appendix 2: Key for the Identification of 10 *Cyclothone* species

The similar appearance of *Cyclothone* species makes it difficult to identify species, particularly when locality data are unknown. To date, published keys include only a few species and rely on examining gill rakers, which can be difficult in fully intact specimens. Based on the morphological characteristics in Appendix 1, a comprehensive key to 10 of the 13 species of *Cyclothone* was constructed. This key does not include *Cyclothone livida*, *C. kobayashi*, or *C. pygmaea* and does not include depth or geographical ranges. . For more specifics on relative size, depth distribution and locality, refer to Fig. A.7.

1 a. Photophores on head and body (Fig. 1) ……..……..... 2
b. Photophores not present on head or body…….... ***C. obscura***
2 a. Teeth gradually increase in length caudally (Fig. 2a)…… ***C. acclinidens***
b. Teeth increase irregularly caudally with 1 or 2 larger teeth separated by several smaller teeth (Fig. 2b) ……..... 3
3 a. Anus located caudal to 1st VAV photophore …… 4
b. Anus located caudal to 2nd VAV photophore ….…… 5
4. One gill raker in angle of first gill arch (Fig. 3a), body coloration white, only a V present for meningeal pigment (Fig. 4a-b).
a. 3 VAVs, 6 OAs (not located off U.S. Pacific coast)...…….. ……. ***C. alba***
b. 4 VAV's, 7 OAs (located off U.S. Pacific coast)……..……... ***C. signata***
5 a. Anus positioned closer to pelvic fins than to anal fin origin ……... 6
b. Anus positioned midway between pelvic fins and anal origin. 5 VAV photophores, anus is under or just rostral to VAV #3, genital opening separate from anal opening (caudal to VAV #3), 9 OA's, curved luminescent gland visible between OP photophores, body coloration dark brown to black ……..... ***C. atraria***
6 a. 9 OA photophores (last two caudal to pelvic fins with anus between OA #8 and #9), body coloration dark, 5 VAV photophores, luminescent gland visible between OP photophores…….....***C. microdon***
b. 7 or 8 OA photophores. Body coloration light to dark brown …… 7
7 a. Area rostral to anal fin origin is transparent ……..……... 8
b. Area rostral to anal fin is pigmented, 4 or 5 VAV photophores, 8 OA photophores (1st is on the vertical from pectoral fin base, 7th is on the vertical from the ventral fin, and 8th is on the vertical from VAV #2), genital and anal opening separate (Fig. 5), internasal area pigmented (Fig. 6b) body coloration light to dark brown …… ***C. pallida***
8 a. 7 OA photophores (1st on vertical from pectoral fin, 7th on vertical from base of anal fin), 4 VAV photophores, less than 30 meningeal pigment spots visible (Fig. 6d-f)…….…… ***C.braueri***
b. 8 OA photophores, body coloration light, 5 VAV photophores ……..…… 9
9 a. Internasal slightly pigmented, OA photophores: 1st on vertical from pectoral fin base, 7th on vertical from the IV #12 or #13, final is behind pelvic fins, separated from others. First 2 VAV photophores nearer than others. More than 30 visible meningeal pigmentation spots (Fig 4g-j)……..... ***C. pseudopallida***
b. Internasal area not pigmented (Fig. 6a). Dorsal and anal fins unpigmented, meningeal pigment does not extend past posterior margin of the eye ……..... ***C. parapallida***

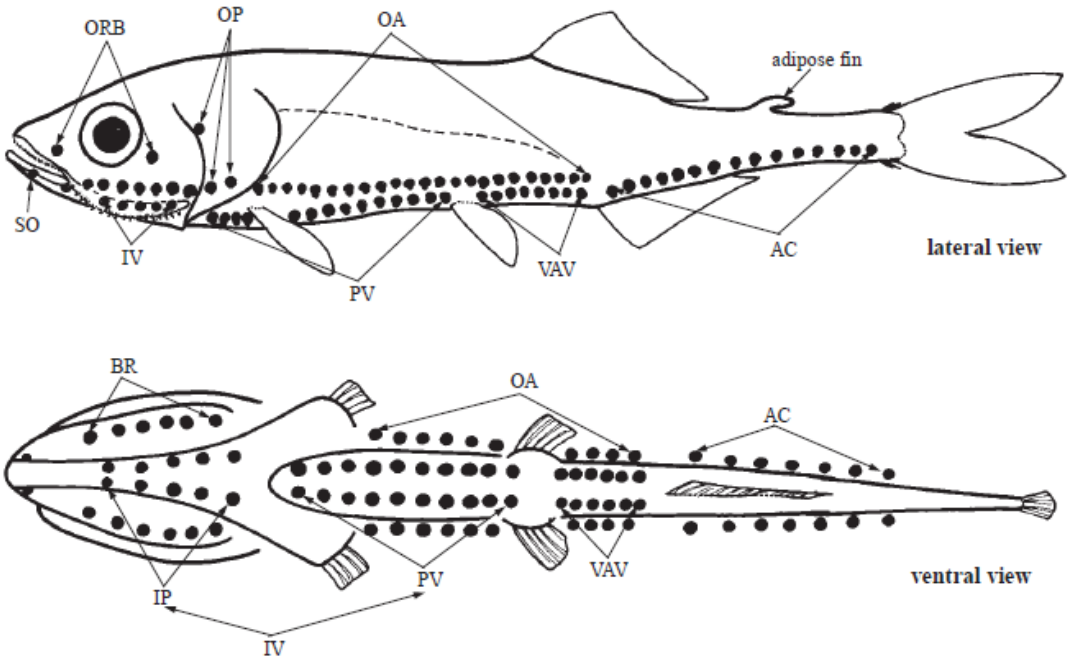

Figure A.1: Definitions and locations of photophore series – image from Harold (2002).

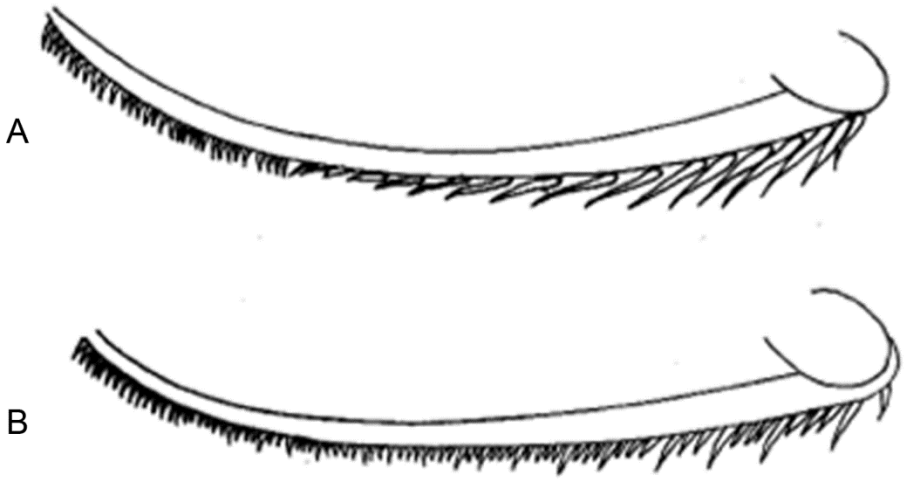

Figure A.2: Examples of teeth on the upper jaw in **A**) *Cyclothone acclindens* showing teeth gradually increasing caudally **B)** in *C. pallida* showing teeth increasing irregularly, with smaller teeth separating larger teeth. Image from Miya (1994).

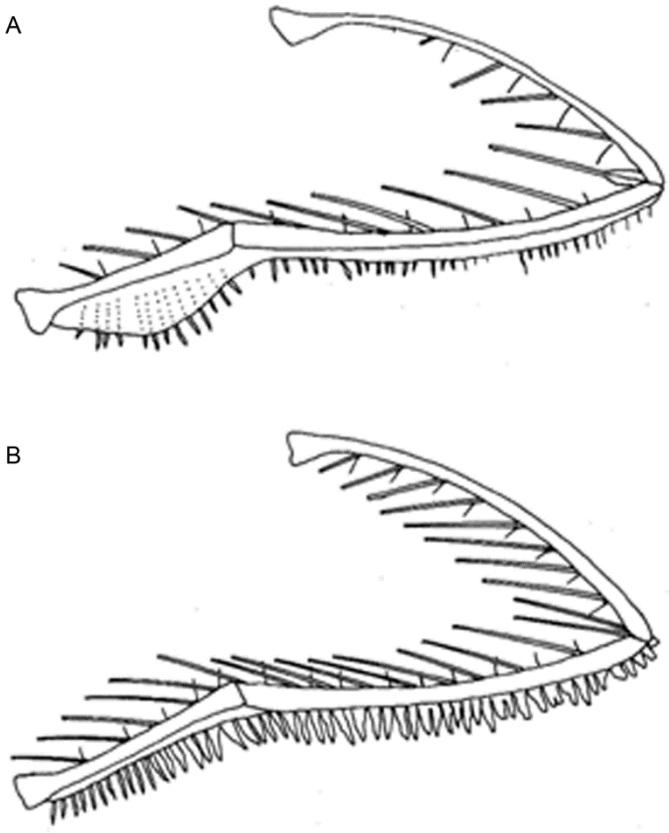

Figure A.3: First gill arch of A) *Cyclothone alba* with only 1 gill raker in angle of gill arch and B) *C. acclinidens* with two gill rakers in the angle of the gill arch. Image from Miya (1994).

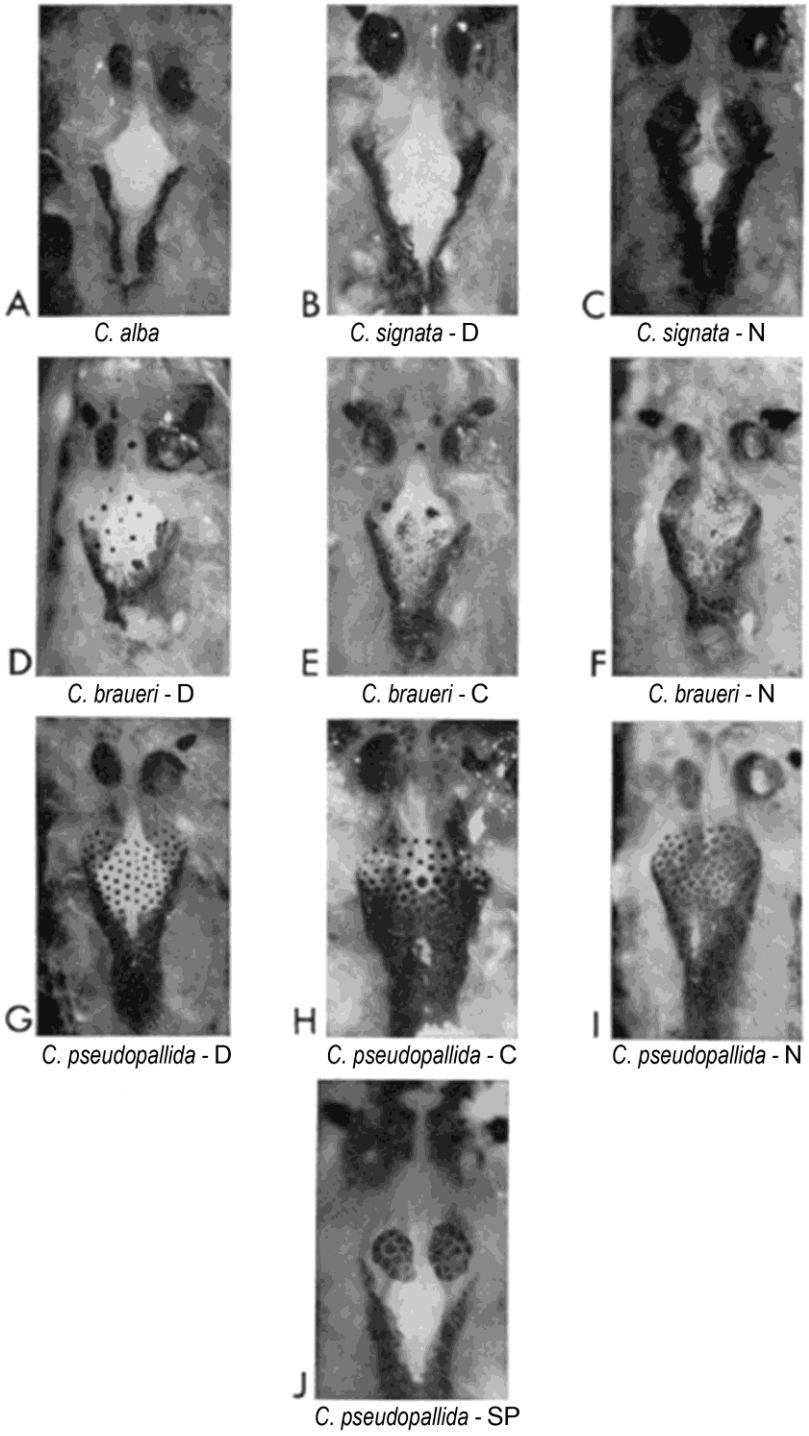

Figure A.4: Meningeal pigmentation patterns visible in lightly colored specimens of *Cyclothone*. Species names and time of capture are listed below each image. C = crepuscular, D = day, N = night,, SP = South Pacific. Image modified from Bond & Tighe (1974).

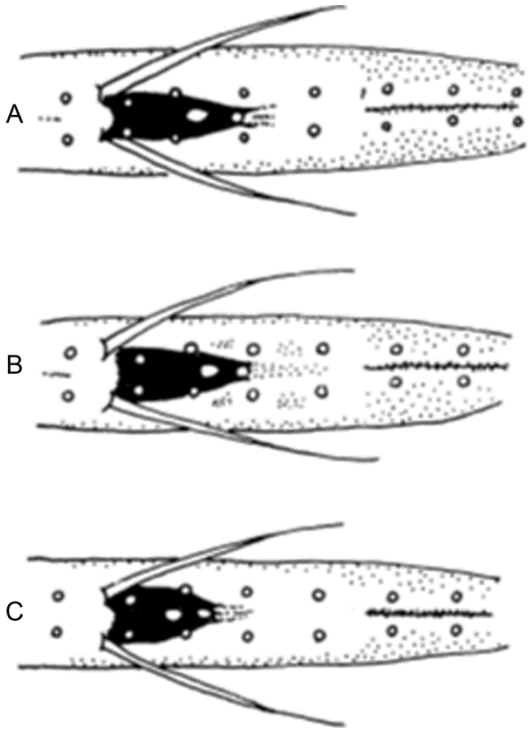

Figure A.5: Variations in pigment pattern around VAV photophores and anus and genital openings in *Cyclothone pallida*. Image from Kawaguchi (1971).

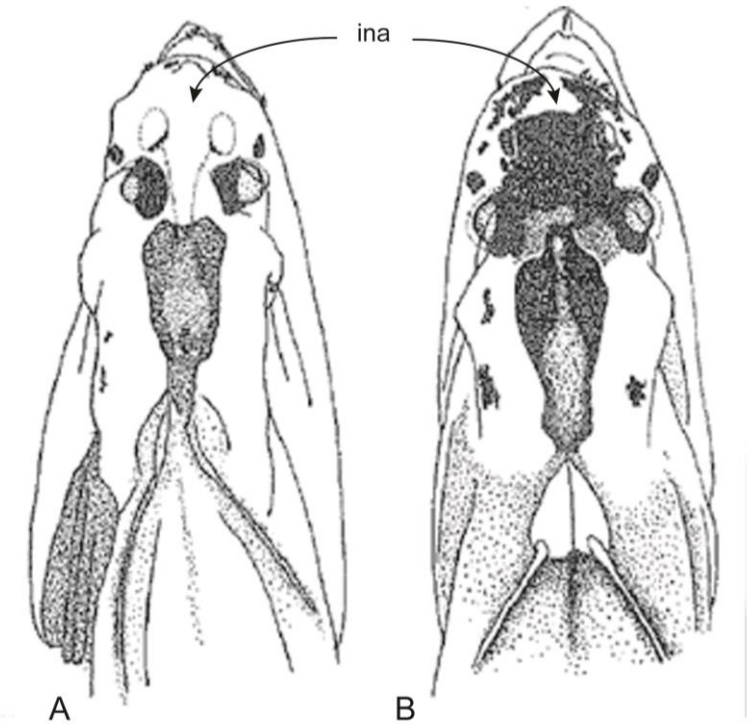

Figure A.6: Dorsal view of head showing internasal area (ina) **A)** unpigmented in *C. parapallida* and **B)** pigmented in *C. pallida*. Image from Badcock, 1982.

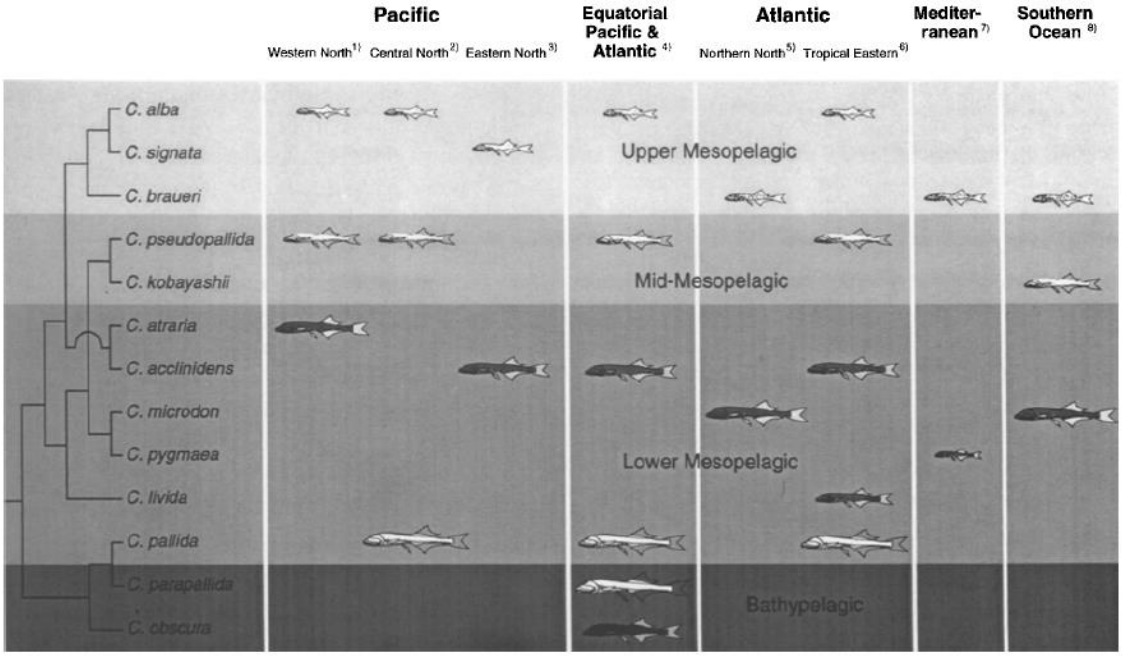

Figure A.7: Combination of species locations, depth ranges, and proportional sizes (according to largest size record) for *Cyclothone* spp. from the Pacific, Atlantic, Southern Ocean and Mediterranean Sea. Note that no data are available for the Indian Ocean. Image from Miya and Nishida (1996).